UNIVERSIDADE DE SÃO PAULO

FFCLRP - DEPARTAMENTO DE FÍSICA

RODRIGO FELIPE DE OLIVEIRA PENA

Emergence of activity fluctuations in cortical network models with heterogeneous neural populations

Emergência de flutuações de atividade em modelos de redes corticais com populações neurais heterogêneas

Ribeirão Preto - SP
2018

RODRIGO FELIPE DE OLIVEIRA PENA

Emergência de flutuações de atividade em modelos de redes corticais com populações neurais heterogêneas

Tese apresentada à Faculdade de Filosofia, Ciências e Letras de Ribeirão Preto da Universidade de São Paulo, como parte das exigências para a obtenção do título de Doutor em Ciências.

Área de Concentração:
Física aplicada à Medicina e Biologia.

Orientador:
Prof. Dr. Antônio Carlos Roque da Silva Filho.

Versão corrigida
Versão original disponível na FFCLRP-USP

Ribeirão Preto - SP
2018

Autorizo a reprodução e divulgação total ou parcial deste trabalho, por qualquer meio convencional ou eletrônico, para fins de estudo e pesquisa, desde que citada a fonte.

FICHA CATALOGRÁFICA

Nome: DE OLIVEIRA PENA, Rodrigo Felipe

Título: Emergência de flutuações de atividade em modelos de redes corticais com populações neurais heterogêneas

Tese apresentada à Faculdade de Filosofia, Ciências e Letras de Ribeirão Preto da Universidade de São Paulo, como parte das exigências para a obtenção do título de Doutor em Ciências.

Aprovado em:____/____/____.

Banca Examinadora

Prof. Dr. : _____ Instituição: _____

Julgamento: _____ Assinatura: _____

Prof. Dr. : _____ Instituição: _____

Julgamento: _____ Assinatura: _____

Prof. Dr. : _____ Instituição: _____

Julgamento: _____ Assinatura: _____

Prof. Dr. : _____ Instituição: _____

Julgamento: _____ Assinatura: _____

Prof. Dr. : _____ Instituição: _____

Julgamento: _____ Assinatura: _____

Dedico este trabalho à minha Jéssica. Pessoa que, por sua vez, escolheu me acompanhar e me apoiar incondicional em todos os momentos, principalmente nos de incerteza que foram muito comuns e os quais ela me resgatou.

AGRADECIMENTOS

À minha família. Meu pai **Jeci**, que sempre confiou em mim e me apresentou dignamente a importância do caminho da honestidade e da persistência. À minha mãe **Maria**, que nunca deixou de sorrir para mim e a me incentivar. Seu apoio e amizade me ajudaram a superar muitos obstáculos. Aos meus irmãos **Leonardo** e **Sophia**, que mesmo estando longe sempre torceram pela minha vitória e me incentivaram nesta jornada;

À minha esposa **Jéssica**, que não só compartilhou comigo de todo o processo que levou ao desenvolvimento desta tese com alto companheirismo, mas também me auxiliou com sugestões e com encorajamento incondicional.

Ao meu orientador, **Prof. Dr. Antônio C. Roque**, por me receber como aluno em seu laboratório. Pela confiança no meu trabalho, respeito, paciência e serenidade em todos esses anos. Enfatizo que seu apoio foi fundamental para desenvolvimento desta tese;

Aos membros da **Banca Examinadora**, por participarem e colaborarem fundamentalmente pela melhora desta Tese;

To **Prof. Michael Zaks** for the patient guidance, encouragement and advice he has provided throughout my time in Germany at the Humboldt University. His confidence in my work were an inspiration to me; I also acknowledge **Petar Tomov** for always being willing to help me when I asked, his collaboration was of very importance to this thesis, specially to the results in Chapter 4;

To **Prof. Benjamin Lindner** for his support and encouragement during my time in the Bernstein Center for Computational Neuroscience. In the course of this research project I benefited from his advice at many stages; I also would like to thank **Davide Bernardi** and **Sebastian Vellmer** who contributed to this research, more specifically during the time I spent in Germany and with Chapter 6

of this thesis;

"... a realidade não é dividida em disciplinas. A natureza não tem capítulos, como em um livro. A divisão é útil, mas é preciso ter em mente que ela é artificial. Imagine a realidade como uma orquestra tocando um concerto de Mozart. Se você ouvir só um dos instrumentos, não compreenderá a mensagem harmônica. O cientista que trabalha sem contato com outras áreas ouve os instrumentos isolados e não sente a orquestra do conhecimento em sua grandiosidade harmônica e melódica."
Sérgio Mascarenhas

Resumo

PENA, R. F. O. **Emergência de flutuações de atividade em modelos de redes corticais com populações neurais heterogêneas**. 2018. 163 f. Tese (Doutorado - Programa de Pós-graduação em Física aplicada à Medicina e Biologia) - Faculdade de Filosofia, Ciências e Letras de Ribeirão Preto, Universidade de São Paulo, Ribeirão Preto - SP, 2018.

Em modelos de redes corticais com neurônios pulsantes, os mecanismos responsáveis pela emergência e impacto de flutuações de atividade neuronal ainda não estão completamente entendidos. Neste trabalho, modelos computacionais de redes corticais foram utilizados para investigar como flutuações rítmicas e não-rítmicas surgem e suas possíveis consequências. Foram estudadas redes com dois tipos de topologia: aleatória e hierárquica modular, esta última inspirada em evidências experimentais para a arquitetura cortical. Foram utilizados três diferentes modelos simplificados de neurônios: integra-e-dispara, Izhikevich e integra-e-dispara exponencial com adaptação. Primeiramente, estudou-se a ocorrência de atividade auto-sustentada em redes hierárquicas modulares compostas por populações de neurônios de classes eletrofisiológicas distintas. Nesses modelos, os padrões de atividade auto-sustentada de longa duração são oscilatórios e seu tempo de vida depende do nível hierárquico e da mistura de neurônios na rede. Em seguida, estudou-se o efeito da introdução de ruído sináptico em modelos de redes aleatórias. Observou-se o aparecimento de alternância intermitente entre atividade rítmica e não-rítmica com características similares a estados corticais síncronos e assíncronos, respectivamente. Desenvolveu-se a extensão de uma abordagem reducionista para redes neuronais homogêneas, em que um esquema iterativo auto-consistente é usado para que um único neurônio gere trens de disparo com propriedades estatísticas de segunda ordem similares às de uma rede, para o caso de redes neuronais heterogêneas. Mostrou-se que essa abordagem captura situações em que flutuações de atividade lentas emergem. Finalmente, utilizou-se o esquema reducionista e ferramentas de teoria de informação para estudar a emergência de flutuações de atividade lentas e sua propagação em redes hierárquicas modulares. Os resultados mostram que a propagação de informação pela rede depende do número de módulos, sugerindo que há um nível hierárquico ótimo para a propagação de informação. Os estudos feitos contribuem para aprofundar o entendimento da relação entre estrutura e composição neuronal em modelos de redes corticais e indicam mecanismos de emergência e manutenção de flutuações de atividade nessas redes.

Palavras-chave: 1. sistemas dinâmicos. 2. redes complexas. 3. córtex cerebral. 4. neurociência computacional. 5. ruído. 6. flutuações.

ABSTRACT

PENA, R. F. O. **Emergence of activity fluctuations in cortical network models with heterogeneous neural populations**. 2018. 163 f. Thesis (Ph.D. - Postgraduate program in Physics applied to Medicine and Biology) - Faculty of Philosophy, Sciences and Literature, University of São Paulo, Ribeirão Preto - SP, 2018.

In cortical network models with spiking neurons, the mechanisms responsible for the emergence and impact of neuronal activity fluctuations are not yet completely understood. In this work, computational models of cortical networks were used to investigate how rhythmic and non-rhythmic fluctuations arise and their possible consequences. Networks with two types of topology were studied: random and hierarchical modular, this latter inspired on experimental evidence about cortical architecture. Three different simplified spiking neuron models were used: integrate-and-fire, Izhikevich, and integrate-and-fire with adaptation. Initially, the types of self-sustained activity patterns that emerge in hierarchical modular networks with mixtures of electrophysiological neuronal classes were studied. In these models, the long-duration self-sustained activity patterns are oscillatory and their lifetime depend on the hierarchical level of the network and its neuronal composition. Next, the effect of the introduction of synaptic noise in random networks was studied. These networks displayed intermittent alternations between rhythmic and non-rhythmic activity patterns with characteristics similar to synchronous and asynchronous cortical states, respectively. A reductionist approach for homogeneous neuronal networks, in which an iterative self-consistent scheme is used so that a single neuron spike train generates second-order statistical properties similar to the ones of a network, was extended to heterogeneous networks. It was shown that this reductionist scheme captures situations in which slow activity fluctuations emerge. Finally, the reductionist scheme and information theoretical tools were used to study the emergence of slow activity fluctuations and their propagation through hierarchical modular networks. The results show that the information propagation in the network depends on the number of modules, suggesting an optimal hierarchical level for information propagation. The studies done contribute to deepen the understanding of the relationship between structure and neuronal composition in cortical network models, and point to mechanisms of emergence and maintenance of activity fluctuations in these networks.

Key-words: 1. dynamical systems. 2. complex networks. 3. cerebral cortex. 4. computational neuroscience. 5. noise. 6. fluctuations.

LIST OF ABBREVIATIONS

RS   Regular spiking excitatory neuron

CH   Chattering excitatory neuron

IB   Intrinsically bursting excitatory neuron

FS   Fast spiking inhibitory neuron

LTS   Low-threshold inhibitiory neuron

HMN   Hierarchical and modular network

LIF   Leaky integrate-and-fire neuron model

AdEx   Adaptive exponential integrate-and-fire neuron model

SSA   Self-sustained activity

mEPSPs   miniature excitatory postsynaptic potentials

mIPSPs   miniature inhibitory postsynaptic potentials

CONTENTS

CHAPTER 1

INTRODUCTION

1.1 General introduction

Humanity seeks the understanding of natural phenomena that happens in the world around us (the *external world*) from as early as its own existence. The study of different patterns, abstractions, and the use of logic, which pertains to the field of mathematics, is known to be done by the Greeks in the 3rd century BC for example. The field of physics, which could be seen as little younger than mathematics, has as major goal the understanding of nature. Although questions concern motion, space, or even time, the final objective is to understand how the universe behaves.

On the contrary, neuroscience differs from these fields in some aspects. The first, and perhaps most important difference, is that neuroscience is not seeking the understanding of the external world; instead, it pursues the understanding of our brain. It may be the only science which allows the real understanding of what is happening in the universe that comprises our minds. Through the studying of neural physiology, neural anatomy, psychology, computational modeling, etc., we seek as ultimate goal to understand what is our brain doing. A second difference is the age of neuroscience. Although some attempts in understanding the brain have been made throughout the whole human history, substantial advances in the field did not start until the late 1890s when Camillo Golgi developed the staining procedure with silver chromate allowing a better visualization of individual neurons. The silver chromate staining allowed Santiago Ramón y Cajal to propose the neuron doctrine which states that the brain has the neuron as its functional unit (Guillery, 2005).

Several attempts have been made since that founding moment to move

forward our understanding of the brain. Nevertheless, little is known. As it was well described by the Austrian-American neuroscientist Eric Richard Kandel (Nobel Prize in Physiology or Medicine), aspects of neuroscience are the "ultimate challenge" for the biological sciences (Kandel, Schwartz, Jessell, et al., 2000). In that sense, scientists with different backgrounds (including the author of this thesis) see that the final goal of neuroscience will not be achieved by an individual scientist working in a single discipline, but by a collective effort of scientists from varied fields: from biological sciences to mathematics, physics, and computational science; from different laboratories around the world.

This work focus on the understanding of biological phenomena through the view of computational and theoretical neuroscience. Efforts were made towards the understanding of brain phenomena via the understanding of brain models. In particular, we investigate how fluctuations in neuronal activity emerge in networks of spiking neurons and what are their consequences. We focus on the cerebral cortex where heterogeneous neuronal populations are known to exist.

1.2   Goals

The goal of this work was to study the emergence of activity fluctuations in cortical network models with heterogeneous neuronal populations. All neuron models and network architectures were chosen to generically represent the cerebral cortex. Heterogeneity was achieved in different directions: topologically by considering networks with hierarchical and modular structure, or intrinsically to the neurons by introducing cells with different firing properties. Rhythmic and non-rhythmic activity fluctuations were studied and mechanisms to generate these fluctuations were linked to synaptic and network noise, types of neurons or topological attributes. Possible implications such as self-sustained activity or propagation of information received special attention during the development of this thesis. Methods of mean-field analysis, dynamical systems analysis, and information theory were developed and applied.

1.3   Contribution

Most theoretical studies of cortical network dynamics have concentrated on networks with non-modular architecture and homogeneous neuronal composition, usually described by unstructured networks with Erdős-Rényi topology (Erdős & Rényi, 1959) populated by leaky integrate-and-fire neurons (Gerstner, Kistler, Naud, & Paninski, 2014). The main contribution of this thesis was to extend these studies to networks with a more elaborate architecture, namely hierarchical modular, which captures elements of the organization of the cortical brain network (Meunier, Lambiotte, & Bullmore, 2010), composed of heterogeneous neuronal populations with distinct firing patterns, modeled by two-dimensional integrate-and-fire neurons (Gerstner et al., 2014). The network models studied here exhibit a rich repertoire of dynamic activity patterns, and this thesis describes, analyses and explains the underlying mechanisms of some of these patterns for the first time.

1.4   Organization of the thesis

The structure of this thesis was inspired on the "traditional complex" arrangement (Paltridge, 2002), where general introduction and methods are followed by studies presented in different chapters with their own introduction, methods, results, and discussion sections. In the end, general conclusions are presented. A summary of the internal structure of each chapter follows:

- In Chapter 2, we review the background and literature. We go through basic neuroscience modeling justifying the use of simplified models as the ones we will employ here. We introduce the reader to basic notions of phase-plane analysis which will be useful for the questions addressed in this thesis.

- In Chapter 3 we present our general methods. There, we explain all the statistical measures used along the thesis. Although the common measures are placed here, in each chapter we also include a more specific methods section.

- In Chapter 4, the first chapter with results, we investigate mechanisms behind the transient oscillatory activity observed in the models. Many of these results

have been published elsewhere (Tomov, Pena, Zaks, & Roque, 2014; Tomov, Pena, Roque, & Zaks, 2016). Using interpretations based on single-neuron and network dynamical systems analyses, we explain why this activity starts and the reason for its eventual complete cessation.

- In Chapter 5 we study how synaptic noise affects spontaneous dynamics in networks with multiple neuron subtypes. Results from this chapter have already been published (R. F. O. Pena, Zaks, & Roque, 2018). We localize the population activity patterns in a two-dimensional parameter diagram, and explain the intermittent dynamics observed in a particular region of the diagram.

- In Chapter 6 we introduce an iterative scheme to describe second-order statistics of a neuron. These results help us to understand how slow-fluctuations build up in a network model from the point of view of a single neuron. Results from this chapter have also been published (R. F. Pena, Vellmer, Bernardi, Roque, & Lindner, 2018).

- In Chapter 7 we finish the presentation of our results by discussing how a hierarchical and modular topology works together with slow activity fluctuations to enhance activity propagation through the network. These results have not yet been published but a manuscript is under preparation.

The thesis organization was done in a way that each chapter can be read independently, but we suggest reading the Methods section first in Chapter 3. Every chapter has its own introduction and a brief summary of specific methods for the questions that are addressed.

1.5 Scientific publications derived from this thesis

During the studies of the author of this thesis aiming for his Ph.D., he published, as first-author or co-author, a number of articles in peer reviewed journals. Some of them are directly related to this thesis, but some are not. The latter are the product of his curiosity and intensive discussions with his supervisor, other professors and close colleagues to whom he is thankful. A complete list with all articles that the

Ph.D. candidate published during his studies (from 2014 to 2018) is displayed below.

Peer reviewed journals:

- **Pena, R.F.O.**, Zaks, M., Roque, A.C. (2018). Spontaneous activity dynamics in random networks of spiking neurons with synaptic noise. *Journal of Computational Neuroscience, 45*:1–28.
  `doi.org/10.1007/s10827-018-0688-6`

- **Pena, R.F.O.**, Ceballos, C.C., Lima., V., Roque, A.C. (2018). Interplay of activation kinetics and the derivative conductance determines resonance properties of neurons. *Physical Review E, 97*:042408.
  `doi.org/10.1103/PhysRevE.97.042408` and *preprint* in `arxiv.org/pdf/1712.00306.pdf`

- **Pena, R.F.O.**, Vellmer, S., Bernardi, D., Roque, A.C., and Lindner, B. (2018). Self-Consistent Scheme for Spike-Train Power Spectra in Heterogeneous Sparse Networks. *Frontiers in Computational Neuroscience, 12*:9.
  `doi.org/10.3389/fncom.2018.00009`

- Amorim, M.R., **Pena, R.F.O.**, Souza, G.M.P.R., Bonagamba, L.G.H., Roque, A.C., and Machado, B.H. (2018). Firing properties of ventral medullary respiratory neurons in sino-aortic denervated rats. *Experimental Physiology,* 1–11.
  `doi.org/10.1113/EP087150`

- Cunha A.O., Ceballos C.C., Deus, J.L., **Pena, R.F.O.**, Oliveira, J.A.C., Roque, A.C., Garcia-Cairasco, N., Leão, R.M. (2018). Intrinsic and synaptic properties of hippocampal CA1 pyramidal neurons of the Wistar Audiogenic Rat (WAR) strain, a genetic model of epilepsy. *Scientific Reports, 8*:10412.
  `doi.org/10.1038/s41598-018-28725-y`

- Lima., V., **Pena, R.F.O.**, Ceballos, C.C., Shimoura, R.O., Roque, A.C., Information theory applications in neuroscience (2019). *Brazilian Journal of*

Education in Physics, *41*:e20180197.
doi.org/10.1590/1806-9126-RBEF-2018-0197

- Shimoura, R.O., Kamiji, N.L., **Pena, R.F.O.**, Cordeiro, V., Ceballos, C.C., Romaro, C., Roque, A.C. (2018). [Re] The cell-type specific cortical microcircuit: relating structure and activity in a full-scale spiking network model. *The ReScience Journal*, *4*:785–806.
doi.org/10.5281/zenodo.1243268

- Ceballos, C.C., **Pena, R.F.**, Roque, A.C., and Leão, R.M. (2018). Non-Decaying postsynaptics potentials and delayed spikes in hippocampal pyramidal neurons generated by a zero slope conductance created by the persistent Na^+ current. *Channels*, *12*:81–88.
doi.org/10.1080/19336950.2018.1433940

- Tomov, P., **Pena, R. F.**, Roque, A.C., and Zaks, M.A. (2016). Mechanisms of self-sustained oscillatory states in hierarchical modular networks with mixtures of electrophysiological cell types. *Frontiers in Computational Neuroscience*, *10*:23.
doi.org/10.3389/fncom.2016.00023

- Tomov, P., **Pena, R.F.**, Zaks, M.A., and Roque, A.C. (2014). Sustained oscillations, irregular firing, and chaotic dynamics in hierarchical modular networks with mixtures of electrophysiological cell types. *Frontiers in Computational Neuroscience*, *8*:103.
doi.org/10.3389/fncom.2014.00103

Manuscripts submitted or in preparation:

- **Pena, R.F.O.**, Lima., V., Shimoura, R.O., Novato, J.P., Roque, A.C., Activity propagation in hierarchical and modular networks with slow fluctuations. **in preparation**.

- **Pena, R.F.O.**, Ceballos C.C., Deus, J.L., Oliveira, J.A.C., Roque, A.C., Garcia-Cairasco, N., Leão, R.M., Cunha A.O., Modeling the temporal

features of synaptic inhibition in hippocampal CA1 pyramidal neurons. **in preparation**.

- Lima, V., **Pena, R.F.O.**, Ceballos, C.C., Shimoura, R.O., Roque, A.C., Asymmetry in the subthreshold resonance properties of neurons generated by high amplitude currents. **in preparation**.
  preprint in arxiv.org/pdf/1804.04748.pdf

- Lima, V., Dellajustina, F., **Pena, R.F.O.**, Shimoura, R.O., Kamiji, N.L., Ceballos, C.C., Borges, F.S., Higa, G.S.V., Kihara, A.H., De Pasquale, R., Roque, A.C., A simple neuron model with a soft threshold and its network consequences. **in preparation**.

- Borges, F.S., Protachevicz, P.R., **Pena, R.F.O.**, Lameu, E.L., Higa, G.S.V., Kihara, A.H., Matias, F.S., Antonopoulos, C.G., De Pasquale, R., Roque, A.C., Iarosz, K.C., Ji, P., Batista, A.M., Low frequency self-sustained activity in balanced networks. **in review**.
  preprint in arxiv.org/abs/1809.01020v1

- Ceballos C.C., **Pena, R.F.O.**, Deus, J.L., Cunha A.O., Leão, R.M., Roque A.C., The impact of the activation rate of I_h on the membrane time constant and synaptic potential decay: a current-clamp and computational modeling study. **in preparation**.

<div align="right">

CHAPTER 2

</div>

BACKGROUND TO THE STUDY AND REVIEW OF THE LITERATURE

2.1 The cerebral cortex

The cerebral cortex is the brain region on which we focus in this thesis. It is a structure of the brain of mammals and comprehends its outermost sheet.

The cortex is responsible for many cognitive and higher brain functions (Kandel et al., 2000; Tranel, Cooper, & Rodnitzky, 2003; Bear, Connors, & Paradiso, 2007). It is divided into two brain hemispheres which contain four anatomical lobes: frontal, parietal, temporal, and occipital. Each lobe is related to a different function, some examples are: the frontal lobe is associated with control of movements and planning; the parietal lobe is associated with somatic sensations; the temporal lobe is associated with hearing and language comprehension; the occipital lobe is related to vision.

The full cortical connectivity at the different scales spanned by it (local circuits to inter-area network) has not been completely determined, as well as their possible functions. Attempts have been made to characterize the cortical anatomy (Thomson, West, Wang, & Bannister, 2002; Binzegger, Douglas, & Martin, 2004; Greenberg, Houweling, & Kerr, 2008; Potjans & Diesmann, 2014). These studies reveal that vertically the cortex is organized in layers where each layer has an enormous neuronal diversity. The cortical layers connect among themselves according to very specific patterns. Horizontal connections are revealed by different techniques, e.g. diffusion MRI, which can measure white matter spreading, and

show a modular organization (Bassett et al., 2010). It is debated whether a modular organization allows parallel processing of information in the cortex, but it does create a heterogeneous organization in the sense that populations are clustered.

Through techniques involving electrophysiological recordings it has been possible to classify neurons based on their responses to current inputs (Connors, Gutnick, & Prince, 1982; McCormick, Connors, Lighthall, & Prince, 1985), and attribute these neurons to given locations in intricate cortical topology (Binzegger et al., 2004). The majority of excitatory neurons in the cerebral cortex are pyramidal and may fire regularly (with or without adaptation) or exhibit an initial burst. On the other hand, most of the inhibitory neurons are basket cells which usually fire with faster frequencies (Shepherd, 2003). Undoubtedly, the cerebral cortex contains heterogeneous neuronal populations.

2.2   Modeling

Theoretical and computational modeling of brain components are not only techniques but comprise a field of research, referred to as computational neuroscience. This field has been largely developed with the intent to investigate and explain several phenomena of the brain. Since the study of the brain is challenging and involves different spatial and temporal scales (Sejnowski, Churchland, & Movshon, 2014), it is not surprising to observe in the literature different types of models on completely different scales as well.

In the following, we will give a background on neuronal and network modeling as well as on dynamical systems analysis, which will be useful for the reader along the thesis.

2.2.1   Neuron Models

We will start by distinguishing between different types of neuronal modeling. There are two main approaches to take when modeling a neuron: biophysical and simplified (see Fig. 2.1 for a schematic explanation of the different types of modeling).

The biophysical type of modeling was introduced by the famous work of Hodgkin and Huxley (Hodgkin & Huxley, 1952), which describes action potentials
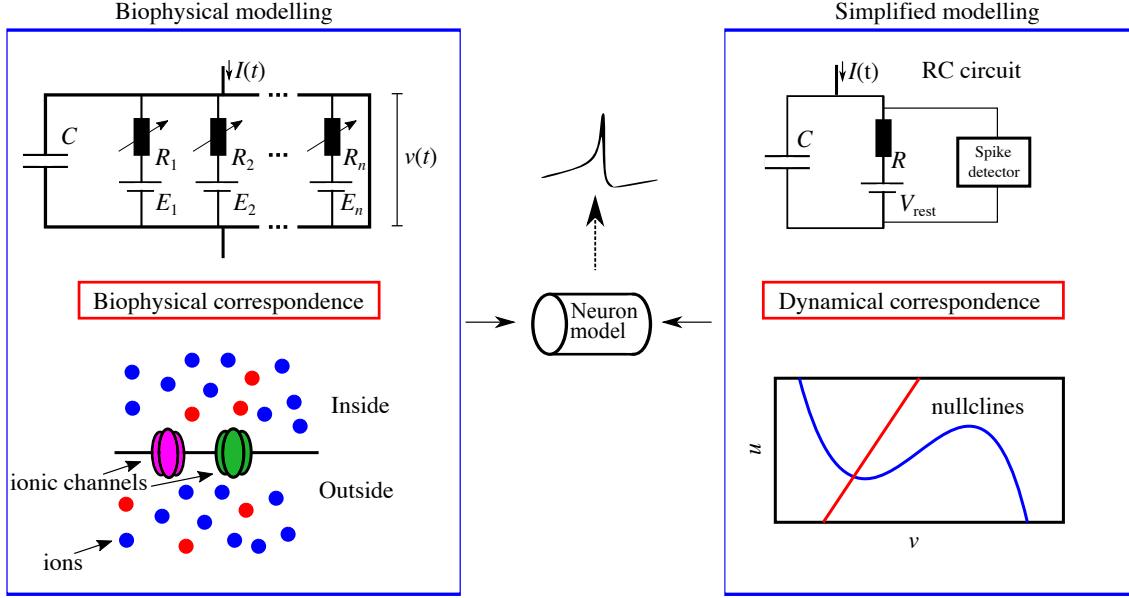
Figure 2.1: *Different approaches to model neurons. Left: Biophysical modeling takes into account ionic channels and because of that has a close biophysical correspondence. Right: Simplified modeling takes into account only the dynamical features to generate a spike and is used to make mathematical analysis such as the ones involving dynamical systems.*

in the squid giant axon. The Hodgkin and Huxley equations outline the ionic mechanisms underlying an action potential and, by coupling the equations for the different ion channels in a neuronal membrane one can create a neuron model with a close biophysical correspondence and make testable predictions.

The simplified modeling approach is interested in reproducing the dynamics of an action potential without necessarily having a biophysical correspondence behind it. This type of modeling has several advantages but also some disadvantages when compared to biophysical modeling. Whereas one can achieve a relatively good neuron model with a simple RC circuit coupled with some spike detector (see Fig. 2.1 right) or by the combination of simple differential equations, these models lack ionic currents which can be experimentally tested. In this thesis, we only focus on simplified neuronal models as we are mostly interested in the single-neuron spiking behavior and on the population behavior. In the following, we will review how simplified models are usually established.

In the class of simplified models that we will treat here, the continuous time evolution of an action potential is not modeled and only the subthreshold dynamics

is described. Because of this, a discontinuity is added to the neuron model and an update rule is introduced which is identified with a reset in the membrane voltage whenever it reaches a certain threshold. Such artifice allows a simplified dynamics which is, in general, easier to be handled.

The first simplified neuron model that we shall describe is the integrate-and-fire neuron model (Lapicque, 1907; Gerstner et al., 2014). This particular neuron model has been a standard choice among the neuroscience community that uses simplified neuron models. It is a very simple model and yet very powerful. Its equation reads:

$$\tau_{\mathrm{m}} \dot{v}(t) = f(v) + \text{input} + \text{update rule}. \tag{2.1}$$

When $v(t) > v_{\mathrm{th}}$, a spike is emitted and, after a refractory period of τ_R, the voltage is reset to $v(t) = v_{\mathrm{r}}$. The parameter τ_{m} in Eq. (2.1) is the membrane time constant, which may be different depending on the electrophysiology of the neuron. The input current may come from different sources (scaled by the membrane resistance R), and is denoted by $RI(t)$.

The choice of the function $f(v)$ is very important to model the correct and desired behavior. Some examples are:

- $f(v) = 0$: perfect integrate-and-fire (PIF);

- $f(v) = -v$: leaky integrate-and-fire (LIF);

- $f(v) = v^2$: quadratic integrate-and-fire (QIF);

- $f(v) = -v + \Delta_T \exp(\dfrac{v - v_{th}}{\Delta_T})$: exponential integrate-and-fire (EIF);

- $f(v) = $ fitting from an experimental data.

Although these neurons are computationally efficient and analytically tractable, they lack some basic features presented in real neurons such as spike-frequency adaptation. One can overcome these limitations by introducing a second variable in the equations, which describes a time-dependent current. With

this second variable the model reads:

$$\tau_{\mathrm{m}}\dot{v} = f(v) - u + \text{input} + \text{update rule}$$
$$\tau_{\mathrm{u}}\dot{u} = g(v, u) + \text{update rule}. \tag{2.2}$$

This second variable in Eq. (2.2) allows a much richer repertoire of behaviors. The u variable provides a negative feedback to the voltage variable v, which works as a memory of the spiking activity of the neuron and produces adaptation in the firing rate. In most cases, the second variable (which we will usually call simply u-variable) is chosen in order to have a linear relation with the voltage. Besides, the first variable v changes accordingly to the type of behavior that one aims to model. The name of the model is taken in accordance with the function $f(v)$. The most accepted choices for $f(v)$ are:

- $f(v) = -v$: linear adaptive integrate-and-fire (adaptive LIF);

- $f(v) = \alpha v^2 + \beta v + \gamma$: quadratic adaptive integrate-and-fire, or Izhikevich neuron model (Izhikevich, 2003);

- $f(v) = $ exponential function : adaptive exponential integrate-and-fire (AdEx model) (Brette & Gerstner, 2005; Gerstner et al., 2014).

As an example which will be largely used in this thesis, we present the Izhikevich neuron model:

$$\begin{cases} \dot{v} &= \alpha v^2 + \beta v + \gamma - u + I(t) \\ \dot{u} &= a(bv - u), \end{cases} \tag{2.3}$$

where α, β, and γ are experimentally fitted to mimic the spiking initiation of a cortical neuron. Observe that the input is time dependent and identified by $I(t)$. In addition, note that here we have $g(v, u) = a(bv - u)$. Whereas the parameter a describes the time scale of the u-variable, the parameter b describes the sensitivity of the u-variable to subthreshold oscillations in the voltage membrane v. In this regard, small (large) a results in slow (fast) recovery, and large b results in subthreshold

oscillations. At the threshold $v(t) = v_{\text{th}}$, which usually is taken at 30 mV for the Izhikevich model. The update rule reads

$$\begin{cases} v(t) & \to c, \\ \\ u(t) & \to u(t) + d, \end{cases} \tag{2.4}$$

where c is the reset voltage (v_{r}) and d is added to the u-variable whenever a spike occurs.

The parameters that are used to generated the neuronal diversity in this type of model are displayed in table 2.1.

	α	β	γ	a	b	c	d
RS	0.04	5	140	0.02	0.2	-65	8
CH	0.04	5	140	0.02	0.2	-50	2
IB	0.04	5	140	0.02	0.2	-55	4
FS	0.04	5	140	0.1	0.2	-65	2
LTS	0.04	5	140	0.02	0.25	-65	2

Table 2.1: *Parameters from the Izhikevich model that characterize five electrophysiological cell classes used in the simulations.*

Examples of neurons that are possible to generate with these parameters are given in Fig. 2.2. In A is presented a regular spiking neuron (RS), in B a chattering (CH), in C a fast spiking neuron (FS), and in D a low-threshold spiking neuron (LTS). While RS and CH are excitatory neurons, FS and LTS are inhibitory neurons. The intrinsically bursting neuron (IB) is an excitatory cell very similar to the RS neuron with the difference that there is an initial bursting prior to the regular behavior.

2.2.2 Phase plane description

To understand the dynamical mechanisms behind these simplified neuron models, it is fundamentally important to describe them in a geometric way. This helps to understand the possible outcomes of the neuron model if stimulation is
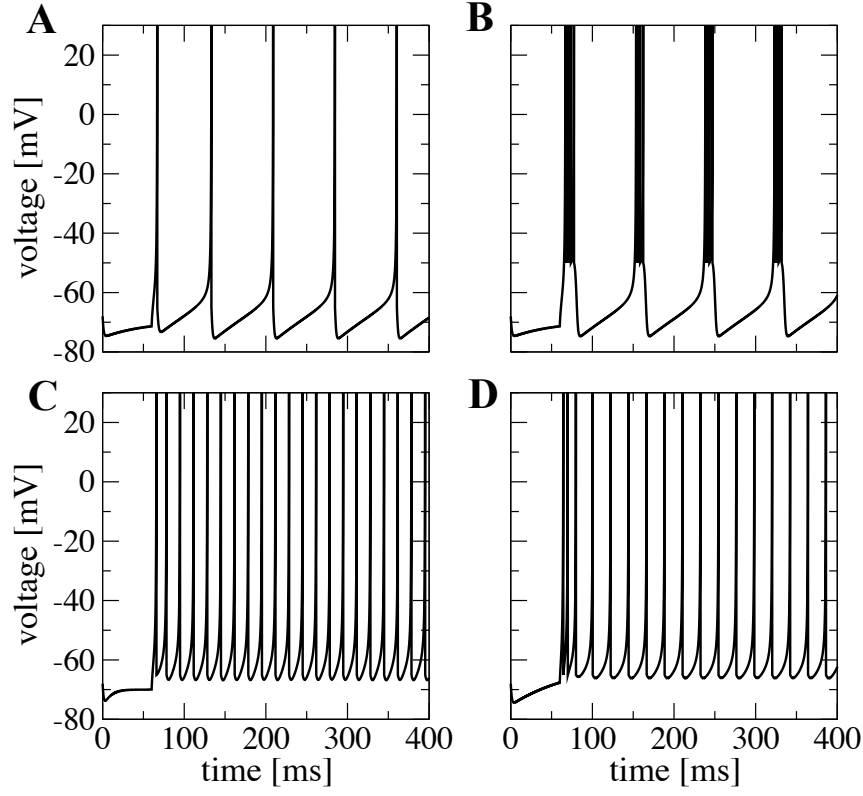
Figure 2.2: *Spiking patterns for electrophysiological cell classes modeled by the Izhikevich formalism.* ***A*** *excitatory neuron RS.* ***B*** *excitatory neuron CH.* ***C*** *inhibitory neuron FS.* ***D*** *inhibitory neuron LTS. Plots where produced with constant* $I = 6$.

applied without the need of solving analytically its differential equations. To do that, we include a phase space description of some important features from these neuron models which might also introduce the reader to basic tools of dynamical systems.

2.2.2.1 Leaky integrate-and-fire neuron model

The LIF neuron model contains only one variable and has its dynamics easily described by its one dimensional phase space (see Eq. (2.1)). By setting the derivative to zero, i.e. $\dot{v} = 0$, one can easily calculate its fixed point

$$v^* = RI(t)$$

where the superscript * identifies the fixed point, i.e. when the derivative $\dot{v} = 0$ we have $v = v^*$. Therefore, the fixed point is completely determined by the input in the

LIF neuron model. As an example, if we set the input $RI = 30$ mV, the trajectory will always be attracted to this value. Since the system tends to evolve attracted to this point we call this particular fixed point an attractor. Given that we want a spiking neuron we have to complete this description introducing a reset mechanism at some threshold value (update rule). In this example, we choose $v_{th} = 20$ mV and $v_r = 10$ mV.

With this LIF neuron model we always have a voltage trace fluctuating mostly between $v_r = 10$ mV and $v_{th} = 20$ mV, being the trajectory attracted towards $v^* = 30$ mV. The velocity of this attraction can be well changed by the arrival of synaptic inputs which, in very large and sparse networks, are usually quasi-random[1]. In Fig. 2.3 we show an example of such neuron model and its phase plane analysis. In Fig. 2.3A the neuron does not receive stimulation and because of that the trajectory is trapped at the fixed point at $v^* = 0$ mV. As the input is incremented to $RI = 30$ mV in Fig. 2.3B we observe a shift of the fixed point to $v^* = 30$ mV where the trajectory is attracted and a fire-and-reset rule applies (see the complete description in the legend of this figure).
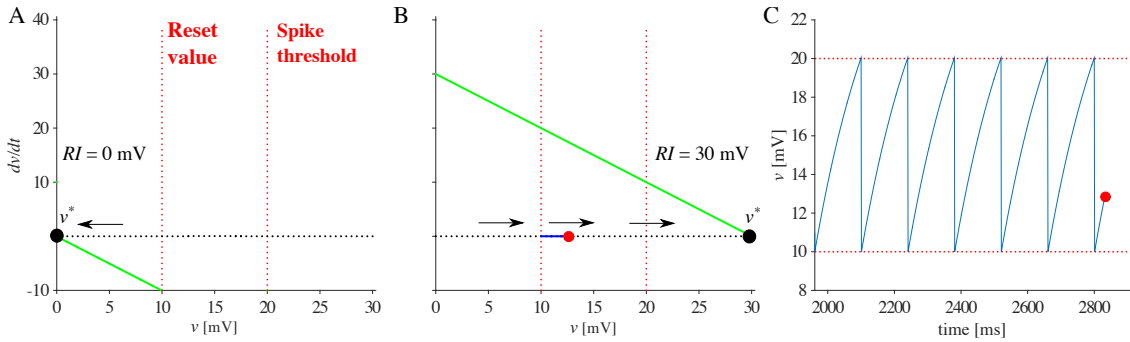
Figure 2.3: ***Leaky integrate-and-fire behavior in a phase plane.*** *Green curve: dv/dt. Black circle: v^*. Red dotted lines: reset voltage and spike threshold, respectively. A: When stimulation is absent, the fixed point is $v^* = 0$ mV and the trajectory stays at this point. Observe that the fixed point is determined by the zero crossing dv/dt. B: By making $RI = 30$ mV the fixed point is changed to $v^* = 30$ mV and the trajectory is now attracted to this point. Since there is a threshold at $v_{th} = 20$ mV the neuron is reset to $v_r = 10$ mV every time the trajectory crosses v_{th}. C: Voltage series of the same trajectory in B.*

---

[1] Quasi-random points fill the space more uniformly than uncorrelated random points. They are evenly distributed. This is the case of synaptic inputs which are subjected to refractoriness.

2.2.2.2   Izhikevich neuron model

In the Izhikevich neuron model, by setting the derivatives to zero we can identify two nullclines which we will refer as v-nullcline or $\bar{u}$ and u-nullcline or u^*. These are identified by the following equations:

$$\begin{cases} \bar{u} & = \alpha v^2 + \beta v + \gamma + I(t) \\[2mm] u^* & = bv. \end{cases} \tag{2.5}$$

Observe that only $\bar{u}$ is time-dependent due to $I(t)$. As I increases, spiking behavior can emerge due to a bifurcation which is basically a qualitative change in the structure of this system due to the increment of I.

In general, four types of bifurcations are used to classify this excitable system (Izhikevich, 2007): saddle-node bifurcation, saddle-node on invariant circle bifurcation, subcritical Andronov-Hopf bifurcation, and supercritical Andronov-Hopf bifurcation.

- In a saddle-node bifurcation, a stable fixed point (the node) and an unstable fixed point (the saddle) approach each other as the bifurcation parameter moves towards the bifurcation point. At the bifurcation point the two fixed points annihilate each other and the trajectory is forced to follow the flow determined by the system dynamics. For example, if there is an unstable fixed point in another region of the phase space the trajectory may be attracted to a limit cycle around this fixed point (if the flow is bounded) and the resulting behavior can be interpreted as a series of spikes with a given frequency.

- The saddle-node on invariant circle bifurcation is a saddle-node bifurcation in which the trajectory is attracted to a limit cycle that passes very close to the point where the node and saddle collided. In this case, when the bifurcation parameter is a little above the transition point the resulting trajectory has very low velocity around the colliding region and the ensuing spiking behavior has a correspondingly very low frequency.

- An Andronov-Hopf bifurcation happens when a stable fixed point loses stability and turns into a limit cycle as the bifurcation parameter passes through the bifurcation point. If the limit cycle is unstable and shrinks into the stable fixed point, the type of bifurcation is called subcritical Andronov-Hopf. If, due to the instability of the newborn fixed point, the trajectory goes towards a limit cycle of larger amplitude this is interpreted as a spiking behavior.

- The supercritical Andronov-Hopf bifurcation happens when the limit cycle that appears through the Andronov-Hopf bifurcation is stable. This limit cycle is created from a stable fixed point which, in turn, becomes an unstable one. When the bifurcation parameter is a little above the bifurcation point, stable oscillations have low amplitude and those are interpreted as subthreshold oscillations.

Understanding the different types of bifurcations that occur in a neuron model is very helpful because one can use this understanding to predict its behavior upon an input.

In the case of the Izhikevich system, two different bifurcations happen when the input current $I(t)$ is increased and those depend on the relation of the parameters a and b (Izhikevich, 2000). If $b < a$ there is a saddle-node bifurcation, if $b > a$ there is a subcritical Andronov-Hopf bifurcation.

As an example, we show the case of the saddle-node bifurcation and how two electrophysiological classes (RS and CH) can be explained through its phase plane analysis. Here, the input current $I(t)$ control the saddle-node bifurcation which is responsible for the creation of the fixed points. When there is no input, the nullcline $\bar{u}$, which is a quadratic equation and so has a parabolic shape, crosses u^* creating two fixed points, a stable and an unstable one. When the input is positive, $\bar{u}$ is shifted upwards and at some point, both fixed points collide and annihilate in a saddle-node bifurcation freeing the trajectory to grow in voltage. We do not allow an infinitely grow by resetting at the threshold. If the trajectory enters the parabola, due to the time-scale separation the velocity will suddenly become very low and the trajectory will be trapped for some transient time. At some point it will be able to escape and develop further spikes.

The interplay of $\bar{u}$, u^*, and the reset values c and d are exactly what will shape the different electrophysiological classes. At Fig. 2.4 we show an example of how the behavior of the neuron can change drastically, from RS to CH, by playing with these features.
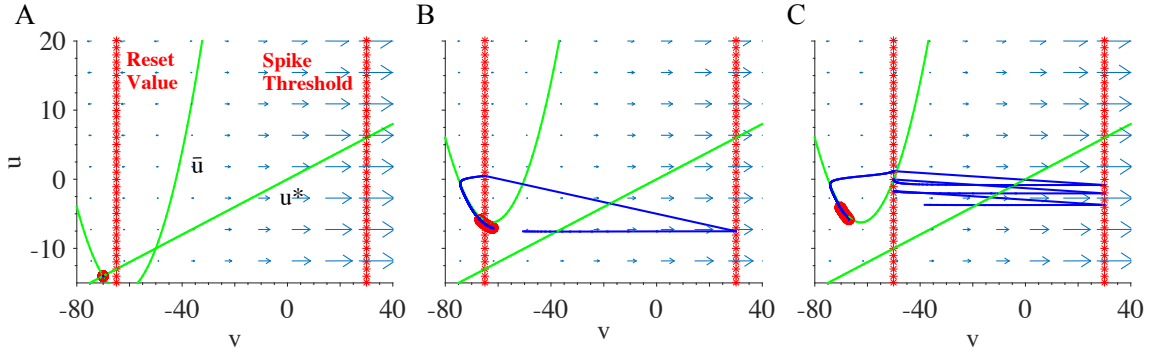
Figure 2.4: *Phase plane for isolated RS and CH neurons. Green curves: nullclines. A: I=0. Nullclines intersect at states of equilibrium. Red circle: stable equilibrium. B and C: Phase portraits at I=10. Blue curves: trajectories. Vertical red lines: values of v at the threshold v_{th} and reset c. B: Regular spiking neuron. C: Chattering neuron.*

Distinctions between the two types at the example in Fig. 2.4 proceed, on the one hand, from different (controlled by parameter d) increments of the variable u after each spike, that are considerably higher for the RS neuron and, on the other hand, from difference in the reset value c. The effect is clearly seen in the plots: in **B** the RS neuron is instantaneously reset to a position above the parabola, whereas the CH neuron performs several cycles (spikes) until the value of u becomes sufficiently large to exceed the nullcline $\bar{u}$.

Another very interesting feature important to our discussion is named rebound spiking. Markedly, this comes exclusively from the particular LTS neuron which can be distinguished from the other neurons in the event of a negative input. After the injection of a negative pulse, LTS neurons are able to spike and this phenomenon will be very important to understand some network mechanisms later on. This may also happen in other neurons depending on the parameter b. To explain how this happens in the Izhikevich dynamical system, we use here a phase space description as shown in the Fig. 2.5.

In the panel at Fig. 2.5 **A** we can see the dynamics during the injection of the negative current pulse with the voltage starting at it's resting state (black square
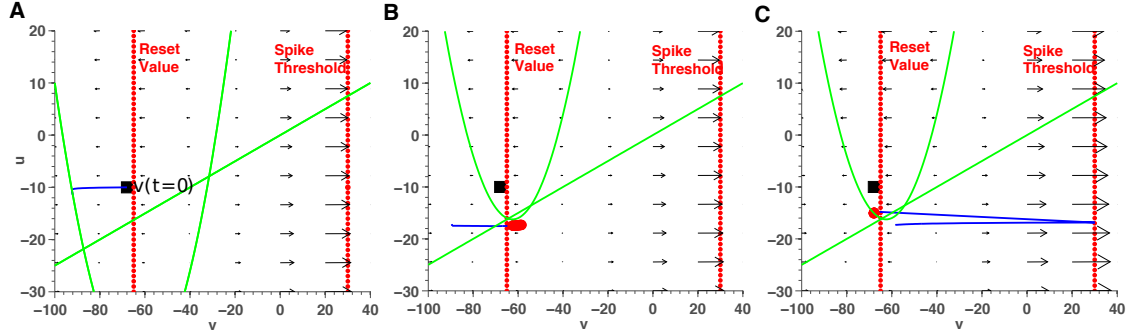
Figure 2.5: *Effect of rebound in the phase plane for isolated LTS neuron. Green curves: nullclines. Thick blue curves: trajectories. Vertical red lines: values of v at the threshold V_{peak} and reset c. A) Dynamics while receiving negative current. B) Dynamics right after the removal of the negative stimuli. C) Rebound spike.*

in the figure). The v-nullcline is shifted downwards and a hyperpolarization follows. When the current is taken out (panel **B)**, the v-nullcline goes back to the normal position. However, at this moment the trajectory is outside the parabola and free to evolve. It quickly develops a spike due to the fast dynamics (panel **C)**.

Due to the parameter b in the LTS neuron, which is different from the other neurons, the inclination of the u-nullcline is higher and the fixed point determined by the crossing of the two nullclines is much lower. This effect increases drastically the chance to observe a rebound and that makes the LTS neurons unique. This kind of behavior is well known in electrophysiological experiments and is used to identify LTS cells among others with the help of negative inputs.

2.2.3 Network Models

In possession of a neuron model as described above, we replicate it into several copies which may differ by intrinsic parameters giving rise to sets of neurons. These sets and subsets of neurons may interact through synaptic connections and this constitutes a network model. The way these interactions happen defines a topology. In this thesis, we concentrate on different topologies as we discuss below.

2.2.3.1 The random network

Here we explain the modeling of a random network. We start with a physiologically motivated ratio of excitatory to inhibitory neurons 4:1; for every

pair of randomly chosen neurons i and j, the probability of connection $i \to j$ is $\epsilon = 0.01$, autapses are not allowed. Also named connectivity, the probability ϵ is independent of the type of neuron (see first panel in Fig. 2.6 for the adjacency matrix, also referred as connectivity matrix) with connections in the same color. This model is also referred as an Erdős-Rényi graph (Erdős & Rényi, 1959) which is a standard choice in many studies of networks, giving its simple nature it allows easy computational and mathematical analysis.

2.2.3.2   The hierarchical and modular network (HMN)

A hierarchical and modular network (HMN) is a common choice of topology for a brain network. Anatomical evidence (Boucsein, Nawrot, Schnepel, & Aertsen, 2011) suggests a hierarchical and modular structure where neurons are grouped into modules (clusters where connections are denser) and connections are more likely to be found between close modules than between faraway ones. To put it another way, modules are encapsulated in a hierarchical topology. This structure is present in both meso- and macroscopic scales, i.e. not only neurons but also regions organize in a hierarchical and modular way (Binzegger et al., 2004; Kaiser & Hilgetag, 2010; Voges, Schüz, Aertsen, & Rotter, 2010).

There are several algorithms that allow the generation of a HMN, here the HMN is generated by the following top-down algorithm (Kaiser & Hilgetag, 2010; Wang, Hilgetag, & Zhou, 2011): We start from the random network and we assign to this network the hierarchical level $H = 0$. At the next step, we randomly divide all neurons into two modules of equal size. All connections *within* the modules are preserved. Since inhibitory connections *between* the modules are not allowed, all such links are rewired: cut (detached from postsynaptic neurons) and redirected back into the modules of their presynaptic neurons, where they are attached randomly. We say that inhibitory neurons are rewired with probability $R_{\mathrm{in}} = 1$. The fate of each excitatory link between the modules is decided at random: with probability $R_{\mathrm{ex}} = 0.1$ a connection is retained, and with probability $(1 - R_{\mathrm{ex}}) = 0.9$ it is cut and rewired back into the module with the presynaptic neuron. In this way, we obtain two modules, sparsely interconnected by excitatory links, and assign to this network the level $H = 1$. This procedure is repeated iteratively to generate other

levels of hierarchy H. In this algorithmic, a network with a hierarchical level H has 2^H modules.
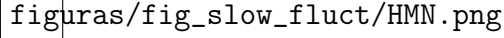
Figure 2.6: *Exemplary networks with different hierarchical levels constructed by the top-down procedure. Upper row: Connectivity matrices for hierarchical levels $H = 0, 1,$ and 2. Bottom row: Schematic representation of the network for the different levels $H = 0, 2,$ and 3 containing 2^{11} excitatory neurons.*

Some examples of HMNs are displayed in Fig. 2.6. In the first row of Fig. 2.6 we present a visualization of the connectivity of a subset of excitatory neurons, it is possible to observe that as H increases, not only the number of modules increases but also the hierarchy: modules are encapsulated in groups of larger modules which communicate with other large groups through sparse excitatory connections. In the second row of Fig. 2.6 we can observe an adjacency matrix, note that whereas the inhibitory neurons are local the long-range connections are exclusively excitatory which is a feature of the cerebral cortex (Bosking, Zhang, Schofield, & Fitzpatrick, 1997; Battaglia, Brunel, & Hansel, 2007).

2.3 Fluctuations, oscillations, and noise

Neurons and networks may exhibit fluctuations, oscillations, and noise. In the light of the clarification and distinction among these close attributes, we shall define their meaning and possible sources.

We start with the definition of **fluctuations**. According to the Oxford dictionary (en.oxforddictionaries.com accessed June 9, 2018), fluctuation means "*An irregular rising and falling in number or amount; a variation*", in that sense we understand for our purposes as fluctuation a non-rhythmic variation of the signal. Adjacent to that, the definition of **oscillation** is close but not the same, the aforesaid dictionary uses fluctuation to define oscillation where it states "*Variation or fluctuation between two states, limits, opinions, etc*". In that sense, we see that oscillations are a more periodic form of fluctuations. We understand for our purposes that rhythmic fluctuations are oscillations and non-rhythmic fluctuations will be simply fluctuations.

Conversely, **noise** may cause fluctuations. Neurons are subject to many different sources of noise (Faisal, Selen, & Wolpert, 2008). These generators of noise are responsible for several changes in the neuronal system. In fact, it is controversial if noise is a true signal or even if it has some function despite disturbing the signal, although there are several examples that have already demonstrated the importance of noise in neuroscience (Benzi, Sutera, & Vulpiani, 1981; Shu, Hasenstaub, Badoual, Bal, & McCormick, 2003).

Among the different sources of noise, the ones which we are mainly interested in this thesis and act on the stochasticity of spiking are channel noise, synaptic noise, and network noise. Although we do not explore all of them, we depict below their sources for comparison.

- **Channel noise** comes from the stochasticity of ionic channels which are submitted to random openings and closings. This type of noise becomes very important in processes that involve signal transduction like mechano-receptors of the auditory system or receptors of the olfactory scheme which are processes governed by a large population of ion channels.

- **Synaptic noise** is a source of noise that may come from different origins. For instance, spiking transmission may failure and this creates some unreliability in the signal transmission that acts as synaptic noise. Another factor might be the spontaneous release of neurotransmitters that happens from time to time. Due to the very large number of synapses, spontaneous transmission is quite often observed. Moreover, there is a variability in synaptic amplitude which is due to the number of synaptic transmitters that vary from vesicle to vesicle that is freed in the synaptic cleft during a synaptic event.

- **Network noise** is considered the largest source of variability of spiking. Since brain networks are large in number of neuronal components and the number of inputs in a given cell is huge, there is a quasi-random arrival of synaptic input which is treated as a noise source.

In this thesis, we will show that noise established in different forms act on neurons and how it can cause not only non-rhythmic but also rhythmic fluctuations.

CHAPTER 3

GENERAL METHODS

3.1 Measures

In this section, we introduce neuron and network measures that will be used below for characterization of the results.

Several of the statistics inspected in this work are based on spike-trains, which are defined as sums of Delta functions

$$x(t) \;=\; \sum_i \delta(t - t_i), \tag{3.1}$$

where t_i is the time instant of the ith spike (we also denote the spike-train with a subscript $x_j(t)$ to indicate that it belongs to a jth neuron when adequate). The instantaneous firing rate ν is the (generally time-dependent) average of the spike train, $\nu = \langle x(t) \rangle$, and can be determined for a specific neuron within the network by an average over different runs with randomized initial conditions. In practice, we often average the rate over the population (if appropriate, i.e. if the neurons are statistically equivalent) which is indicated by $\langle . \rangle$ (ensemble average) and over time:

$$\nu \;=\; \frac{1}{T} \int_0^T \langle x(t) \rangle \, dt. \tag{3.2}$$

The network time-dependent firing rate is defined as

$$r(t; \Delta t) = \frac{1}{N \Delta t} \sum_{j=1}^N \int_t^{t+\Delta t} x_j(t') dt', \tag{3.3}$$

23

where we fix the time window $\Delta t = 1$ ms.

For the calculation of spectral measures, we define the Fourier transform by

$$\tilde{x}(f) \;=\; \int_0^T dt e^{2\pi i f t} x(t), \tag{3.4}$$

where T is our time window and is set in our simulations to a standard value of $T = 2$ s if not mentioned otherwise. In the simulations, we generally neglect a transient period of 1 s before extracting the statistics over the next T seconds (we will indicate the value of T).

We will use two power spectra: the spike train power spectrum and the voltage time series power spectrum. The first one is defined for each neuron j as

$$S_{xx,j}(f) = \frac{\langle \tilde{x}_j \tilde{x}_j^* \rangle}{T}, \tag{3.5}$$

where $\tilde{x}_j^*$ is the complex conjugate of $\tilde{x}_j$. Note that $\langle . \rangle$ represents an ensemble average. The power spectrum of the voltage time series is obtained in the same way, replacing in Eq.(3.5) the spike train $x_j(t)$ by the voltage time series $v_j(t)$. In the case of the spike train power spectrum, the units are 1/s whereas the units of the voltage spectrum are $\mathrm{mV}^2/\mathrm{Hz}$.

An average over a subset that includes K neurons renders the average power spectrum:

$$\bar{S} = \frac{1}{K} \sum_{j \in K} S_{xx,j}(f). \tag{3.6}$$

We note that the spike-train power spectrum saturates for infinite frequency at the firing rate, $\lim_{f \to \infty} \bar{S}(f) = \nu$ (Lindner, 2009; Grün & Rotter, 2010). Besides, two important statistical measures can be extracted from the spike-train power spectrum. The first is the Fano factor FF which is defined as the variance of the spike count $N = \int_0^T dt\, x(t)$ over its mean, an expression that can be related to the power spectrum at zero frequency:

$$FF = \frac{\langle \Delta N^2 \rangle}{\langle N \rangle} = \frac{S_{xx}(f \to 0)}{\nu}. \tag{3.7}$$

The second statistical measure is the correlation time τ_c. Following (Neiman, Yakusheva, & Russell, 2007) and (Wieland, Bernardi, Schwalger, & Lindner, 2015), we consider the spike train's correlation function $c(\tau) = \langle x(t)x(t+\tau) \rangle -$

$\langle x(t) \rangle \langle x(t+\tau) \rangle$ (note that here $\langle . \rangle$ indicates a time average) and its continuous part $\hat{c}(\tau) = c(\tau) - \nu\delta(\tau)$ to define the correlation time as an integral over the squared and normalized $\hat{c}(\tau)$

$$\tau_c = \int\limits_{-\infty}^{+\infty} d\tau \left[\frac{\hat{c}(\tau)}{\hat{c}(0)} \right]^2 = \int\limits_{-\infty}^{+\infty} df \frac{(S_{xx}(f) - \nu)^2}{\nu^4}, \tag{3.8}$$

an integral which in turn can be related to an integral over the power spectrum via the Parseval theorem[1] on the right side.

We quantify the degree of oscillatory activity in the network via the spectral entropy H_s (Blanco, Garay, & Coulombie, 2013; Sahasranamam, Vlachos, Aertsen, & Kumar, 2016). Spectral entropy is computed from the power spectrum of time-dependent firing rate in Eq.(3.3) as

$$H_s = \frac{-\sum_k S_{rr}(f_k) \log S_{rr}(f_k)}{\log N_b}, \tag{3.9}$$

where N_b is the number of frequency bins and $S_{rr}(f_k)$ is the value of the normalized (i.e. $\sum_k S_{rr}(f_k) = 1$) power spectrum of the network time-dependent firing rate $r(t; \Delta t)$ at the kth bin. In our simulations we use N_b=1000. In the case of broadband noise activity, the power spectrum of the network firing rate is flat and the spectral entropy is maximal: $H_s = 1$. If, in contrast, all power is concentrated at one frequency, a case of single-frequency network oscillations, the spectral entropy vanishes: $H_s = 0$.

To quantify the degree of synchrony in the network, we use the phase locking value (PLV) which is a standard measure to evaluate phase synchronization (Lachaux, Rodriguez, Martinerie, & Varela, 1999; Celka, 2007; Rosenblum, Pikovsky, Kurths, Schäfer, & Tass, 2001; Aydore, Pantazis, & Leahy, 2013; Lowet, Roberts, Bonizzi, Karel, & De Weerd, 2016). Unless otherwise stated, the time average used to calculate the PLV is always taken over a simulation interval of $T = 2000$ ms. We define the PLV as the average over K neuron pairs and T sample time points:

$$PLV = \frac{1}{K} \sum_{\{ij\}}^{K} \left| \sum_{t}^{T} e^{i\Delta\Phi_{xy}(t)} \right|, \tag{3.10}$$

---

[1] The Parseval theorem states that the integral of the square of a function is related to the integral of the square of the same function Fourier transformed.

where $\Delta\Phi_{xy}(t)$ are the phase differences $\rho_x\Phi_x(t) - \rho_y\Phi_y(t)$ from two randomly chosen spike-trains $(x(t), y(t))$ that are obtained using the Hilbert transform. The values ρ_x and ρ_y define the frequency ratio and, expecting similar firing rates, we set $\rho_x = \rho_y = 1$. The PLV is bounded between 0 (asynchrony) and 1 (synchrony).

3.2   Numerical integration and computational platform

Numerical integration of the differential equations was performed by different numerical methods depending on the network and neurons involved. In Chapter 4, we used the 4th order Runge-Kutta method with step size $h = 0.01$ ms. In Chapter 5, where there are equations involving noise, the differential equations were integrated with the Heun algorithm (Mannella, 2002) with step size $h = 0.01$ ms. In Chapters 6 and 7, we used the Euler method with step size $h = 0.1$ ms. We used C++ and Python to write the computational codes, and Matlab and XMgrace to visualize and analyze the results. In addition, different Python packages were used to analyze and visualize results such as Brian 2, SciPy, NumPy, Matplotlib, Pandas, and NetworkX. We employ parallel computing techniques when necessary to speed up simulations.

Simulations were performed with the use of the NeuroMat cluster (FAPESP project 2013/07699-0) which is composed of 4 computational nodes each one with 2 CPUs Xeon E5-2650 v3 (20 physical cores with addition of 20 virtual cores), 128 GB RAM, 2 TB HDD, and 3.2 TB HDD shared.

EMERGENCE OF OSCILLATORY ACTIVITY IN A SELF-SUSTAINED ENVIRONMENT

4.1 Introduction

This chapter focus on the description of oscillatory self-sustained activity (SSA). This regime corresponds to rhythmic fluctuations (see Sect. 2.3). Our goal is to obtain a general understanding of how oscillatory dynamics emerge in a self-sustained setup, as well as understand how SSA is influenced by a hierarchical and modular topology and by a mixture of neuronal components.

Self-sustained activity is a spontaneous and persistent activity observed in many situations in the brain. Regimes of SSA may be found ranging from asynchronous to synchronous activity and this depends on different factors. For instance, during anesthesia or slow-wave sleep SSA is usually observed in an oscillatory regime (Steriade, Nunez, & Amzica, 1993; Contreras & Steriade, 1995). During wakefulness, SSA is observed in an asynchronous regime with neurons firing irregularly. Recordings of SSA include *in vivo* cortical slab preparations (Timofeev, Grenier, Bazhenov, Sejnowski, & Steriade, 2000) and *in vitro* slices (Plenz & Aertsen, 1996; Sanchez-Vives & McCormick, 2000; Shu, Hasenstaub, & McCormick, 2003).

We will start by describing the experimental methodology necessary to obtain the SSA. We proceed by investigating different characteristics of SSA that are obtained by varying the parameters. We also relate the dynamics of the single-neurons during the SSA to the dynamics of the global system, i.e.

the entire network. Using a phenomenological approach, we explain when the transient dynamics will start and when it will end as well as why modularity favors sustainment of activity.

4.2 Methods

In this Chapter, we will be working with the Izhikevich neuron model and different electrophysiological classes.

Every connection in the network is created by a conductance-based synaptic model. Upon a synaptic event coming from a presynaptic neuron, the conductance of the postsynaptic j neuron $(G_j^{\text{ex/in}}(t))$ is incremented by a $g_{\text{ex/in}}$ amount which is followed by an exponential decay with time constant $\tau_{\text{ex/in}}$. This behavior is described by

$$\frac{dG_j^{\text{ex/in}}(t)}{dt} = -\frac{G_j^{\text{ex/in}}(t)}{\tau_{\text{ex/in}}} + g_{\text{ex/in}} \sum_i \delta(t - t_i), \tag{4.1}$$

where we separate among excitatory/inhibitory conductances.

In the neuron, synaptic current is disturbed as it dependents on $G_j^{\text{ex/in}}(t)$:

$$I_{syn,j}(t) = G_j^{\text{ex}}(t) \left(E_{\text{ex}} - v_j\right) + G_j^{\text{in}}(t) \left(E_{\text{in}} - v_j\right), \tag{4.2}$$

where $E_{\text{ex/in}}$ represent the reversal potentials and characterize excitatory/inhibitory effects.

We adopt the parameters $E_{\text{ex}} = 0$ mV, $E_{\text{in}} = -80$ mV, $\tau_{\text{ex}} = 5$ ms and $\tau_{\text{in}} = 6$ ms (Dayan & Abbott, 2001; Izhikevich & Edelman, 2008).

We will be exploring networks containing $N = 2^{10}$ neurons in different hierarchical levels. We use powers of 2 due to ease the use of the hierarchical and modular network construction algorithm. For every network, we tried different neuronal compositions: the excitatory:inhibitory ratio is always 4:1. From the excitatory neurons, RS is always present and a certain percentage (which will always be indicated) will be either CH or IB. The inhibitory neurons may be of the FS or LTS type. A summary of the models used in this Chapter is identified in the Table 4.1.

Models considered in this part	
Populations	Excitatory (mixture of RS,CH, or IB) and inhibitory (FS or LTS)
Neuron models	Izhikevich
Synapse models	Conductance-based, event-driven with exponential decaying
Network	Random and hierarchical and modular
Network size	$N = 2^{10}$, $N_{ex} = (4/5)N$
Connectivity	Random with $\epsilon = 0.01$ and rewiring $R = 0.9$
Initial conditions	Vary according to: time of stimulation t_{stim}, proportion of stimulated neuron P_{stim}, and amplitude of stimulation I_{stim}
External input	Absent

Table 4.1: *Summary of models used in Chapter 4.*

As we are interested in evaluating SSA, we define a measure to extract the sustainment of activity in a network. Let's start defining that for a given neuron i the time of the last spike in its spike-train as

$$t_i^{\text{last}} = \max\{t_i\}. \tag{4.3}$$

For the network lifetime (δ) we take the maximum t_i^{last} from the set of neurons in the network

$$\delta = \max\{t_i^{\text{last}} : i = 1, \ldots, N\}. \tag{4.4}$$

4.2.1 Ensemble of initial conditions

After having constructed the network and populated the nodes with neurons, the dynamics should be initiated somehow. If no initial stimulation is applied to the network we would not observe any activity and the voltage series of all neurons would not leave a fixed point at the resting state. Together with that, the initial investigation has a lot of uncertainties about the structure of the network's phase space where the dynamics should oscillate.

Given that the number of equations involved in the network is high enough to make it difficult a complete analytical analysis without simplifications, we base our

study on statistical descriptions. Supported by distributions in a sufficiently large ensemble of initial conditions that change in their preparation, we will investigate dynamical behavior of the network.

For the preparation of ensembles we do not choose initial conditions at random in the high-dimensional phase space of the network: a representative sampling would be hardly available computationally. Instead, we start at the state of rest and vary in duration of stimulation t_{stim}, intensity of initial stimulation I_{stim}, and proportion of stimulated neurons in the network P_{stim}. A representation of this method is displayed in Fig. 4.1.
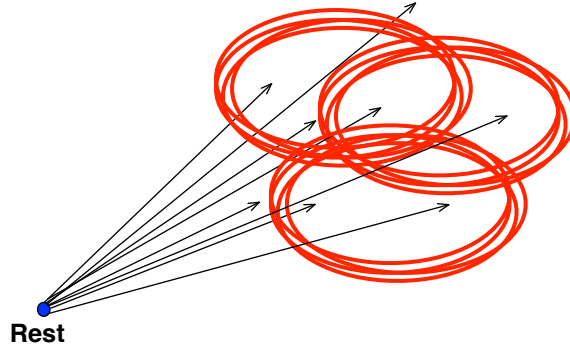
Figure 4.1: *Representation of the ensemble of initial conditions.* *The idea is to draw a set of different initial conditions that will lead the system to the physiological oscillatory state and leave its dynamics evolving freely. We vary t_{stim}, I_{stim}, and P_{stim}.*

4.3 Results

4.3.1 Exploring the space of possibilities

We would like to start exploring our system by examining the lifetime dependencies in a diagram spanned by g_{in} (abscissas axis) and g_{ex} (ordinates axis). To build such diagram we discretized on a 50×50 grid with $\Delta g_{\text{ex}} = 0.002$ and $\Delta g_{\text{in}} = 0.02$, where every point is simulated with 10 different initial conditions. In Fig. 4.2 we present these results for an exemplary network with level $H = 1$ and populated by 20% of the excitatory neurons being of CH type and the inhibitory neurons of the LTS type.
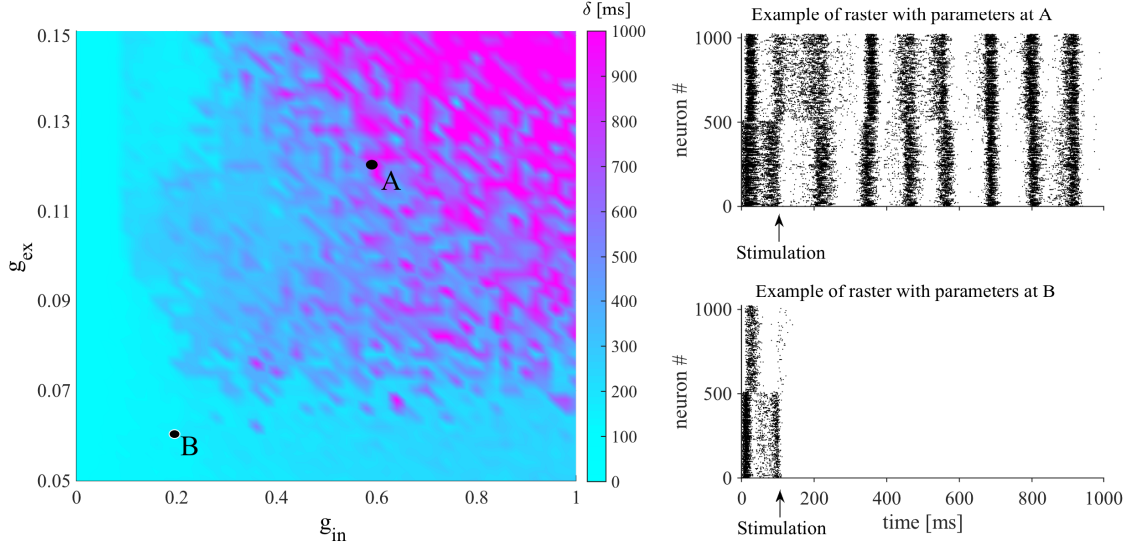
Figure 4.2: *Values of δ on the parameter plane of synaptic strengths.*
Simulations were carried out in a network with hierarchical level H = 1, 20% of excitatory neurons of the CH type, inhibitory neurons of the LTS type. Left: Parameter plane $g_{ex}-g_{in}$ discretized on a 50×50 grid with $\Delta g_{ex} = 0.002$ and $\Delta g_{in} = 0.02$. Every point is simulated 10 times with parameters $P_{stim} = 1/2$, $10 \leq I_{stim} < 20$ and $t_{stim} = 100$ ms. Points are interpolated. Right: Raster plots taken at the (g_{ex}, g_{in}) points indicated in the left plot.

Results presented in the diagram in Fig. 4.2 are similar to other combinations of electrophysiological classes and hierarchical levels (differences will be discussed below). For all combinations of (g_{ex}, g_{in}), there was no case of non-oscillatory SSA recorded and, in all cases where SSA was observed, it was oscillatory. The examples of rasters in the right of Fig. 4.2 demonstrate the latter effect, it is also possible to observe a small difference between the modules. Regarding the diagram, its major characteristic is the fragmented shape located in the upper right corner, possibly due to the small number of initial conditions studied so far.

A key feature observed is that there is some sensitivity to initial conditions, i.e. lifetime of SSA has some probability and, in addition, this probability grows as the strengths (g_{ex}, g_{in}) are increased. High sensitivity to initial conditions is a feature of chaos. However, in this area of the diagram (g_{ex}, g_{in}) chaos is not an attractor due to the fact that after some short period the activity ceases. Systems in which, for a given set of initial conditions, chaos is present for a short period followed by an abrupt cessation of the chaotic dynamics are known as systems exhibiting transient chaos. (Lai & Tél, 2011).

A second property of transient chaos is the existence of an escape rate κ, i.e. in a sufficiently large ensemble of initial conditions, the lifetimes δ should follow an exponential distribution where the number $n(T)$ of systems with lifetime larger than T approximately obeys

$$n(T) \sim e^{-\kappa T}, \tag{4.5}$$

where κ is the escape rate. For an ensemble of transiently chaotic trajectories, the value of $\tau_{\text{dec}} = \kappa^{-1}$ defines the characteristic time of decay of SSA in ms.

To evaluate if an escape rate is indeed a property of our system, we took different points $(g_{\text{ex}}, g_{\text{in}})$ from the diagram in Fig. 4.2 and ran a sufficiently large number of initial conditions with varying P_{stim}, I_{stim}, and t_{stim}: $P_{\text{stim}} = 1, 1/2, 1/8,$ $1/16$, $I_{\text{stim}} = 8,9,...,20$, and $t_{\text{stim}} = 50,52,...,300$ ms, totalizing 6552 different initial conditions. In Fig. 4.3 we present these results.
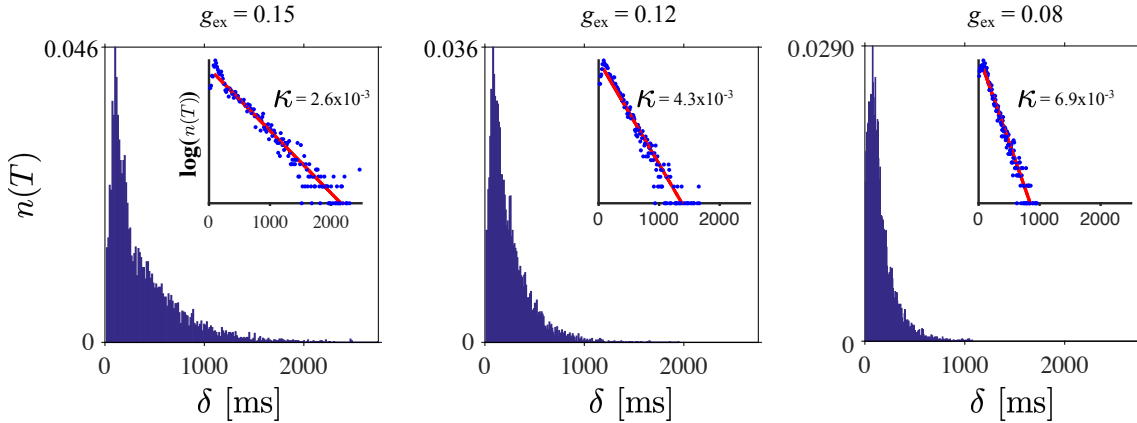
Figure 4.3: *Distributions of δ for varying initial conditions. Inhibitory conductances fixed at $g_{\text{in}} = 0.7$, excitatory ones have their values displayed atop. Other parameters are as in Fig. 4.2. Each panel contains normalized distributions of $n(T)$. Insets: ordinate values on the logarithmic scale for the same histograms, straight lines are fitted exponential dependencies, values of κ are displayed in each inset.*

Different properties can be extracted from Fig. 4.3. In the first place, the escape rate is present and has some dependency on the synaptic coupling. For a fixed g_{in}, as g_{ex} is increased κ is decreased, i.e. the probability of having long-living SSA increases. Despite this example, we have also verified that the same effect happens with varying g_{in} for a fixed g_{ex}. The fact that a distribution is behind every $(g_{\text{ex}}, g_{\text{in}})$ combination makes it difficult to delineate a border among SSA and non-SSA regimes, that is why the diagram in Fig. 4.2 has a fragmented shape. As

we did, the best option seems to be an evaluation of the κ values. In addition, in absence of inhibition ($g_{\mathrm{in}} = 0$) or very little excitation ($g_{\mathrm{ex}} = 0.05$) it was not observed any case of long-living SSA in the tested initial conditions.

The effects observed: sensitive dependence of individual trajectories on initial conditions, and exponential distribution of lifetimes in the large ensemble of trajectories are indeed two characteristic attributes of the so-called transient chaos (Lai & Tél, 2011), and, based on this, we conjecture that the oscillatory self-sustained activity in the network is transiently chaotic.

Regarding the different hierarchical levels and combinations of neuronal classes, as the general behavior depicted in the diagram of Fig. 4.2 is rather similar, with small differences, we will summarize below the observations:

- Increase of level H increases the magenta region in the diagram where long-living SSA is observed.

- If the second excitatory population (despite the RS group) is of the CH type, there is an enlargement of the ($g_{\mathrm{ex}}, g_{\mathrm{in}}$) area where long-living SSA is observed.

- If the second excitatory population is of the IB type, there is no prominent difference in the ($g_{\mathrm{ex}}, g_{\mathrm{in}}$) diagram.

- Changing inhibitory neurons FS to LTS increases in great proportion the long-living SSA region.

An extended investigation is presented in Table 4.2 where values of κ were obtained for selected combinations of ($g_{\mathrm{ex}}, g_{\mathrm{in}}$) chosen to be located in the upper right corner in the diagram of Fig. 4.2, different mixtures of neurons, and H (see legend). The results of the table show that it is not only the region of long-living SSA that is enlarging but each ($g_{\mathrm{ex}}, g_{\mathrm{in}}$) point is becoming more likely to exhibit longer SSA when CH proportion or H is increased. Moreover, the effect of changing LTS to FS neurons is also easily observed in Table 4.2.

Regions in the parameter space where the combination ($g_{\mathrm{ex}}, g_{\mathrm{in}}$) is increased beyond the values displayed here correspond to non-realistic firing rates, above 70 Hz, in comparison with firing rates found in cortical neurons (Softky & Koch, 1993; Maimon & Assad, 2009; Haider, Häusser, & Carandini, 2013). While looking

		LTS				FS			
		(g_{ex}, g_{in})				(g_{ex}, g_{in})			
	H	(0.12,0.7)	(0.15,0.7)	(0.12,1)	(0.15,1)	(0.12,0.7)	(0.15,0.7)	(0.12,1)	(0.15,1)
RS	0	0.0053	0.0083	0.0022	0.0048	0.0164	0.0181	0.0140	0.0138
	1	0.0029	0.0043	0.0014	0.0019	0.0111	0.0138	0.0080	0.0097
	2	0.0021	0.0017	0.0011	0.0011	0.0045	0.0028	0.0037	0.0028
20%CH	0	0.0075	0.0031	0.0049	0.0022	0.0134	0.0082	0.0095	0.0084
	1	0.0037	0.0022	0.0023	0.0017	0.0109	0.0088	0.0094	0.0081
	2	0.0017	0.0008	0.0013	0.0007	0.0045	0.0028	0.0034	0.0025
40%CH	0	0.0009	—	0.0008	0.0006	0.0062	0.0016	0.0056	0.0021
	1	0.0009	—	0.0008	0.0005	0.0079	0.0045	0.0071	0.0046
	2	0.0002	0.0008	0.0006	0.0007	0.0008	0.0005	0.0007	0.0005
20%IB	0	0.0092	0.0091	0.0078	0.0096	0.0198	0.0210	0.0176	0.0203
	1	0.0073	0.0078	0.0041	0.0058	0.0149	0.0183	0.0129	0.0144
	2	0.0036	0.0022	0.0023	0.0017	0.0055	0.0037	0.0043	0.0036
40%IB	0	0.0111	0.0081	0.0085	0.0076	0.0201	0.0199	0.0214	0.0186
	1	0.0112	0.0094	0.0073	0.0082	0.0176	0.0194	0.0160	0.0159
	2	0.0050	0.0024	0.0033	0.0019	0.0065	0.0041	0.0048	0.0038

Table 4.2: *Values of κ computed by simulating 10^6 different initial conditions and varying the neuronal composition, hierarchical level, and (g_{ex}, g_{in}) combination. The indication '—' means that SSA was not reported. The network contains 4:1 excitatory/inhibitory neurons where the inhibitory are either LTS or FS. The excitatory are always RS and some percentage of CH or IB (0%,20%,40%). These mixtures of neurons are indicated in the columns and rows of the table.*

at individual traces, it was possible to identify that the non-realistic firing rates were mostly due to CH and LTS neurons which could achieve frequencies around 600 Hz. In this regard, we consider not necessary to study these regions in this work and that is why they were eliminated.

4.3.2 The inner dynamics

Here and in the next sections of this chapter, we study only networks with fixed g_{ex}=0.15 and g_{in}=1 parameters so that we guarantee high probability of
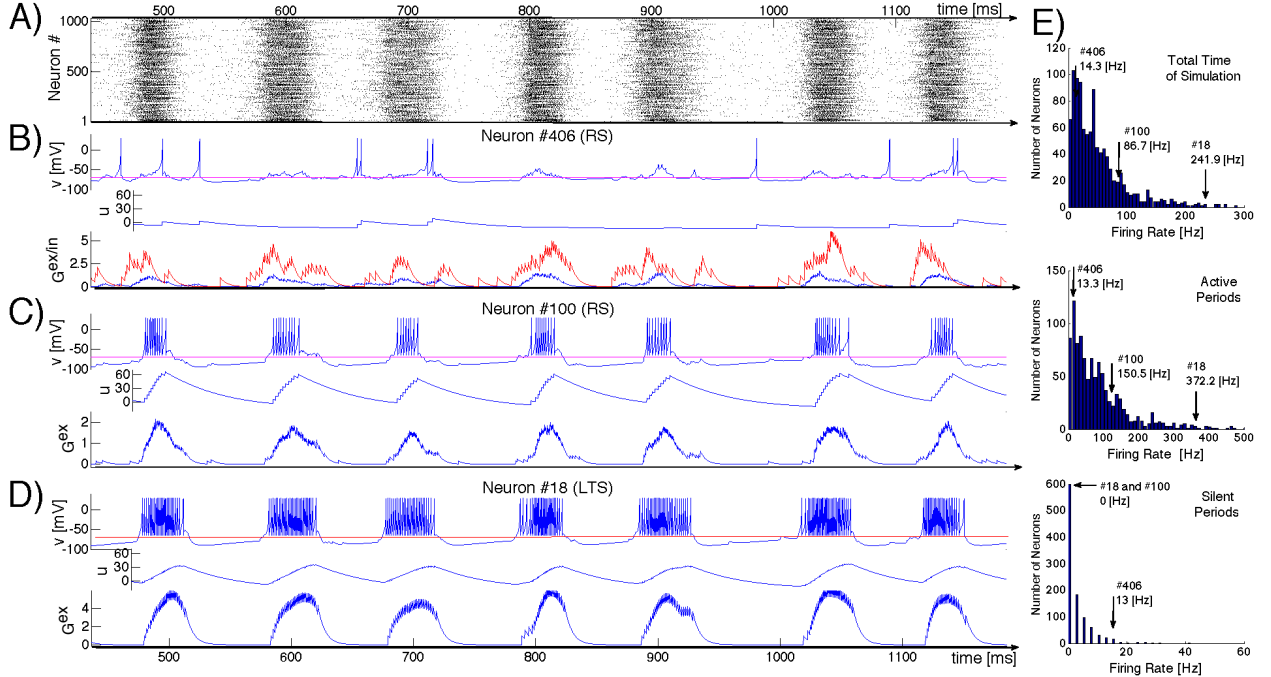
Figure 4.4: *SSA state in a network of hierarchical level H=0 with LTS inhibitory neurons and a mixture of excitatory neurons: 80%RS and 20%CH. A) Raster plot: spiking activity of the network within 700 ms. B),C),D) Evolution of variables for three exemplary neurons. Top panels: voltage v, middle panels: recovery variable u, bottom panels: synaptic conductances G^{ex} (in blue) and G^{in} (in red). Neurons # 406 and # 100 are excitatory RS. Neuron # 18 is inhibitory LTS. E) Distributions of mean firing rates for all neurons in the network: for the whole duration of the SSA state (upper histogram), for the epochs of high network activity (middle histogram), and for the epochs of low network activity (bottom histogram). Positions of three neurons shown in B),C) and D) in these distributions are indicated by arrows.*

long-living SSA appearance. We shall look at the inner dynamics of SSA from the point of view of its individual participants. Fig. 4.4 presents a typical oscillatory SSA state in the network. Its top panel (Fig. 4.4A) shows the raster plot of the system, and the panels below show time series representing the dynamical states of three sample units: two excitatory neurons and one inhibitory neuron (respectively, Fig. 4.4B, Fig. 4.4C, and Fig. 4.4D) aligned with the raster plot. For each of the neurons we plot the membrane potential v, the membrane recovery variable u as well as the synaptic conductances $G^{ex/in}$.

Although both excitatory neurons belong to the same RS type, their behavior is remarkably different. Neuron #406 exhibits irregular spiking at low firing rate (~ 14Hz), seemingly uncorrelated with epochs of high global network activity. This

low frequency can be understood, taken into account the dominating presynaptic inhibitory input: the spikes always occur when the excitatory conductance exceeds the inhibitory (see $G^{\text{ex/in}}$ in Fig. 4.4B, where the inhibitory input is represented in red and the excitatory in blue). The time series of the membrane potential $v(t)$ confirms that during the epochs of high global network activity the neuron is developing an "up" state with depolarized membrane potential (e.g. the range between 580ms and 620ms in Fig. 4.4). During such epochs, global activity enhances both inhibitory and excitatory synaptic conductances, but the former is larger and, hence, for most of the time the spiking is hampered. Fig. 4.4E shows that this neuron shares a typical firing rate of the whole ensemble and lies at the peak of the firing rate distribution: the majority of the RS neurons behaves similarly.

In contrast, neuron #100 exhibits bursting-like behavior, strongly correlated with global network activity. Its firing rate is ∼86Hz, if estimated over the whole length of simulation; the actual firing rate, restricted to epochs of high global network activity, reaches 150Hz, while no spike occurs during the inactive epochs. This unit represents a more exotic subclass of RS neurons: they possess unusually high firing rates and, in fact, behave like CH neurons. Notably, within the distribution of the firing rates, neuron #100 is not placed at the very end, since that distribution includes also "genuine" CH neurons that naturally tend to have higher spiking frequencies. In the same network, this exotic behavior was also observed for LTS neurons (cf. Fig. 4.4D); in the corresponding architectures it was found for FS and IB neurons as well.

The RS neuron #100 is, in a sense, an extreme case: it does not receive any inhibitory presynaptic input from the network and, as shown in Fig. 4.4, always behaves like a CH neuron. There are, however, numerous RS neurons that receive inhibitory input but nevertheless tend to have higher firing frequencies than the typical neuron #406: they can exhibit bursting-like behavior within one epoch of high global network activity, while producing few spikes within another epoch or even completely skipping it (not shown here). Similar behavior of RS neurons naturally embedded in a network was observed empirically in (Kang & Kayano, 1994; Steriade, 2001) where *"work in cortical slices also showed that regular spiking neurons may develop their type of discharges into those of fast-rhythmic-bursting*

neurons by repeated application of depolarizing current pulses." Chattering behavior has also been reported for inhibitory neurons in cortical slices (Steriade, Timofeev, Dürmüller, & Grenier, 1998; Steriade, 2004), contradicting the common opinion that chattering-like spiking patterns occur only in pyramidal neurons (Gray & McCormick, 1996).

A closer comparison shows that the spiking patterns of the inhibitory and the excitatory neurons, albeit qualitatively similar, bear apparent distinctions: as a rule, an epoch of high activity for the LTS neuron in the panel D) starts earlier, breaks up later and is "denser" (contains more spikes) than for its RS counterpart from the panel C). As their name tells, the LTS neurons need less presynaptic excitatory input in order to spike. Hence, the lower excitatory input generated by their environments at the beginning and at the end of active epochs suffices to sustain their firing.

4.3.3 The global dynamics: a phenomenological approach

Ensembles of trajectories created with the help of the above procedure where initial conditions are chosen with different P_{stim}, t_{stim}, and I_{stim} yield global characteristics of dynamics but say only a little about the local structure of the phase space in the neighborhood of the chaotic set. To resolve this structure, we create an auxiliary ensemble in the following way.

1. At fixed parameter values we take from the ensemble a single orbit with SSA lifetime larger than 2000 ms (over 20 subsequent epochs of high global activity); this ensures that the orbit stays close to the chaotic set sufficiently long. Below, we call this orbit a *reference trajectory* $\mathcal{R}(t)$.

2. On $\mathcal{R}(t)$, we choose fifty equidistant positions $\mathcal{P}_k$, $k = 1, .., 50$ at the time values

$$\mathcal{P}_k = \mathcal{R}(t_0 + k\,\Delta t), \tag{4.6}$$

with t_0=370ms and Δt=7ms. The offset ensures that by the time t_0 the reference trajectory has reached the region of the chaotic set (this has been established visually from the irregular shape of oscillations). The choice of Δt enables us to have within each epoch of global activity and subsequent inactivity $\approx$15 positions $\mathcal{P}_k$: a reasonably dense covering of $\mathcal{R}(t)$.

3. In each position the system is perturbed six hundred times, by stimulating for 3 ms each eighth neuron with the external input current $I_{\text{ext}}=10$. For every perturbation the 128 stimulated neurons are chosen at random. The stimulation interval is much shorter than the characteristic time of the system ≈ 100ms, therefore within it the perturbed orbits stay sufficiently close to the reference trajectory.

4. After the perturbation the system is left to evolve freely, and the resulting lifetime δ is recorded.

This local procedure creates 50 sets of "secondary" initial conditions, each one with 600 points close to one of $\mathcal{P}_k$. Since, by construction, all these sets lie at different locations along the reference trajectory, they provide information about local dynamics near the chaotic state, and, in particular, on the rates of escape from it.

In Fig. 4.5 **A** we show the raster plot of the reference trajectory $\mathcal{R}(t)$ with the perturbation positions $\mathcal{P}_k$ in blue lines where the local perturbations were generated at each $(t_0 + k\,\Delta t)$. In Fig. 4.5 **B** we present the projection of $\mathcal{R}(t)$ and $\mathcal{P}_k$ on the plane of two artificial collective coordinates $\langle v \rangle$ and $\langle u \rangle$: instantaneous mean values of, respectively, voltage and membrane recovery variable over all 2^{10} neurons.

In Fig. 4.5 **C1**–**C4** we present lifetime distributions δ for some of the perturbation positions $\mathcal{P}_k$. Unlike Fig. 4.3, the distributions are non-monotonic and exhibit local maxima (peaks), which means that trajectories leave the chaotic set in specific places (an effect not observed when choosing initial conditions as at the beginning of this Chapter). Furthermore, if vicinities of all segments of the reference trajectory would offer the same possibility of immediate escape to the state of rest, the lifetimes δ of trajectories originating from different local sets would be comparable. Our numerical data unambiguously state that this is not the case. Rather, they indicate that escape occurs only from a relatively small local region responsible for the instability, to which we shall refer as a "hole". In Fig. 4.5 **B** the approximate location of this region is indicated in gray. Each passage of the ensemble of trajectories past the "hole" results in the loss of some approximately constant proportion of the ensemble; these orbits leave the ensemble and soon land
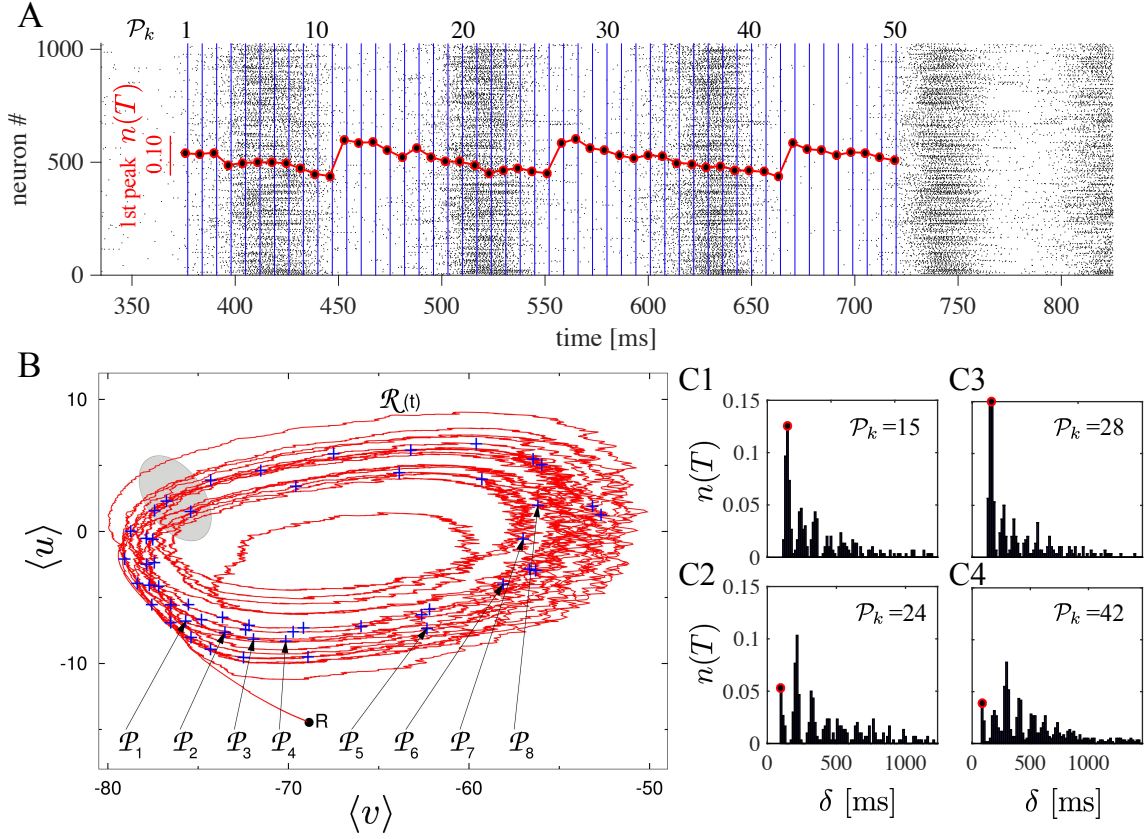
Figure 4.5: ***Probing the neighborhood of the chaotic set.*** *Panel **A** contains the raster plot of the spiking activity in the network during the motion on the reference trajectory. Blue lines: positions of perturbation along the reference trajectory $\mathcal{R}(t)$. $n(t)$ values of first peaks in all perturbation positions $\mathcal{P}_k$ are represented inside the raster plot as a red curve with black circles. Panel **B** shows the reference trajectory $\mathcal{R}(t)$ on the phase plane of averaged values of voltage and membrane recovery variable. Pluses: positions of perturbations $\mathcal{P}_k$ along $\mathcal{R}(t)$. Gray region: approximate location of the "hole" (see explanations in the text). R: state of rest. Panels **C1**−**C4** are exemplary distributions of lifetimes at some perturbation positions $\mathcal{P}_k$.*

at the state of rest. Ensembles of trajectories that start at local sets situated near the entrance to the "hole" tend to have shorter average lifetimes than ensembles that originate from local sets situated far from it. This latter statement can be well observed in the red curved graphically represented together with the raster plot in Fig. 4.5 **A**. Following the raster plot, one can see passages through the "hole" as the first peak of $n(T)$ in every position of $\mathcal{P}_k$ where $n(T)$ suffers an apparent discontinuity and is shifted upwards.

4.3.4   Hierarchy

In Sect. 4.3.1 we commented that our observations show that lifetime δ increases if the hierarchical and modular level H is increased. Given the explanations of the "hole" in Sect. 4.3.3, here we explain this lifetime increase with H in terms of the "hole".

Each module can be seen as a random network, sparsely connected to other modules. Depending on its neuronal composition, each module can sustain activity for a certain time, whereas sparse excitatory coupling enables the modules to activate each other in alternating succession. Hence, there is a probability that each module, before decaying itself to rest, (re)activates a neighboring one. This viewpoint conforms with the above phenomenological analysis when we assume that every module possesses its own "hole". If a module falls into its "hole" while a neighboring module is still active, there is a chance that the former will be reactivated by the latter. Hence, for activity to die out, the modules should enter their "holes" approximately simultaneously; asynchrony between the modules would sustain the activity.

This effect is illustrated by the sample raster plot in Fig. 4.6 for a network with four modules ($H = 2$). The blue lines indicate beginnings of epochs of high network activity *within* a module, and the red lines denote the respective ends of these epochs. By the time ≈ 300 ms the modules 3 and 4 stop firing; slightly later, the firing in them is (non-simultaneously) resumed, apparently under the influence of the still active module 1. Observing further evolution of the network we see that the SSA in the modules 3 and 4 ceases completely at $t \approx 500$ ms for more than 100 ms, before being reactivated by signals from modules 1 and 2.

The chances of reactivation depend on the number of excitatory connections from the active module to the inactive one. While constructing the network (cf. Sect. 2), we can make a distinction between the hierarchically close and hierarchically distant modules: in the considered example, the excitatory connectivity between the close modules is nearly twice as high as between the distant ones. Hence, for hierarchically close modules the probability of mutual reactivation in the case when one of them falls into the "hole" is distinctly higher than for the modules that are hierarchically distant.
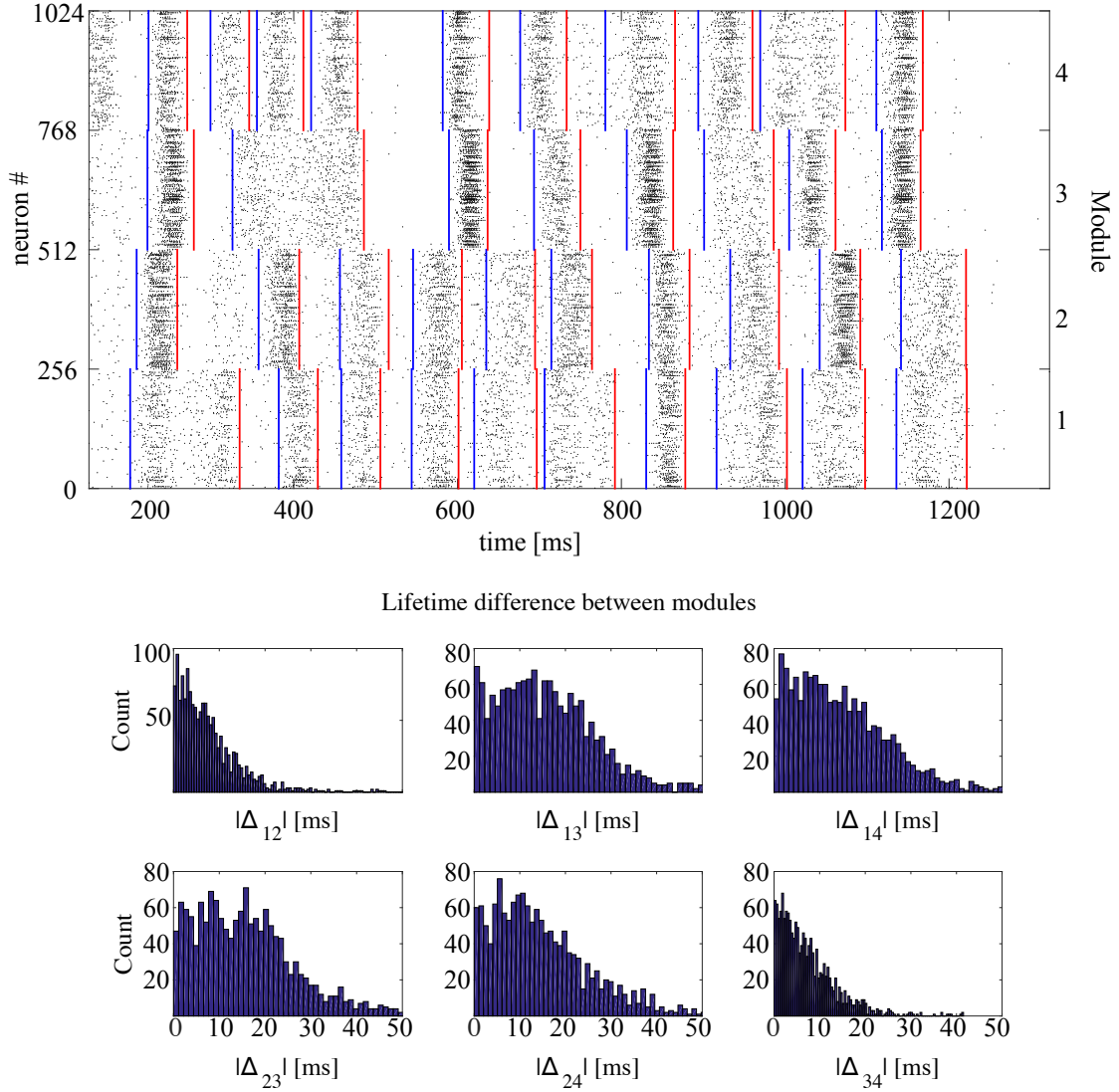
Figure 4.6: *Synchronization and temporal shifts between modules.* *The network of modularity level H=2, consists of LTS inhibitory neurons and RS excitatory neurons. A) Sample raster plot of activity in a network. The blue and red lines indicate, respectively, the beginning and end of epochs of high network activity.*
B) Histograms of the difference Δ_{ij} between the ends of the last active epoch in the modules i and j   (i,j=1,2,3,4) from 4×10^3 trials

This conjecture is corroborated by Fig. 4.6 that represents the histograms of temporal differences Δ_{ij} between the endpoints of *the last* active epochs, respectively, in modules i and j ($i,j=1,2,3,4$). The histograms were computed for all pairs of modules over 2^{12} different initial conditions.

Conversely, if we compare the time differences between the moments when the

modules enter their "holes" in the very last activity epoch, the probability to observe a noticeable time difference is higher for modules that are hierarchically distant. This is confirmed by the distributions of Δ_{12} and Δ_{34} from Fig. 4.6 (bottom).

Summarizing, the explained mechanism of stabilization of SSA is twofold:
1) through excitatory intermodular connections, the modules are able to mutually reactivate each other, so that cessation of activity in one of them can be reversed due to the influence of the neighboring modules.
2) due to the sparseness of connections between the modules, the coupling between them is too weak to induce the full synchrony. Therefore, the events (onset and decay of the active epoch) in different modules do not coincide in time. As a consequence, when activity decays in one of the modules, it is often still present in one or several of the other modules, and there are good chances that the neighbors will awake the dormant module to a new activity.

In this situation, an increase of the overall connectivity would enhance the first aspect but definitely lower the second one. Higher *intermodular* connectivity can impose synchrony which will be harmful in the long run: when activity in all modules synchronously halts, nobody is left to initiate the revival.

4.4   Discussion

In this Chapter, we studied small networks of 2^{10} neurons. The networks were populated by different electrophysiological classes in which 20% of the neurons were always inhibitory and 80% excitatory. We varied mixtures of neurons and the level H of the hierarchical and modular architecture.

The results of simulations show that after the end of stimulation the network displays a series (from several to several hundreds) of alternating epochs of global activity and inactivity that, on the level of separate neurons, do not reproduce each other and seem completely irregular. The series is followed by abrupt relaxation to the state of rest: in fact, activity is *transiently self-sustained*. Dynamics was aperiodic; the interval between the starting points of consecutive epochs of activity was typically in the range from 100 to 110 ms.

Remarkably, the entire duration of the process, as well as the number of

the observed epochs of high activity, were highly sensitive to initial conditions: a minor variation in e.g. the length or strength of the initial stimulation often replaced a process with only a few such epochs by a process with several dozens of alternating onsets and breakdowns of activity, or vice versa. There seemed to be no precursor of the forthcoming termination of SSA: the last epochs of global activity qualitatively differed from all preceding ones neither in amplitude, nor in duration. We conjectured that the observed oscillatory SSA states were transiently chaotic.

In fact, during the active phase, projections of trajectories in the phase space of the system remind typical examples of deterministic chaos. The trajectory in Fig. 4.5 **B** is reminiscent e.g. of the Rössler attractor (Rössler, 1976). However, conventional indicators of chaos like Lyapunov exponents and fractal dimensions of the chaotic set are hardly applicable here due, first, to the high order (> 3000 variables) of the dynamical system and, second, to the finite lifetime of individual trajectories, which in many cases is too short to gather sufficient statistics. Hence, we were forced to use indirect evidence for our conclusions on the character of dynamics: our judgments were based on distributions of the activity lifetimes in the network. We interpret the lifetime as the length of the time interval between the end of stimulation and the firing of the very last spike anywhere in the network. We characterized the lifetime decay by an exponential fitted decay time constant κ. Variation of parameters g_{ex} and g_{in} results in variation of the value of κ, but the exponential character of the distribution persists.

To interpret the behavior in the high-dimensional phase space of the model, we used the phenomenological idea of a relatively small and confined "hole" through which trajectories may escape from the chaotic set during their evolution. This allowed us to explain qualitatively the global oscillations in the network and their unpredictable breakdowns at the ends of the high activity phases, as well as the exponential distributions of the SSA lifetimes. Reasoning along the same lines, we explained the facilitating effect of modularity upon SSA. Hierarchically distant modules tend to have higher degrees of asynchrony during their activities, and therefore tend to fall into their "holes" at different times. Hence, a rise in the hierarchical level of the network, by increasing the number of modules, enhances intermodular asynchrony and the likelihood of maintaining the SSA. Important

for the effectiveness of the modularity effect is the sparseness of intermodular connectivity.

Overall, the results of this Chapter elucidate the dynamics of the system and how self-sustained oscillatory activity takes place in it.

DYNAMICS OF OSCILLATORY SPONTANEOUS ACTIVITY IN RANDOM NETWORKS WITH MULTIPLE NEURON SUBTYPES AND SYNAPTIC NOISE

5.1 Introduction

Simultaneous recordings from large neuronal populations disclose complex spatio-temporal firing patterns characterized by rhythmic oscillations with variable degrees of synchrony (Buzsáki & Draguhn, 2004; Bonifazi et al., 2009; Uhlhaas et al., 2009; Colgin, 2011). Recent evidence suggests that in the cortex these patterns range from a "synchronized" state, characterized by low-frequency oscillation in the population firing rate and up/down switching in the single-neuron membrane potential, to a "desynchronized" state, marked by a roughly constant population firing rate and irregular single-neuron firing (Harris & Thiele, 2011; Vyazovskiy et al., 2011; Sachidhanandam, Sreenivasan, Kyriakatos, Kremer, & Petersen, 2013; Miller, Ayzenshtat, Carrillo-Reid, & Yuste, 2014; Okun et al., 2015; Jercog et al., 2017). Synchronous states are more prominent during slow-wave sleep and anesthesia whereas asynchronous firing activity is prevalent in the states of wakefulness and REM sleep (Steriade, Timofeev, & Grenier, 2001; El Boustani, Pospischil, Rudolph-Lilith, & Destexhe, 2007; Greenberg et al., 2008; Sanchez-Vives, Massimini, & Mattia, 2017). Notably, the degree of synchrony in cortical and subcortical regions varies with time, often with intermittent switches between synchronous

and asynchronous states (Ahn & Rubchinsky, 2013; Hahn et al., 2017; Ahn & Rubchinsky, 2017).

There is a widespread assumption that prevalence of synchrony or asynchrony in the network activity depends on the relative strength of excitatory and inhibitory synaptic inputs (van Vreeswijk, Sompolinsky, et al., 1996; Amit & Brunel, 1997b; Renart et al., 2010; Landau, Egger, Dercksen, Oberlaender, & Sompolinsky, 2016). In the context of networks of leaky integrate-and-fire (LIF) neurons, the balance between average excitatory and inhibitory synaptic inputs is known to result in quantitative characteristics of network activity that resemble those of asynchronous cortical states (Brunel, 2000; Mattia & Del Giudice, 2002; Cessac & Viéville, 2008; Vogels & Abbott, 2005; Kumar, Schrader, Aertsen, & Rotter, 2008; Wang et al., 2011; Litwin-Kumar & Doiron, 2012; Kriener et al., 2014; Ostojic, 2014; Potjans & Diesmann, 2014). In the absence of such balance, the network displays behaviors akin to synchronous cortical states (Vogels, Rajan, & Abbott, 2005).

Networks in which the nodes feature more complicated dynamics than LIF neurons and are able to reproduce intrinsic firing patterns of contrasting cortical neurons, e.g. based on the Izhikevich (Izhikevich, 2003, 2007) or the AdEx (Brette & Gerstner, 2005; Gerstner et al., 2014) models, demonstrate higher diversity of temporal patterns. In the region of parameter space where inhibitory synaptic strength exceeds excitatory synaptic strength, mixtures of neurons with different individual firing characteristics perform collective spontaneous oscillations that resemble the alternation of up and down states observed in the synchronized cortical state (Tomov et al., 2014, 2016). This suggests that not only synaptic balance of excitation/inhibition but also heterogeneities in the neuronal composition of the network may have an impact on the dynamic pattern of the network.

Yet another factor, capable of influencing the interplay between oscillatory and non-oscillatory states, is the intrinsic randomness of synaptic channels. More specifically, stochasticity expressed by synaptic noise originates from spontaneous neurotransmitter release in the synaptic cleft which generates miniature excitatory (inhibitory) postsynaptic potentials, the so-called mEPSPs (mIPSPs) or simply minis (Kavalali, 2015; Pulido & Marty, 2017). Characteristics of miniature postsynaptic potentials as amplitude and frequency have been demonstrated to

depend on the sleep/wake state (Liu, Faraguna, Cirelli, Tononi, & Gao, 2010). From the theoretical point of view, synaptic noise has been used in cortical models as a source of transitions between different dynamical network states (Compte, Brunel, Goldman-Rakic, & Wang, 2000; Renart, Brunel, & Wang, 2003; Holcman & Tsodyks, 2006; Moreno-Bote, Rinzel, & Rubin, 2007; Parga & Abbott, 2007).

Previous work has shown that up-down oscillations can appear in different setups. One of them considers neurons with an adaptive variable, within e.g. AdEx (Destexhe, 2009) or Izhikevich (Tomov et al., 2014) formalism. Another setup uses noise to provoke the switching between the two states (Holcman & Tsodyks, 2006; Jercog et al., 2017). Here, by combining adaptation with noise, we show that noise is not mandatory for the up-down oscillations but favors their occurrence when it is present. In this study we demonstrate that a network of Izhikevich neurons with stochastic synaptic inputs displays a rich variety of dynamic states with different levels of oscillations and degrees of synchrony. We locate these states in the parameter space spanned by the ratio between inhibitory and excitatory synaptic increments and the synaptic noise magnitude. As expected, noise transforms the transient dynamics observed in previous studies into persistent states with well established properties. Independently of network composition and relative inhibitory synaptic strength, for low intensities of synaptic noise the persistent states are asynchronous and non-oscillatory. For higher noise magnitudes, the type of persistent state depends on the relative inhibitory synaptic strength.

Remarkably, in the region of the parameter space where inhibitory synaptic increments are greater than excitatory synaptic increments the persistent state displays intermittent spontaneous transitions between two dynamic regimes: an active state characterized by rhythmic alternations of tonic firing and silence, and a quiescent state characterized by low-rate irregular network firing. In the active state, the average neuronal membrane voltage oscillates between depolarized and hyperpolarized states in a manner that resembles cortical up/down oscillations, whereas in the quiescent state the average membrane potential remains close to the resting value. We characterize this intermittent state by means of firing rates, power spectra, voltage series, and explain the observed phenomena in terms of the behavior of network-embedded neurons viewed in their single-neuron phase subspaces.

This work extends previous studies on activity pattern dynamics in random networks of LIF neurons to random networks with more involved on-site dynamics. To test the validity of our observations against the change of the chosen neuronal model, we performed similar computations for the same networks composed of the AdEx neurons, reproducing all basic effects found for the Izhikevich model. This paves way to a broader conjecture that two-dimensional neuron models with a slow recovery variable can naturally account for oscillations between depolarized and hyperpolarized states, mimicking up/down states. In this context, the synaptic noise can transform transient oscillatory network activity into a persistent complex state with intermittent switches between two different dynamic regimes.

5.2 Methods

5.2.1 Neuron and network model

In this Chapter we work with a standard random network model where directed connections between every two nodes exist with a fixed probability ϵ. To keep cortical sparseness we have chosen a low connection probability $\epsilon = 0.01$ and size $N = 2^{10}$. This renders the expected number of incoming connections per node (average in-degree) $\epsilon(N-1) \approx 10$. The network is mixed: it includes both excitatory and inhibitory nodes. The sizes of excitatory and inhibitory subpopulations are taken in the proportion $4:1$ (Brunel, 2000). Each network node is a neuron modeled by the Izhikevich formalism (Izhikevich, 2003) (see description in Chapter 2) with parameters that ensure diverse dynamics on the individual level.

Our choice of the Izhikevich neuronal model is based on its ability to mimic, by means of setting the appropriate values of parameters a, b, c, d, the behavior of neurons from different electrophysiological classes (Nowak, Azouz, Sanchez-Vives, Gray, & McCormick, 2003; Contreras, 2004). Among those, we concentrate in this study on the excitatory regular spiking (RS) and chattering (CH) neurons, and on the inhibitory fast spiking (FS) and low-threshold spiking (LTS) neurons. In Fig 2.2 one can see examples of individual dynamics for different classes: the neuronal types differ in frequency, adaptation, and in rheobase current. We consider network compositions where all inhibitory neurons belong to the same class: all of them are

either of the LTS type or of the FS type. In the excitatory subpopulation we take the case when all neurons belong to the RS type, and the case when the RS neurons are mixed with CH. A thorough discussion of different aspects of the Izhikevich neuron model can be found in (Izhikevich, 2007).

In this chapter, the last term in the first equation of Eq.(2.3), which is the synaptic current described by Eq.(4.2), has the addition of the synaptic noise. For that, we note that the current is controlled by conductances $G_j^{\mathrm{ex/in}}$ and reversal potentials $E_{\mathrm{ex/in}}$, responsible for excitatory/inhibitory effects. Whenever an excitatory (inhibitory) neuron spikes, an increment g_{ex} (g_{in}) is added to the conductances G^{ex} (G^{in}) of all its postsynaptic neurons; thereafter the conductances decay exponentially with time constant $\tau_{\mathrm{ex/in}}$. This is well known as a conductance based synaptic model, described by the differential equation

$$\frac{dG_j^{\mathrm{ex/in}}(t)}{dt} \quad = \quad -\frac{G_j^{\mathrm{ex/in}}(t)}{\tau_{\mathrm{ex/in}}} \quad + \quad g_{\mathrm{ex/in}}\sum_i \delta(t \ - \ t_i) \quad + \quad \sqrt{2Dn_j}\xi_j(t), \quad (5.1)$$

where summation is performed over all time instants t_i of preceding presynaptic spikes. We adopt the same parameters as in (Tomov et al., 2016): $E_{\mathrm{ex}} = 0$ mV, $E_{\mathrm{in}} = -80$ mV, $\tau_{\mathrm{ex}} = 5$ ms and $\tau_{\mathrm{in}} = 6$ ms.

The last term in Eq.(5.1) is the synaptic noise source. Since, for simplification, the noise sources are treated as being independent or weakly correlated, a superposition of a large number of such inputs is approximated by a simple Gaussian white noise process. We assume that ξ_j is Gaussian with zero mean and unit variance: $\langle\xi(t)\rangle = 0$ and $\langle\xi(t)\xi(s)\rangle = \delta(t - s)$. Note that in spite of the zero mean of the Gaussian process, the mean value of the synaptic input current $I_{syn,j}$ stays non-zero which, in its turn, is determined by both $G_j^{\mathrm{ex/in}}$ and $E_{\mathrm{ex/in}}$. So, the Gaussian process only has the effect of causing displacements in the synaptic current but does not act as a driving force. Concerning the variance, since the sum of independent random normally distributed variables is normally distributed as well, the overall variance of the stochastic process for a neuron j is chosen to be proportional to the total number of excitatory/inhibitory inputs n_j that this neuron receives. Thereby, for neurons with different numbers of presynaptic partners, the intensity of the noisy input is different. Altogether, evolution of conductances for each neuron consists of the stochastic Ornstein-Uhlenbeck process

([Uhlenbeck & Ornstein](), 1930) in the time intervals *between* the presynaptic spikes and of discontinuous jumps upwards of the size $g_{\mathrm{ex/in}}$ at the instants of arrival of those spikes. This stochastic model, similar to the point-conductance model described in ([Destexhe, Rudolph, Fellous, & Sejnowski](), 2001), has its power-spectral density and variance completely determined ([Gillespie](), 1996). In distinction to ([Destexhe et al.](), 2001), in our case randomness is generated within the synapses and is, in general, non-Poissonian.

The complete set of parameter values used in the simulations of this study is summarized in Table 5.1. Note that that the values of parameters α, β, γ in the voltage equation are shared by all neuronal types.

Common parameters in Eq.(2.3)	α	β	γ	v_{th} [mV]		
	0.04	5	140	30		
Parameters of Eq.(2.3) for						
different firing patterns	**a**	**b**	**c [mV]**	**d**		
Excitatory RS	0.02	0.2	-65	8		
Excitatory CH	0.02	0.2	-50	2		
Inhibitory FS	0.1	0.2	-65	2		
Inhibitory LTS	0.02	0.25	-65	2		
Synaptic parameters	$g_{\mathrm{ex}}^{\mathrm{max}}$	$g_{\mathrm{in}}^{\mathrm{max}}$	τ_{ex} [ms]	τ_{in} [ms]	E_{ex} [mV]	E_{in} [mV]
	0.15	1	5	6	0	-80
Network parameters	size N	ratio exc:inh	connectivity			
	2^{10}	4:1	$\epsilon = 0.01$			

Table 5.1: Parameters used in the simulations.

5.2.2 *PLV*

In our simulations, we constructed parameter space plots of the synchrony index PLV for different numbers K of neuron pairs and observed a saturation in the plots for increasing values of K above 50. This indicates that PLV becomes independent of the number of neuron pairs for $K \geq 50$. To ensure this independence,

in computations we took $K = 60$. See Chapter 3 for a description of the *PLV* measure.

5.2.3 Numerically integrating the synaptic equations

The numerical integration of the stochastic differential equations involved in this chapter is done with the help of the Heun's method (Mannella, 2002). The Heun's method for stochastic differential equations is an improved Euler's method or sometimes referred as a two-stage Runge-Kutta method. The method can be described as follows:

- Consider a given system of stochastic differential equations such as $\dot{x}_i = f_i(x) + g_i(x)\xi(t)$, where the stochastic process $\xi(t)$ is identified as a Gaussian zero-mean unit-variance, i.e. $\langle\xi(t)\rangle = 0$ and $\langle\xi(t)\xi(s)\rangle = \delta(t-s)$.

- At the level of the discretization, we consider that the integration time step is called h and we introduce a stochastic variable Y_i with zero-mean and unit-variance. Due to discretization at every time step h, we skip some period in time and, because of that, we have to define a stochastic variable that will take into account the amount added by the Gaussian variable. One easily can identify this amount by observing that the sum of Gaussian variables is still a Gaussian variable with its statistics, mean and variance, completely determined by the sum of the former ones. To enumerate, if $A \sim \mathcal{N}(\mu_A, \sigma_A^2)$ and $B \sim \mathcal{N}(\mu_B, \sigma_B^2)$, then $Z = A + B$ with $Z \sim \mathcal{N}(\mu_A + \mu_B, \sigma_A^2 + \sigma_B^2)$. Last but not least, we define

$$Z_i(h) = \sqrt{h}Y_i, \tag{5.2}$$

and with that, we keep correct statistical properties: zero-mean and a sum of variances.

- Finally, the Heun's method reads

$$x_{i,aux} = x(0) + \sqrt{2D}Z_i(h) + f_o h$$
$$x_i(h) = x(0) + \sqrt{2D}Z_i(h) + \frac{h}{2}(f_o + f(x_{i,aux})), \tag{5.3}$$

where $f_o = f(x(0))$.

5.3 Results

5.3.1 Preliminaries and the deterministic setup

To single out the effects caused by the introduction of synaptic noise, we first characterize the system in the non-perturbed state, i.e. in the absence of noise. Below, we refer to this case as the deterministic setup.

At the chosen parameter values the global state of rest is stable. Since in the deterministic setup no activity can be excited from that state without an initial disturbance, we start simulations by applying brief electric stimulation to arbitrarily selected neurons. Different stimuli are constructed by varying

- the amplitude of the input current from $I_{\text{stim}} = 10$ to $I_{\text{stim}} = 20$;

- the duration of the input current from $t_{\text{stim}} = 50$ ms to $t_{\text{stim}} = 300$ ms; and

- the proportion of stimulated neurons: 1, 1/2, 1/4, 1/8, 1/16.

The initial kick provided by brief stimulation has a sole role to put the system into a state other than rest. After the stimulation ends, the network is left to evolve freely and its dynamics is recorded. Eventually all trials end up in the state of rest. In most cases evolution is not a straightforward decay but a long dynamical transient; its duration strongly (by several orders of magnitude) varies, depending on the initial conditions. On discarding the cases where the free activity was shorter than 400 ms, we are left with a set of trials in which the network displayed long-living self-sustained activity; duration of the latter stage justifies a closer look at its intrinsic characteristics.

We have studied different combinations of the conductance increments $(g_{\text{in}}, g_{\text{ex}})$ and observed rather distinct behavior as shown in Fig 5.1. The choice of g_{ex} and g_{in} directly affects the network balance and shapes thereby its dynamics (Vogels et al., 2005).

Depending on the ratio $g_{\text{in}}/g_{\text{ex}}$, the self-sustained activity displayed by the network belongs to one of two categories outlined in (Tomov et al., 2014). The first

one, shown in the left column of Fig 5.1, is a relatively constant network activity state where neurons spike in an asynchronous and non-oscillatory fashion. For the given example, this is confirmed by the high value of the spectral entropy ($H_s = 0.87$) and the low phase locking value ($PLV = 0.39$). The reason for the constant network activity can be seen from the behavior of the voltage traces for two randomly selected neurons at the bottom of the left column of Fig 5.1: the neurons fire irregularly, but their firing rates are so high that the collective activity is constant.

The second category, shown in the right column of Fig 5.1, is an oscillatory state ($H_s = 0.39$) characterized by regular periods of high mean firing rate intercalated with periods of very low firing. The average voltage indicates that the bulk of neurons is fluctuating between depolarization and hyperpolarization. The PLV for this state is higher ($PLV = 0.60$) indicating that neurons fire/stay silent with a higher degree of synchrony. Voltage traces for two randomly picked neurons (see bottom plot in the right column of Fig 5.1) show bursts of closely spaced spikes during high activity phases intercalated with periods of hyperpolarization below the reset value during low activity phases. This behavior was explained by us earlier (Tomov et al., 2016) in terms of the dynamics of the recovery variable u in the single neuron phase plane of the Izhikevich neuron.

The example given in the middle column of Fig 5.1 illustrates the transition between the two above categories. This transition occurs when the inhibitory synaptic increment overcomes the excitatory synaptic increment as reported in (Tomov et al., 2014). The network activity in the transition region looks as a mixture of constant and oscillatory activity, with intermediate values of the synchrony ($PLV = 0.45$) and oscillatory activity ($H_s = 0.56$) indexes. Voltage traces for two randomly chosen neurons (bottom of middle column) show high firing rates like in the first category (a tendency for constant activity), but now there are short periods of activity break like in the second category (oscillatory activity).

Naively, $g_{\mathrm{in}}/g_{\mathrm{ex}} = 4$ may seem to be a balanced situation, as reported elsewhere (Brunel, 2000). Here, however, we are dealing with neurons from different electrophysiological classes, and their firing rates differ as well. In addition, we are using a conductance based synaptic model where the synaptic current is voltage-dependent. In that sense, the mean time-averaged synaptic input for a

given neuron j can be roughly estimated as

$$I_j(t) \approx g_{\text{ex}} C_{\text{ex}} \nu_{\text{ex}} \tau_{\text{ex}} (E_{\text{ex}} - \langle v \rangle) - g_{\text{in}} C_{\text{in}} \nu_{\text{in}} \tau_{\text{in}} (E_{\text{in}} - \langle v \rangle), \qquad (5.4)$$

where $C_{\text{ex/in}}$ are the numbers of excitatory/inhibitory inputs to neuron j, $\nu_{\text{ex/in}}$ are the mean firing rates of the excitatory/inhibitory populations, and $\langle v \rangle$ is a representative voltage. The expression in Eq.(5.4) elucidates that the notion of "balance" is subtle, and its reduction to just $g_{\text{ex/in}}$ and $C_{\text{ex/in}}$ may be misleading. Usually, when LIF neurons are considered, equal mean firing rates of excitatory and inhibitory neurons, as well as equal relaxation times $\tau_{\text{ex,in}}$ are assumed, hence the balance requires only that $g_{\text{in}}/g_{\text{ex}} = C_{\text{ex}}/C_{\text{in}}$, which, in the widely studied situation with the number of excitatory connections four times higher, results in $g_{\text{in}}/g_{\text{ex}} = 4$. In contrast, in a network like ours, with $\nu_{\text{in}} > \nu_{\text{ex}}$, there is no balance at $g_{\text{in}}/g_{\text{ex}} = 4$, instead there is a voltage dependent input current: if $\langle v \rangle$ is depolarized (hyperpolarized), negative (positive) currents drive the neuron.
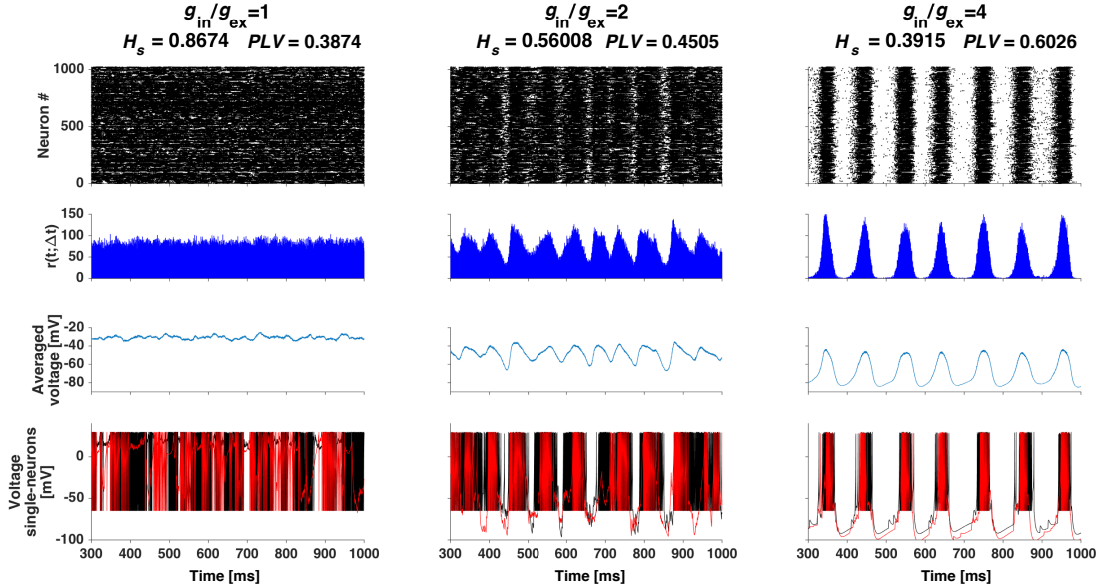
Figure 5.1: *Self-sustained firing pattern changes under variation of $g_{\text{in}}/g_{\text{ex}}$ ratio in the deterministic setup. The network is composed of RS and LTS neurons. Each column represents a combination of $g_{\text{in}}/g_{\text{ex}}$ indicated atop together with the corresponding spectral entropy H_s and synchrony index PLV. From top to bottom: raster plot, network firing rate, average voltage and voltage traces of two arbitrarily selected neurons (in black and red respectively).*

Altogether, these preliminary examples confirm that the deterministic setup, depending on the ratio $g_{\text{in}}/g_{\text{ex}}$, is able to generate oscillatory or constant activity. In

the following, we concentrate on the oscillatory situation, when inhibition overcomes excitation.

In Fig 5.2 we present an exemplary simulation in the deterministic setup and extended statistics from the set of long-lived realizations with synaptic increments $g_{\text{ex}} = 0.15$ and $g_{\text{in}} = 1$ (this set contains 487 simulations, thus allowing good statistics). In this case the majority of neurons oscillates between a depolarized state and a hyperpolarized state, well visible in Fig 5.2 **B** and on the bimodal distribution in Fig 5.2**F**, computed from the entire set of simulations with varied initial stimulation. For individual neurons these preferred subthreshold membrane potentials are known as "up" and "down" states (Wilson, 2008), and in the context of the ensemble of neurons it seems natural to view these two states as collective "up" and "down", respectively. As seen in Fig 5.2 **A-E**, a typical period of oscillations is close to 100 ms ($f \approx 10$ Hz).

For a typical neuron in the ensemble, Figs 5.2 **D-E** illustrate the temporal evolution of the voltage and the membrane recovery variable, respectively, during the same simulation. There is strong correlation between firing of this neuron and the periods of high activity of the whole network, although some other neurons also fire when the network activity is low. These latter are inhibited during the high activity epochs and become disinhibited when the overall network activity is low. We have shown elsewhere the importance of this disinhibitory effect to sustain the long-lived activity of the network in the oscillatory situation (Tomov et al., 2016).

Remarkably, not only the voltage series in Fig 5.2 **D** features two different states (a hyperpolarized one and a depolarized one) but also the membrane recovery variable, which clearly grows when the network activity is high and slowly relaxes when the activity is low. This is a global phenomenon: in all simulations there are peaks of the variable u. In the distribution shown in Fig 5.2 **G**, the maximum is broad due to the time-scale separation of the variables: u is slower than v and its relaxation takes much longer. In (Tomov et al., 2016) we have shown the importance of the recovery variable for the breakdown of global high-activity epochs, which produces the up and down oscillatory pattern.

Fig 5.2 **H** presents a histogram of durations in collective up and down states. The term "up" refers here to different states in which the network activity is above
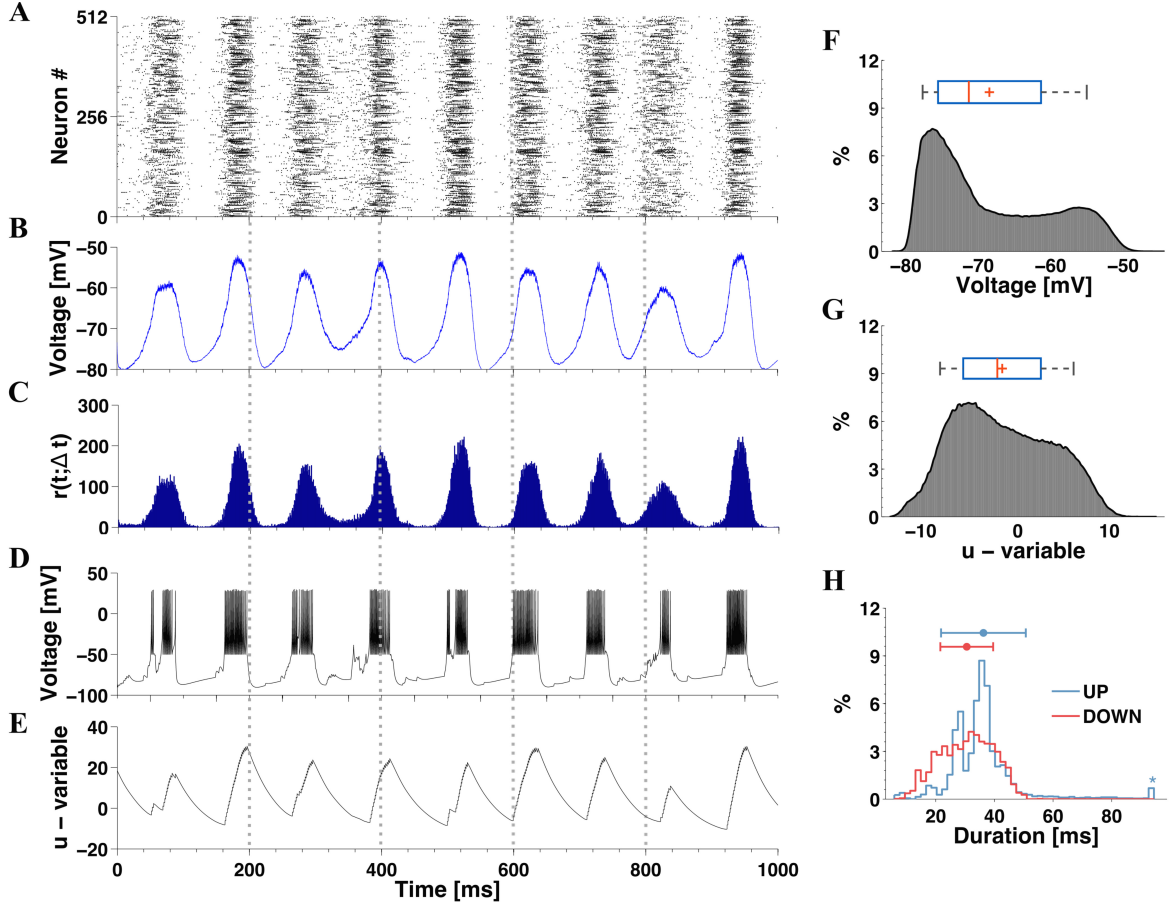
Figure 5.2: *Up and down network oscillations in the noiseless case when* $g_{in} > g_{ex}$. *The network is composed of 16%CH, 64%RS and 20%LTS neurons, with* $(g_{ex}, g_{in}) = (0.15, 1)$. *Panels* **A-C** *show the raster plot for half of the neurons in the network, average voltage and time-dependent firing rate from a sample simulation with long-lived self-sustained activity. Panels* **D-E** *show the voltage v and membrane recovery variable u extracted from a sample neuron in this simulation. Histograms* **F-G** *show the distributions of average v and average u based on data from all long-lived simulations. In the box plots above the histograms the red lines and the pluses denote, respectively, the median and the mean. Histogram* **H** *presents the distribution of stay duration in the collective up and down states based on all simulations, as well as mean and standard deviation; the outlier is indicated by the star in the end of the distribution.*

20% of its average value, whilst the voltage for the majority of neurons is at a depolarized value. A collective "down" state is identified whenever the bulk of the neurons reaches a hyperpolarized state close to -80 mV.

Recall that eventually the system ceases to oscillate, and voltages of all neurons invariably converge to the rest value.

5.3.2   Setup with synaptic noise

Introduction of synaptic noise drastically changes one important aspect, both in the individual and in the collective dynamics: the state of rest, albeit formally stable, ceases to be the ultimate attractor. A neuron is an excitable system, and in the noisy setup it is just a matter of time when a sufficiently strong fluctuation (or a cumulative effect of many fluctuations) drives it across the spiking threshold. For an ensemble this implies disordered sporadic firing of its members, which, under favorable conditions, can turn into ordered collective activity. If deterministic aspects dominate in dynamics, this activity will temporarily end in the state of rest, only to be recreated by new fluctuations.

5.3.2.1   Isolated neurons

Consider an individual neuron that obeys Eq.(2.3) with the synaptic current I given by Eq.(4.2) and synaptic conductances $G^{\text{ex/in}}$ governed by Eq.(5.1) with noisy input. An isolated neuron, by definition, has no synaptic inputs; nevertheless, stochastic fluctuations of its synaptic conductances can result in action potentials. In this situation, to study the influence of noise on the resting neuron we, without loss of generality, set $n_j = 1$ in Eq.(5.1). Take the initial conditions for the neuron at its state of rest and set its synaptic conductances to zero, so that the initial current is absent. As time goes on, the conductance evolves stochastically; to ensure that it stays positive, we impose a reflecting condition at zero (which, in the long run, very slightly shifts upwards the mean value of $\xi(t)$). As a result, a stochastic current $I(t)$ is generated. As long as $I(t)$ is absent or sufficiently small, the neuron stays at rest. As soon as the instantaneous current I exceeds the critical value $I_{\text{crit}}(t) = \dfrac{(\beta - b)^2}{4\alpha} - \gamma$, with α, β, γ, b being the parameters of the Izhikevich model (2.3), the state of rest disappears (the mechanism is explained below in Sect. 5.3.4), the voltage variable v starts to grow monotonically, and the neuron fires.

Since presynaptic inputs are absent in this isolated neuron description (see Eq. 5.1), computation of the first firing time for an isolated neuron turns into a variant of the mean first passage time problem (Siegert, 1951) for the Ornstein-Uhlenbeck process. Numerically, we find this quantity by averaging over a sufficient number of trials.

Regarding dependency of $I_{\text{crit}}(t)$ on the electrophysiological class, we note that the parameters α, β and γ are common for all classes, leaving b as the only parameter that matters. In this context, b determines the current threshold value. Furthermore, three of the four considered neuronal classes share the same value of b, whereas the LTS neuron has a higher value of b, ensuring early initiation of spikes. Hence, it suffices to compare two neurons: LTS and e.g. RS. In Fig 5.3 we plot the computed dependences of the time of first spike on the synaptic noise intensity.
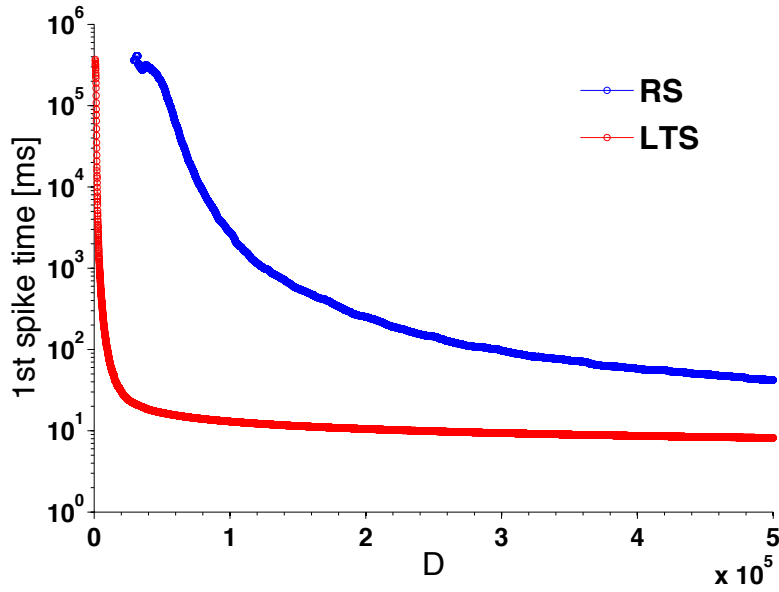
Figure 5.3: *Average time of first spike for the Izhikevich neuron model driven by synaptic noise.* *D: noise intensity. Blue curve: RS neuron. Red curve: LTS neuron.*

Notably, from the point of view of the random network, each curve in Fig 5.3 shows the behavior for all neurons of its respective kind, regardless of their in-degree: according to Eq.(5.1), an increase of the in-degree (in other words, of the number of independent Gaussian noises acting upon the synapse) rescales the variance and is therefore equivalent to the corresponding increase of D at constant degree. Recall that in the studied networks most of the neurons have in-degree ≈ 10. Altogether, the influence of the number of synaptic connections is clear: the higher the in-degree, the higher the variance of the input noise, the faster the neuron crosses the threshold and emits a spike.

5.3.2.2 Network with weak synaptic noise

We begin the discussion of synaptic noise in the network by presenting a case where its introduction induces activity with properties strongly different from those in the deterministic setup. For the same set of parameter values as in the deterministic case of Fig 5.2, instead of initial stimuli, we add in accordance with Eq.(5.1) small ($D = 2.5 \times 10^{-6}$) stochastic fluctuations to the synaptic variables. This results in activity with very low firing rates, exemplified in panels **A-C** of Fig 5.4. The high spectral entropy ($H_s = 0.82$) and the very low synchrony ($PLV = 0.0298$) indicate a non-oscillatory and asynchronous type of activity. The voltage distribution in Fig 5.4 **D** stands in contrast to the deterministic case: it is unimodal, the maximum lies at the mean, and the relevant voltage values are close to the resting potential. The firing rates in Fig 5.4 **E** are close either to 1 Hz (excitatory neurons) or to 8 Hz (inhibitory neurons). The state of the network in the weak synaptic noise setup corresponds well to the so-called asynchronous irregular (AI) state (Brunel, 2000; Vogels et al., 2005).

5.3.3 Onset and classification of intermittent oscillatory and quiescent activity in the synaptic noise setup

Here we describe various collective states induced in the network by synaptic noise. Experience gained from the study of the deterministic setup allows us to expect that, along with the synaptic noise intensity D, the crucial parameter in this context is the ratio $g_{\text{in}}/g_{\text{ex}}$: the proportion between inhibitory and excitatory synaptic strengths (Brunel, 2000; Girones & Destexhe, 2016). We start by exploring the behavior of the spectral entropy H_s and the synchrony measure PLV in the two-dimensional diagram spanned by parameters $g_{\text{in}}/g_{\text{ex}}$ and D (Fig 5.5).

As seen in the diagrams in Fig 5.5, both $g_{\text{in}}/g_{\text{ex}}$ and D are responsible for shaping the activity pattern of the network. Let us begin with the diagram for spectral entropy in Fig 5.5 **A**. For weak synaptic noise ($D \lessapprox 5 \times 10^{-6}$) the network displays non-oscillatory behavior independently of the ratio $g_{\text{in}}/g_{\text{ex}}$. For the narrow horizontal band defined by $5 \times 10^{-6} \lessapprox D \lessapprox 10^{-5}$, the state of the network is oscillatory and the degree of oscillatory activity is higher for $g_{\text{in}}/g_{\text{ex}} \lessapprox 2$. On the other hand, for $D \gtrapprox 10^{-5}$ the situation is inverted and the region determined by
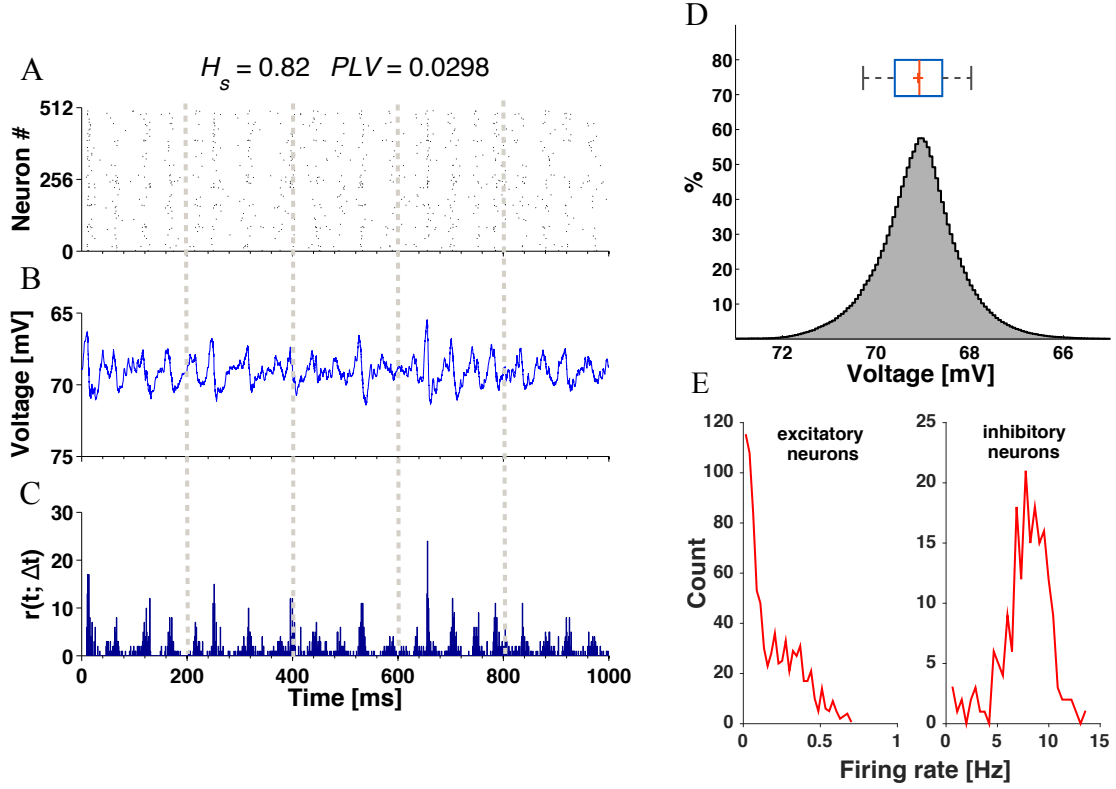
Figure 5.4: *Asynchronous irregular state in the presence of weak synaptic noise. The network, composed of 16%CH, 64%RS and 20%LTS neurons, evolves without initial stimulation. Synaptic increments: $(g_{ex}, g_{in}) = (0.15, 1)$. Intensity of synaptic noise: $D = 2.5 \times 10^{-6}$. Panels **A-C** present, respectively, raster plot for half of the neurons in the network, average voltage and time-dependent firing rate for the network. Above them the values of H_s and PLV are cited. Panels **D-E** are histograms with distributions of average voltage and firing rates. For the firing rates, excitatory and inhibitory populations are presented separately, as indicated in the titles of **E**.*

$g_{in}/g_{ex} \lessapprox 2$ displays non-oscillatory activity while most of the remainder of the diagram features oscillatory activity. Within this latter part of the diagram, increase of both noise and inhibitory synaptic strength lowers the degree of oscillatory activity until in the upper right corner the activity turns non-oscillatory.

Now let us turn to the diagram for the synchrony PLV in Fig 5.5 **B**. The region of weak synaptic noise ($D \lessapprox 5 \times 10^{-6}$) displays asynchronous behavior independently of g_{in}/g_{ex}. Under such weak noise firing remains an individual event for noise-perturbed neurons, rather than a collective effect. Along the narrow horizontal band of the diagram determined by $5 \times 10^{-6} \lessapprox D \lessapprox 10^{-5}$, the synchrony index has mostly intermediate values with a narrow high-synchrony region around
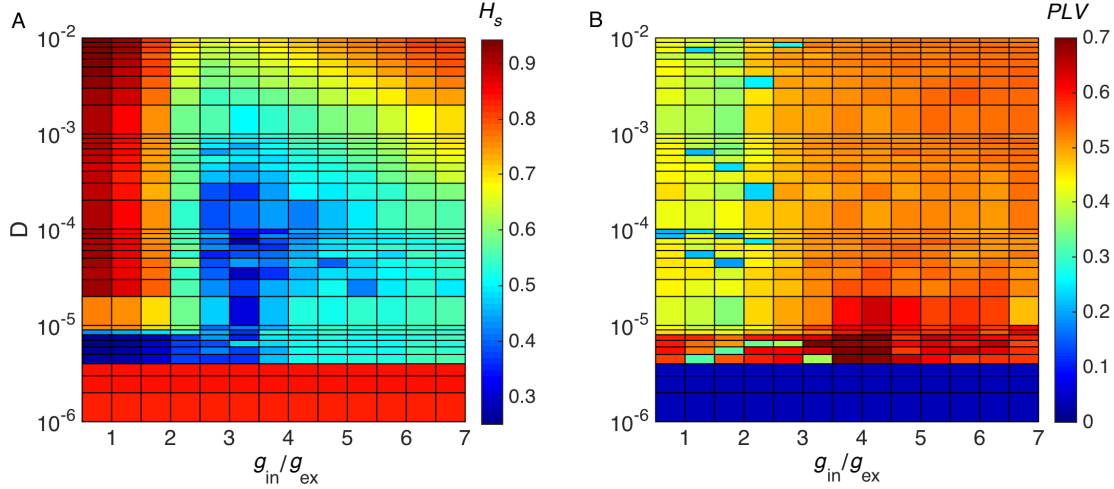
Figure 5.5: *Spectral entropy H_s and synchrony index PLV for the synaptic noise setup. Two-dimensional space where ordinate represents the synaptic noise intensity D and abscissa, the ratio of synaptic increments g_{in}/g_{ex}. The coordinate mesh is linear (from 0.5 to 7) with respect to g_{in}/g_{ex} and logarithmic with respect to the synaptic noise intensity (from $D = 1 \times 10^{-6}$ to $D = 1 \times 10^{-2}$). Panel **A**: Colors represent spectral entropy H_s (values close to zero correspond to oscillatory states and values close to 1 correspond to non-oscillatory states). Panel **B**: Colors represent synchrony evaluated by means of the phase locking value PLV (values close to zero correspond to asynchronous states whereas values close to 1 correspond to synchronous state).*

$g_{in}/g_{ex} \approx 4$. In the remainder of the diagram the behavior along horizontal scans in the diagram is roughly the same: in the entire region determined by $g_{in}/g_{ex} \lessapprox 2.5$ the activity is asynchronous, whereas outside that region the degree of synchrony has intermediate values.

The combined information in the two diagrams of Fig 5.5 is qualitatively summarized in a schematic diagram drawn in Fig 5.6. The states in this diagram are denoted in accordance with two measures of network activity in Fig 5.5: H_s quantifies the degree of oscillatory activity and PLV quantifies the degree of synchrony. Selected samples from the different regions are also displayed on the right of Fig 5.6 to show the time-dependent network firing rates for the corresponding combinations of H_s and PLV.

The region of weak synaptic noise lies at the bottom of the diagram in Fig 5.6. The type of network activity there is asynchronous non-oscillatory, already described in subsection 5.3.2.2. It is similar to the asynchronous irregular (AI) activity observed in networks of LIF neurons (Brunel, 2000; Vogels et al., 2005).
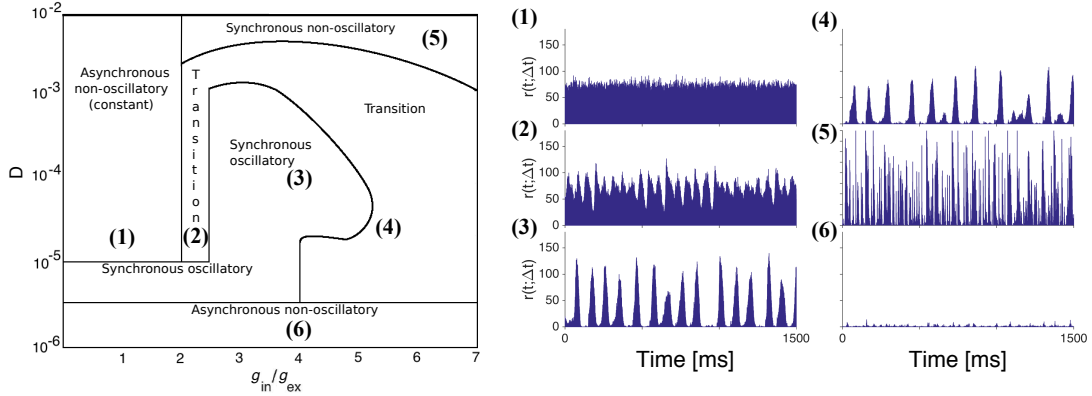
Figure 5.6: *Network activity patterns in the synaptic noise setup. A schematic representation of the D vs. g_{in}/g_{ex} diagram of Fig 5.5 combining the information on degree of oscillatory activity (H_s) and degree of synchrony (PLV) disclosed in that figure. The names of the activity types are given inside the regions bounded by full lines. The synchronous non-oscillatory type is equivalent to the constant type used to describe network states in the deterministic setup. The region marked as "transition" corresponds to states with intermediate levels of oscillatory activity and synchrony. On the right side of the diagram we present the time-dependent firing rate $r(t; \Delta t)$ of the network for six selected $(D, g_{in}/g_{ex})$ combinations. Numbers on the left-hand top of the panels indicate the corresponding points in the diagram to the left.*

The region stretches along the full length of the horizontal axis, indicating that the generic features of the network activity for weak synaptic noise are insensitive to the ratio between excitation and inhibition.

For stronger synaptic noise the structure of the diagram in Fig 5.6 is more complex. The network displays synchronous oscillatory activity within an irregular shaped region in the center of the diagram, adjoined by a narrow horizontal strip in the bottom part. This is similar to the synchronous regular (SR) type of activity found in networks of LIF neurons (Brunel, 2000; Vogels et al., 2005). In the remainder of the third of the diagram where $g_{in}/g_{ex} < 2$ the activity is asynchronous non-oscillatory. Its pattern is similar to the constant pattern shown in the left column of Fig 5.1. On the other hand, through the upper two-thirds of the diagram for $g_{in}/g_{ex} > 2$ the activity is synchronous non-oscillatory. Thus, for very strong synaptic noise the network activity is non-oscillatory and can be synchronous or asynchronous depending on the g_{in}/g_{ex} ratio.

Finally, the diagram in Fig 5.6 includes the region marked as "transition". It

contains most of the right third of the diagram, with the exception of the regions of weak and strong synaptic noise mentioned above, and extends to the central part of the diagram where it separates the synchronous oscillatory from the asynchronous non-oscillatory regions. This corresponds to a region with intermediate degrees of oscillatory activity (the greenish region in the diagram for H_s in Fig 5.5 **A**) and synchrony (red-orange to yellow-orange colors in the diagram for *PLV* in Fig 5.5 **B**). Therefore, states in the transition region should occupy intermediate position between constant and oscillatory states like the state in the middle column of Fig 5.1.

Interested in the behavior of the network in the transition region, we focus here on a part of the diagram in Fig 5.6 determined by $(g_{in}, g_{ex}) = (1, 0.15)$, which implies $g_{in}/g_{ex} \approx 6.66$, and $10^{-5} \lesssim D \lesssim 10^{-4}$. This corresponds to the greenish (light orange) region on the lower right-hand side of the diagram for H_s (PLV) in Fig 5.5 **A** (**B**). Spectral entropy and *PLV* here are both close to 0.5 meaning that states with intermediate levels of oscillatory activity and synchrony may be encountered.

In Fig 5.7 we illustrate dynamics for the point given by $D = 1 \times 10^{-5}$ and $(g_{in}, g_{ex}) = (1, 0.15)$ in the diagram in Fig 5.6. This point is in the transition region on the lower right-hand side of the diagram described above, which is characterized by intermediate values of H_s and *PLV*.

Remarkably, a typical record of a long simulation trial in this region of the diagram consists of alternating states (Fig 5.7): an oscillatory one, akin to oscillations presented in the deterministic setup in Fig 5.2, and a state with very low firing rates similar to the one in Fig 5.4. From time to time transitions between these states occur, seemingly without any precursors. Compared to deterministic simulations, an additional feature is distinct in the histogram of mean voltage: a pronounced maximum at the state of rest. Accordingly, the temporal evolution of voltage is organized around three characteristic values, instead of two known from the deterministic setup. Three red dashed lines in Figs 5.7 **B-C** mark three relevant states; from top to bottom, they denote depolarization, the state of rest and hyperpolarization. Note that the histogram in **B** can be viewed as a combination of the voltage histograms from Figs 5.2 and 5.4.

The average spectral entropy calculated over the quiescent/oscillatory states

in Fig 5.7 is $H_s = 0.74/H_s = 0.37$, indicating non-oscillatory activity in the first case and oscillatory activity in the second one.
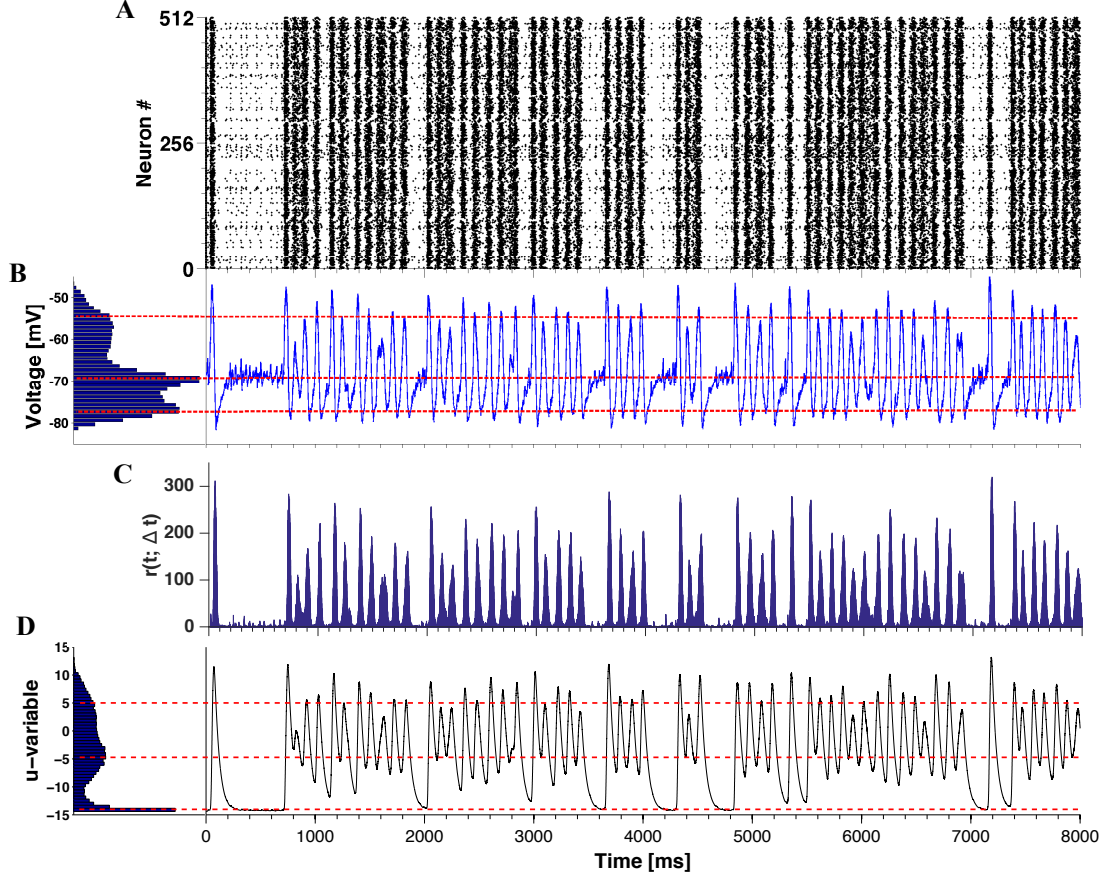
Figure 5.7: *Intermittent transitions between active oscillatory and quiescent regimes in the presence of synaptic noise. Plots generated for a network with 16%CH, 64%RS and 20%LTS neurons, $D = 1 \times 10^{-5}$ and $(g_{in}, g_{ex}) = (1, 0.15)$. Panel **A**: Raster plot for half of the neurons in the network. Panel **B**: voltage v histogram (left) and time course of average voltage over all network neurons (right). Panel **C**: time-dependent firing rate of the network. Panel **D**: Recovery variable u, histogram (left) and time course of average recovery value over all network neurons.*

We classify the observed states based on two attributes: network activity and average voltage. Like previously, the average voltage series was used to detect the up and down states (see Fig 5.2 **H**). The states close to rest are identified through very low network activity,

In terms of activity, we introduce the following distinction:

- **quiescent period** is the time interval when the time-dependent firing rate of the network $r(t, \Delta t)$ is below its maximum by at least 20%, and most of the

single neurons have voltage values close to the resting state. During a quiescent period there can be sporadic noise-induced spikes but no collective dynamics. The state is similar to an asynchronous irregular (AI) state of networks of LIF neurons (Brunel, 2000; Vogels & Abbott, 2005) with low firing rate, and to a desynchronized cortical state as described in the Introduction.

- **active period** is the time interval when the network exhibits oscillatory activity, alternating between high depolarized and hyperpolarized mean voltage values: collective up and down states. Such behavior can be related to the self-sustained activity developed in *in vivo* cortical slice preparations and during slow-wave sleep and anesthesia (Steriade et al., 2001; Tomov et al., 2016; Sanchez-Vives et al., 2017).

These definitions, in combination with the values of the average voltage, facilitate identification of different collective states. Certain states that look very similar on the raster plot turn out to differ in typical voltage values. For instance, both the down state and the quiescent period feature in the raster plot almost no activity, but can be easily discerned in terms of the average voltage.

In Fig 5.8 we show various regimes at different values of D. Three samples corresponding to the time interval of 2 s are, from top to bottom: $D = 0.5 \times 10^{-5}$, $D = 1.5 \times 10^{-5}$, and $D = 4.5 \times 10^{-5}$, respectively. In panels **A1**, **B1**, and **C1** green dots denote states with instantaneous voltage values close to the resting state, blue dots denote hyperpolarized voltage (down state), and red dots denote depolarized voltage (up state). The plot highlights the crucial role of synaptic noise level in changes of typical duration at each of these states. It is easier to generate oscillatory states (alternating between up and down states) when the network is subjected to stronger synaptic noise. In contrast, the "green" states close to rest (quiescent periods), prevalent at low synaptic noise amplitudes, occupy a much smaller proportion of time when synaptic noise becomes sufficiently intensive.

Comparison of raster plots in Fig 5.8 indicates that when noise intensity D is increased, the waves of activity start to merge. This hinders identification of states, based on the raster plot alone. The spectral entropy and the synchrony index increase with the noise intensity until a saturation is reached and then they slightly
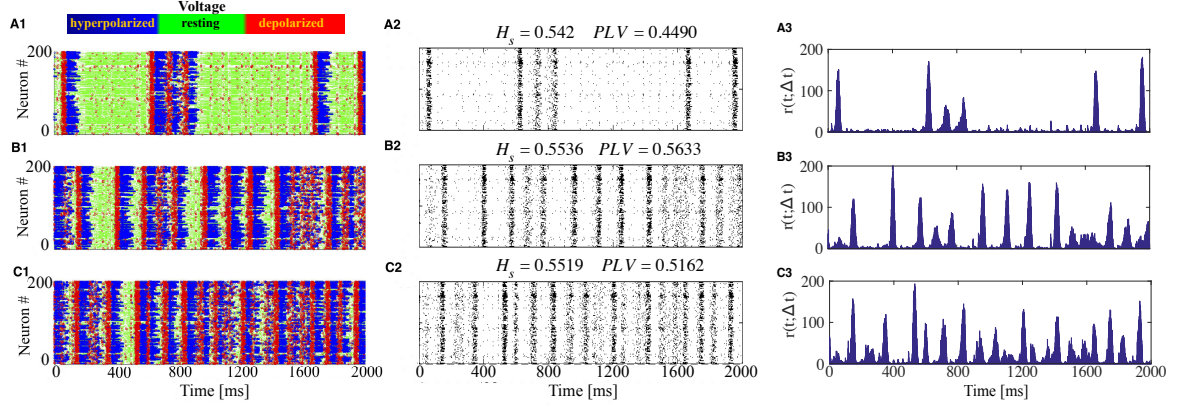
Figure 5.8: *Increase of synaptic noise favors up-down oscillations.* *The network has the same composition as in Fig 5.7 with varying synaptic noise intensity D. **A**: D = 0.5 × 10⁻⁵, **B**: D = 1.5 × 10⁻⁵, **C**: D = 4.5 × 10⁻⁵. In **A1**, **B1**, and **C1** blue dots correspond to depolarization (up state), red dots to hyperpolarization (down state), and green dots to voltage near the resting state. **A2**, **B2**, and **C2**: raster plots for 200 neurons in the network with corresponding H_s and PLV values atop each plot. **A3**, **B3**, and **C3**: time-dependent firing rates.*

decrease. We expect that at very high levels of noise the activity becomes constant (synchronous non-oscillatory), with rather high firing frequencies (see the schematic diagram in Fig 5.6).

In the frequency domain, variation of the noise level leads to redistribution of power in the Fourier spectra of both the spike trains and the voltage series. Fig 5.9 presents spectra for the same noise intensities as in Fig 5.8: from top to bottom, $D = 0.5 \times 10^{-5}$, $D = 1.5 \times 10^{-5}$, and $D = 4.5 \times 10^{-5}$. All spectra were averaged over ensembles of 200 neurons, see Eq. (3.6). The shapes of spectral curves for spike trains and for voltage values are similar; the only noticeable difference is the somewhat faster decay at high frequencies in the voltage spectra. The left column shows mixtures of RS and LTS neurons; the right column corresponds to networks with RS and FS neurons. Under low levels of noise, spectral power is concentrated at very low frequencies, waves of collective activity are quite rare and, when they occur, they are mostly isolated events. On increasing the intensity D, waves of collective activity become more frequent whereas the periods of quiescence get shorter. During the periods of oscillatory activity, neurons are either firing at high frequency in the up state or rarely firing in the down state. This results in the increase of spectral power at low frequencies, with a distinct maximum near 10 Hz.
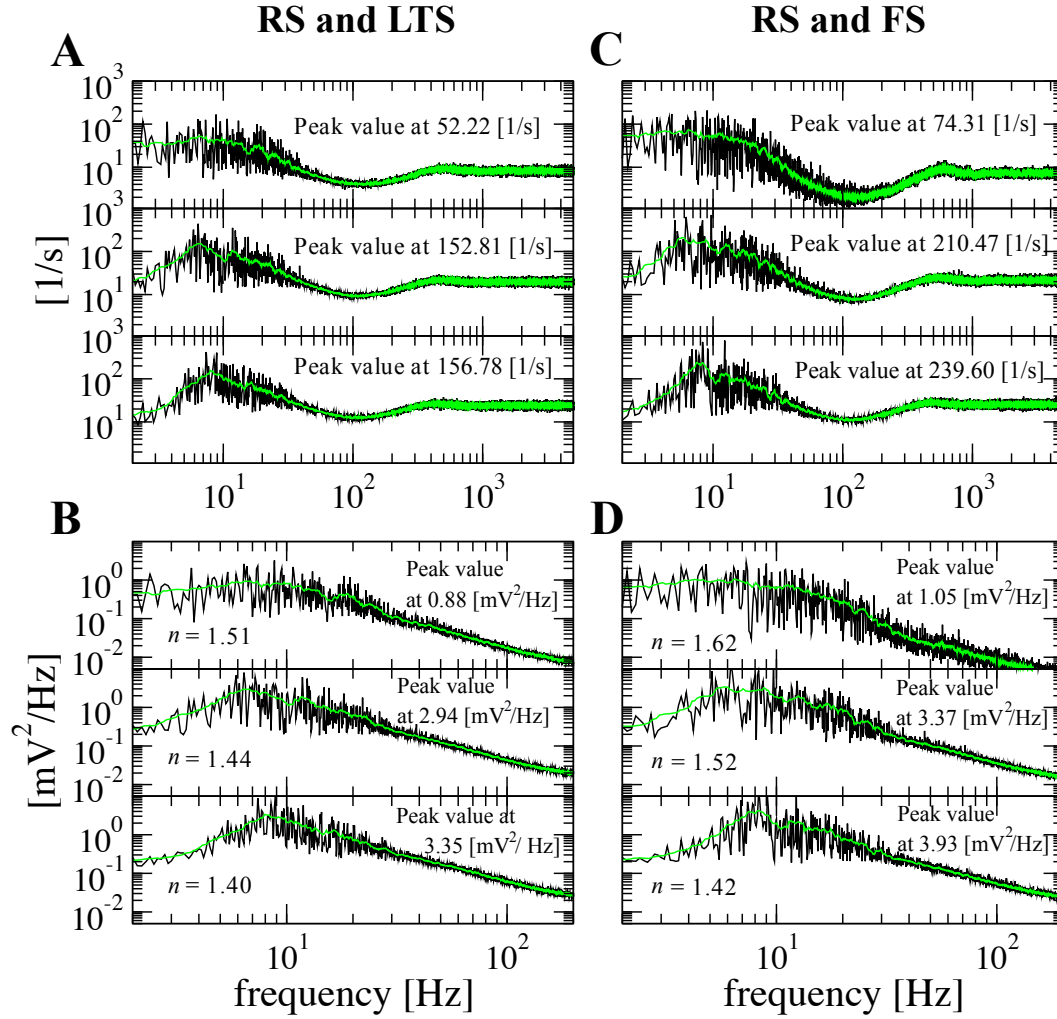
Figure 5.9: *Averaged power spectra at different noise intensities.* *Simulation length: 10 s. Left column: network with inhibitory LTS neurons. Right column: network with inhibitory FS neurons. Every panel (**A**,**B**,**C**,**D**) contains three subpanels displaying three levels of noise intensity from top to bottom: $D = 0.5 \times 10^{-5}$, $D = 1.5 \times 10^{-5}$, and $D = 4.5 \times 10^{-5}$. Black curves in **A** and **C**: averaged spectra of spike trains for 200 randomly chosen neurons. Black curves in **B** and **D**: averaged spectra of voltage for the same 200 neurons. Green curves: moving average over 20 points. Peak values are indicated in the plot and were evaluated from the green curves neglecting the zeroth frequency bin. In the bottom panels we display the factor n for the $1/f^n$ decay extracted between 10 and 200 Hz.*

Comparison of left and right columns in Fig 5.9 shows that spectral curves for networks with inhibitory LTS and FS neurons are similar. Comparing the peak values indicated in the panels. we see that spectral power in the networks with FS neurons is slightly higher.

Remarkably, these power spectra, computed for single neurons, bear

resemblance to experimentally obtained spectral curves. In the case of the voltage spectra (Figs. 5.9 **B** and 5.9 **D**), the $1/f^n$ behavior is reported in experiments on up-down states with n in the range 1 to 3 (Bédard & Destexhe, 2009; Millman, Mihalas, Kirkwood, & Niebur, 2010; Baranauskas et al., 2011). Furthermore, our results match the experimental observation that the spike-train power spectra have striking differences in comparison to the voltage-series power spectra (Bair, Koch, Newsome, & Britten, 1994) .

In the spike-train power spectra (Figs. 5.9 **A** and 5.9 **C**), there is no $1/f^n$ scaling. As the noise intensity D is raised, the value related to the zeroth frequency bin of the spectra decreases. This indicates that irregularity is becoming less apparent given that $\lim_{f \to 0} \bar{S}(f)$ is related to the Fano factor which is a measure of irregularity (Middleton, Chacron, Lindner, & Longtin, 2003; R. F. Pena et al., 2018).

Regarding the $1/f^n$ scaling, observed both experimentally and theoretically (Beggs & Plenz, 2003; Kinouchi & Copelli, 2006), in our case we see that noise acts upon the scaling (cf. n values in Fig 5.9 **B,D**). It has been shown elsewhere (Baranauskas et al., 2011) that the shape of up-down transitions in the membrane potentials could be a determining factor for modulation of the $1/f^n$ scaling with $n = 2$. Our observations provide support to this experimental evidence. At unbounded growth of D, transitions should vanish, and, as a consequence, n decreases.

Additionally, increase of noise shifts the peak values and peak frequencies in both spike-train and voltage power spectra; compare the peak values in different subpanels. The existence of spectral differences where peaks becomes apparent or not is well known to be present in the cerebral cortex during different states such as slow wave sleep and wake (Buzsáki, 2006).

We have seen that synaptic noise enforces alternation of collective states and influences durations of stay in each of them. Below, we explain how the dynamics of a single neuron, embedded in the synaptic noise setup, is reflected in the collective properties of activity, how the transitions are affected by the composition of the network, and how the picture changes at different levels of noise.

5.3.4 Single neuron phase plane description of the synaptic noise setup

A deeper understanding of the single neuron behavior in the synaptic noise setup can be gained from analysis of the course of its phase plane dynamics during the simulation. Setting the derivatives $\dot{v}$ and $\dot{u}$ in Eq.(2.3) to zero renders the nullclines of the voltage and the membrane recovery variable which we denote below as $\bar{u}$ and u^*, respectively.

$$\begin{cases} u & = \bar{u} = \alpha v^2 + \beta v + \gamma + I(t), \\[2mm] u & = u^* = bv. \end{cases} \tag{5.5}$$

with $\bar{u}$ being a (time-dependent) quadratic parabola and u^* a straight line. Synaptic noise enters this configuration implicitly, through its contribution to the current I.

Under the employed parameter values (see Table 5.1 above) and $I = 0$, the nullclines intersect in two points of the phase plane. These points correspond to equlibria of the system; the left of them is stable: without input current, neuron exhibits no activity. When the instantaneous value of the current is increased, the nullcline $\bar{u}$ is shifted upwards on the phase plane, and the equilibria move towards each other. At the value $I_{\mathrm{sn}}(t) = \dfrac{(\beta - b)^2}{4\alpha} - \gamma$ they merge and disappear in a saddle-node bifurcation. Absence of equilibria is sufficient to ignite a spike: the voltage grows until it reaches the threshold. In fact, if the value of the parameter b exceeds that of the parameter a (this holds for all four considered neuronal types), spiking starts at even weaker current: at $I_H = \dfrac{(\beta - b)^2 - (a - b)^2}{4\alpha} - \gamma$ the subcritical Andronov-Hopf bifurcation takes place, the equilibrium loses stability and the solutions spiral out from its vicinity towards the spiking threshold. Recall that the values of α, β, γ are common for all neuronal types (cf. Table 5.1). Hence, the onset of spiking at I_H is dictated for each type of neuron by the pertaining a and b (the remaining parameters c and d characterize the reset and are irrelevant in this context: a neuron that has made it to the reset, is already in the spiking state).

Evolution of every individual neuron is governed by its instantaneous location on the phase plane with respect to the nullclines; its dynamics is affected not only by its own state, but by the time-dependent (due to external and synaptic currents)

position of the nullcline $\bar{u}$. This allows us to see the collective dynamics from the local point of view of its individual participant; for it, the rest of the network is a background mechanism that moves the nullcline $\bar{u}$ upwards and downwards.

Remarkably, this motion is not always negligible in comparison to dynamics of the neuron on the phase plane: on arrival of synaptic input, the nullcline $\bar{u}$ is swiftly shifted in the vertical direction. Sometimes this leads to spectacular effects: a rapid fall of $\bar{u}$ may drag it across the instantaneous position of the neuron on the plane and thereby halt and reverse the developing action potential. Such events, however, are seldom in a network like ours with its moderated connectivity, therefore most of the time the vertical displacements of the nullcline $\bar{u}$ stay noticeably slower than the motion of the neuron.

With this local view in mind, we present in Fig 5.10 and Fig 5.11 the same simulation as in Fig 5.7 focusing on the individual dynamics of two representative neurons, arbitrarily picked among the populations of, respectively, the neurons that fire only during the active periods and the neurons that fire throughout all stages of evolution. As we will see, distinctions in the behavioral patterns can be traced down to the phase planes of the neurons.

We begin from the neuron # 240 which fires only during the active periods, showing it in the time range between 3800 ms and 4400 ms. We split this range, which contains both active and quiescent states, into 6 smaller intervals Δt_i, each one of either 50 or 100 ms duration. The upper panel in Fig 5.10 shows the entire range and its breakdown into the set of Δt_i. The lower panels present for every Δt_i the voltage series and the trajectory on the phase plane. Notably, in the hyperpolarized (down) state below reset, the neuron typically is close to the instantaneous location of $\bar{u}$, hence its motion is slow.

We summarize our observations as follows:

- Interval Δt_1: in the beginning, the neuron has just ended its evolution in an up state and passes through a down state. There, the trajectory mostly stays inside the parabola of the voltage nullcline $\bar{u}$ below the reset value. Since the system is located above nullcline u^* of the recovery variable, the latter decreases. The down state can be viewed as a period of relaxation where the voltage is hyperpolarized. The trajectory slowly moves towards the state of
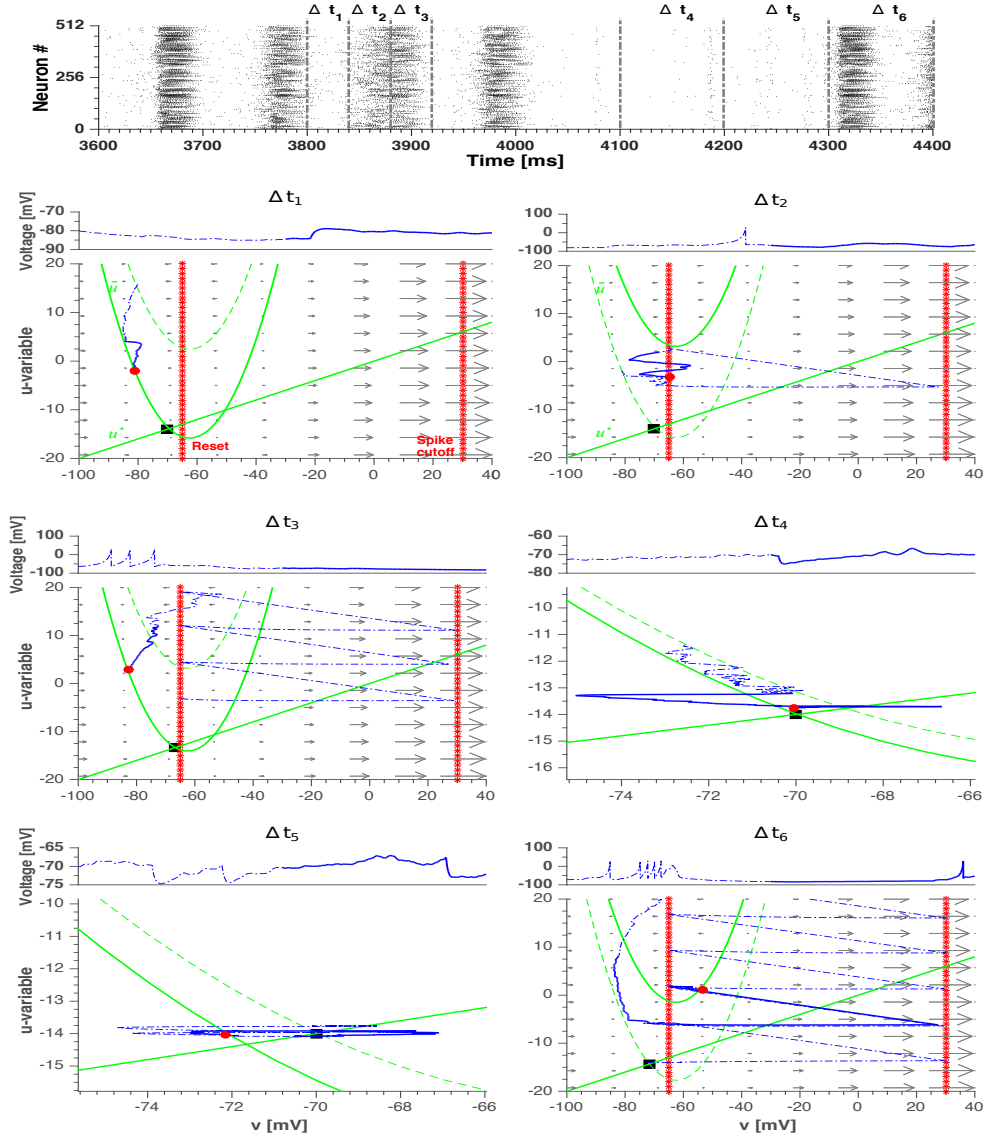
Figure 5.10: *Single neuron phase plane depiction of a neuron that fires during the active periods in the synaptic noise setup. Upper panel: a zoom of the simulation from Fig 5.7, split into 6 time intervals Δt_i. The first 3 intervals have a duration of 50 ms and the last 3 have a duration of 100 ms. Lower panels: voltage series and dynamics on the phase plane of neuron # 240 in subsequent intervals Δt_i. Arrows indicate the vectors $(\dot{v}, \dot{u})$; since v is much faster than u, the vectors are nearly horizontal. Blue dashed line: the first half of evolution in a given Δt_i. Blue solid line: the last half of evolution in a given Δt_i. Red circle: location of the neuron at the end of the time interval. Black square: location of the state of rest with $v = v_{rest}$ and $u = u_{rest}$. Dotted red lines: reset value of voltage and spike cutoff. Green lines: Nullclines $\bar{u}$ and u^*, according to Eq. (5.5). The location of the parabolic nullcline $\bar{u}$ is time-dependent; its position at the beginning (respectively, end) of Δt_i is shown with dashed (respectively, solid) green line.*

rest (marked as a black square in Fig 5.10).

- Interval Δt_2 : Before the trajectory arrives at the resting state, the neuron receives excitatory input from its presynaptic partners and the voltage nullcline $\bar{u}$ is shifted upwards, then the neuron resumes the up state and fires several times. The dynamics of $\Delta t_1 + \Delta t_2$ is largely repeated every ≈ 100 ms.

- Interval Δt_3: Since most of the neurons are firing, their recovery variables are growing (recall that at every spike, d is added to the value of the variable u). At very high u the negative feedback to the voltage variable v is so strong that the neuron is forced to stop firing and follows the same path as in Δt_1 (see (Tomov et al., 2016) for a description of this effect). The majority of the neurons in the network stops firing due to the same reason, and the network does not supply synaptic input, hence the conductances $G^{\text{ex/in}}$ relax. As a result, the nullcline $\bar{u}$ lowers and the neuron approaches the state of rest.

- Interval Δt_4: This is the middle of a quiescent period. The zoomed image shows how the neuron slowly moves towards the state of rest. The membrane recovery variable u monotonically decays. Synaptic noise perturbs the trajectory, but falls short of initiating a new up state.

- Interval Δt_5: the neuron crosses the nullcline u^* of the recovery variable u. The latter does not decrease anymore while the voltage is fluctuating due to noisy synaptic input.

- Interval Δt_6: finally the noise and/or arrival of inputs from presynaptic neurons are able to initiate a new active period.

The sequence of events in Fig 5.10 discloses a major role of the membrane recovery variable u both in the transition from up state to down state and in the subsequent initiation of the new active phase by the noisy input. Because of high tonic firing during an up state, the total synaptic current into a neuron like #240 is very intense and roughly constant (its fluctuation amplitude depends on the synaptic noise level). Hence, the nullcline $\bar{u}$ stays close to its highest position in the u-v diagram while the neuron climbs towards it due to the increments received by its

recovery variable u after each spike. Finally, the neuron gets inside the parabolic nullcline $\bar{u}$, has its firing probability decreased and eventually stops firing. The fact that the whole network enters a down state when this happens suggests that most neurons behave like #240, i.e. they dominate dynamics in the network. Excursion of the neuron to the left from the reset line while it is inside the parabola $\bar{u}$ is the mechanism responsible for the hyperpolarized voltages seen in the down states of oscillatory regimes both in the deterministic (cf. Fig 5.1) and noisy (cf. Fig 5.7) setups. During a quiescent period, the nullcline $\bar{u}$ is dragged to the bottom of the diagram putting the neuron close to rest. This explains the absence of hyperpolarized voltages during quiescent periods (cf. Fig 5.7). In this situation the neuron is also close to the nullcline u^*, so its eventual high jump to the region of the diagram below the nullcline u^* makes the neuron fire again and a new active period begins.

The behavior of the neuron #240 in Fig 5.10 somewhat mimics the overall behavior of the network: it is highly active during up states of active periods and silent during down states of active periods and quiescent periods. In the following, we will refer to neurons of this type as "typical" in the sense that they represent the behavior of the majority of the network nodes.

The firing pattern of typical neurons is contrasted by the behavior displayed in Fig 5.11. There, we show dynamics of the neuron #69, chosen because of its atypical behavior: it fires at all stages: in the up and down states of the active period and during the quiescent period. Dynamical features of this neuron are complementary to the ones of the typical neuron in Fig 5.10, and a combination of the views given by them offers a deeper understanding of the mechanisms responsible for the intermittent changes between active and quiescent states.

A summary of our observations for the "atypical" neuron reads as follows:

- Interval Δt_1: contrary to the typical neuron, # 69 starts its evolution with a low value of the recovery variable u. This indicates that during the previous up state the neuron did not fire much. The nullcline $\bar{u}$ also begins this time interval at a low position, meaning that it did not receive many increments. This suggests that the neuron is heavily inhibited when the network is at a high firing state, possibly being postsynaptic to a large pool of inhibitory neurons. Hence, it is more likely that the neuron emits spikes during down states: there
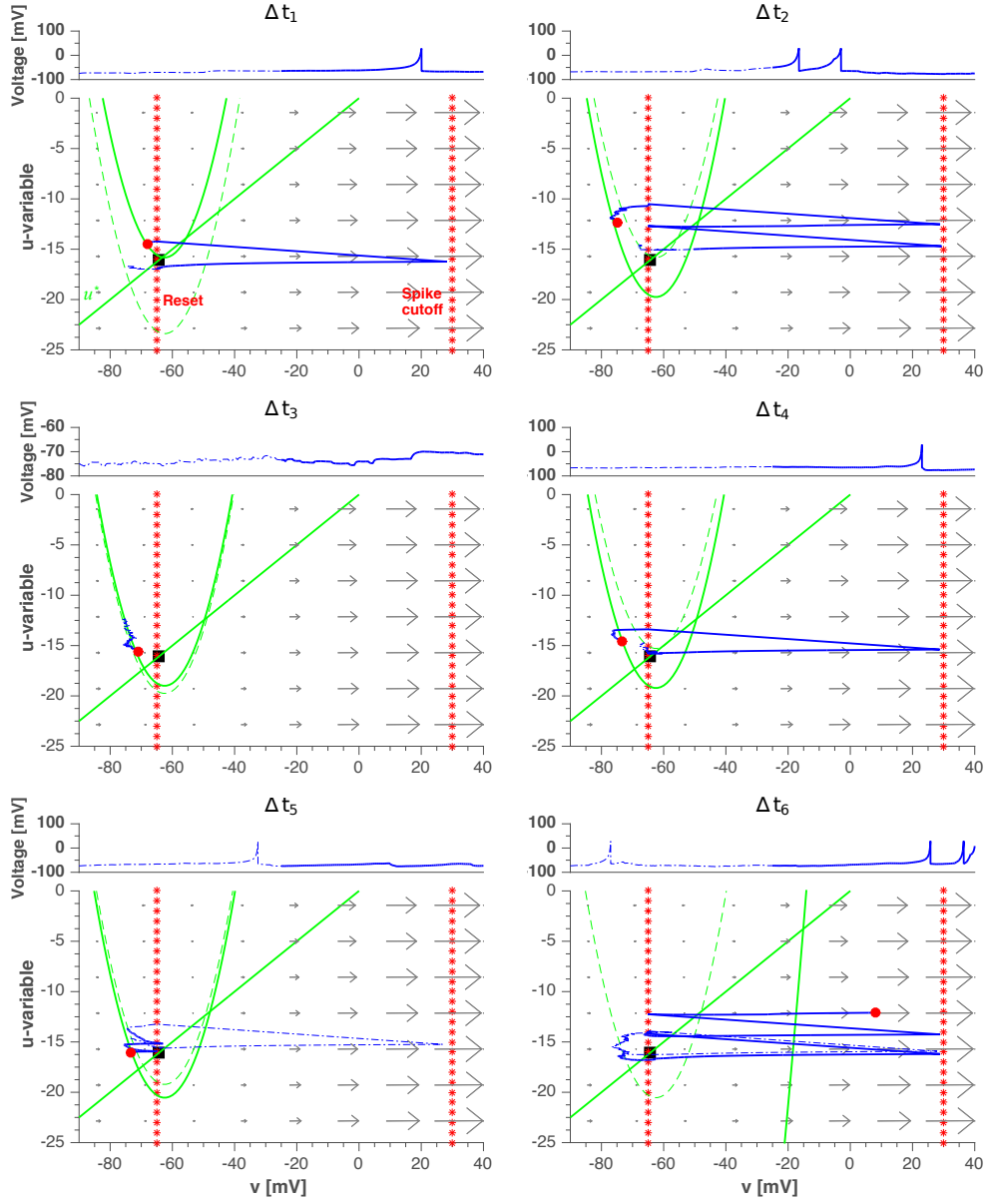
Figure 5.11: *Single neuron phase plane depiction of a neuron that fires during all periods in the synaptic noise setup. Each panel contains voltage series and dynamics on the phase plane of neuron # 69 for the same time range (3800–4400 ms) and the same six time intervals of 100 ms as for the neuron in Fig 5.10. Arrows in the plot indicate ($\dot{v}, \dot{u}$). Blue dashed line: the first 50 ms of evolution. Blue solid line: the last 50 ms of evolution. Red circle: location of the neuron at the end of the time interval. Black square: location of the state of rest with $v = v_{rest}$ and $u = u_{rest}$. Dotted red lines: reset value of voltage and spike cutoff. Green lines: Nullclines $\bar{u}$ and u^*, according to Eq (5.5). The location of the parabolic nullcline $\bar{u}$ is time-dependent; its position at the beginning (respectively, end) of Δt_i is shown with dashed (respectively, solid) green line.*

it receives less inhibition from its presynaptic neurons, which, like the typical neuron in Fig 5.10, are relaxing toward rest. Due to synaptic noise or eventual inputs from other similar neurons, the neuron $\#$ 69 fires at a low rate during the down state.

- Interval Δt_2: When the network enters the up state (second half of the time interval), the neuron is again strongly inhibited and emits fewer spikes than a typical neuron.

- Interval Δt_3: The network up state continues and ends, whereas the neuron has a low probability of firing.

- Interval Δt_4: This is the middle of the quiescent period. Note that by the end of the time interval the nullcline $\bar{u}$ moves down, indicating a net inhibitory input to the neuron (an early sign of the recovery of network activity which will come in the next time steps). Even weak synaptic noisy inputs can make it fire. Since the firing rate depends on the synaptic noise level, the duration of the quiescent period depends on it as well.

- Interval Δt_5: The situation is still as in the last time interval, but now we see a clear sign of the strong inhibition received by the neuron. After a spike in the first half of the time interval, when it is close to emitting a new spike, the neuron receives a strong inhibitory kick which hyperpolarizes its voltage and prevents the spike. The voltage grows again but another strong inhibitory impulse serves for the next setback. The inhibitory inputs come from neurons in the pool of presynaptic inhibitory neurons to $\#$ 69, which are starting to "wake up" on the eve of a new active period. As a consequence of the inhibitory inputs, the nullcline $\bar{u}$ moves further down.

- Interval Δt_6: The network enters the up state of an active period and most neurons are active again (like the typical $\#$ 240 in Fig 5.10). This makes $\#$ 69 fire but because of the heavy inhibition, not at a high rate of the typical neuron. Evidence of the strong increase in the inhibitory input received by this neuron comes from the dramatic downward movement of the nullcline $\bar{u}$ out of the scale of the plot.

Excitatory neurons like the one in Fig 5.11, which fire at low rates at all periods, will be called here "quiet" neurons (elsewhere, in the context of the deterministic setup, we called them "moderately active neurons" (Tomov et al., 2016)). Quiet neurons are fewer than typical neurons; for the network of Fig 5.7, they, on the average, constitute about a quarter of the population.

The sequence of events depicted in Fig 5.11 underscores the importance of inhibition and synaptic noise in shaping the network activity during both down states and quiescent periods. Strongly inhibited during up states, the quiet neurons become disinhibited by the end of those states and serve as a source for most of the spikes occurring during down states and quiescent periods. Thus, the firing pattern in the down states and quiescent periods is basically due to the recurrent excitatory synaptic connections among quiet neurons. The weak noise limit (cf. Fig 5.4) discloses the nature of the intrinsic activity pattern generated by the population of quiet neurons: it is highly asynchronous and non-oscillatory; remarkably, it is also weak. This confirms, on the one hand, that the population of quiet neurons is small, and explains, on the other hand, why the network activity during down states and quiescent periods is asynchronous and irregular.

Due to the weakness of intrinsic activity of quiet neurons, the likelihood that their pool can trigger a high firing (up) state in the network is low and the synaptic noise level plays a pivotal role in controlling this likelihood. At low synaptic noise level, the weak activity of the quiet neurons can restore the up state when the network is at a down state, but this can be repeated generating a sequence of up-down oscillations only for a short transient time. After the transient the network enters a quiescent period: a persistent low activity regime characterized by asynchronous non-oscillatory activity. When the network is in a quiescent period, the activity of the quiet neurons is too weak to start a high firing state in the network; a certain minimal synaptic noise level is necessary to trigger this state. In the absence of this minimal synaptic noise level, the network activity remains in the quiescent regime as seen in the diagrams of Figs 5.5 and 5.6. When the synaptic noise intensity increases above minimum level, the recurrent excitation amongst quiet neurons gets stronger, as well as the synaptic noise inputs to typical neurons, and the probability of the network exiting a quiescent period increases.

The above discussion highlights a fundamental difference between down states and quiescent periods. In the weak synaptic noise regime, when the network activity is dictated by quiet neurons, their weak agitation is able to restore a high firing state in the network when the latter is in a down state but not when it is in a quiescent period. This phenomenon bears some similarity to the behavior observed previously by us in deterministic networks of two-dimensional nonlinear integrate-and-fire neurons in the absence of external inputs (Tomov et al., 2014, 2016). There, the network state oscillates for a transient time between up and down states, before decaying to rest (cf. the behavior of the network in the deterministic setup in Sect. 5.3.1). The decay to rest always occurs when the state of the network in its high-dimensional deterministic phase space passes through a particular region of the phase space (a "hole") which, when represented in the two-dimensional space of average voltage $\langle v \rangle$ and recovery $\langle u \rangle$ variables, overlaps with the region traversed by the network when it is in a down state (Tomov et al., 2016). The analogy between down/rest state for the deterministic network without external input and down/quiescent state for the network in the synaptic noise setup suggests a further analogy between the hole in the high-dimensional phase space of the deterministic network and a hole in the high-dimensional phase space of the stochastic network. The difference is that when the network state in the stochastic high-dimensional phase space falls into its corresponding hole it escapes to a quiescent state instead of the resting state, and it can leave this quiescent state when the synaptic noise intensity is above a minimum level.

To show that the recovery variable u has a stronger impact on the cessation of activity than the inhibitory neurons, in Fig 5.12 we compare the effects of this variable and the synaptic currents I_{syn} on the same neurons as in Fig 5.7. In Fig 5.12 we present for selected time points both variables (u, v) for 200 neurons randomly picked from the network, and their total synaptic input I_{syn}.

The first row in Fig 5.12 refers to an up-down transition: For $T = 3880$ ms, which is the middle of the up state, some neurons have high values of u (due to the constant increments the u variable receives after each spike, cf. Eq. (2.4)) and consequently strong negative feedback. The consequence of this negative feedback is to hyperpolarize the neurons, which can be seen in the graphs for $T = 3900$ and
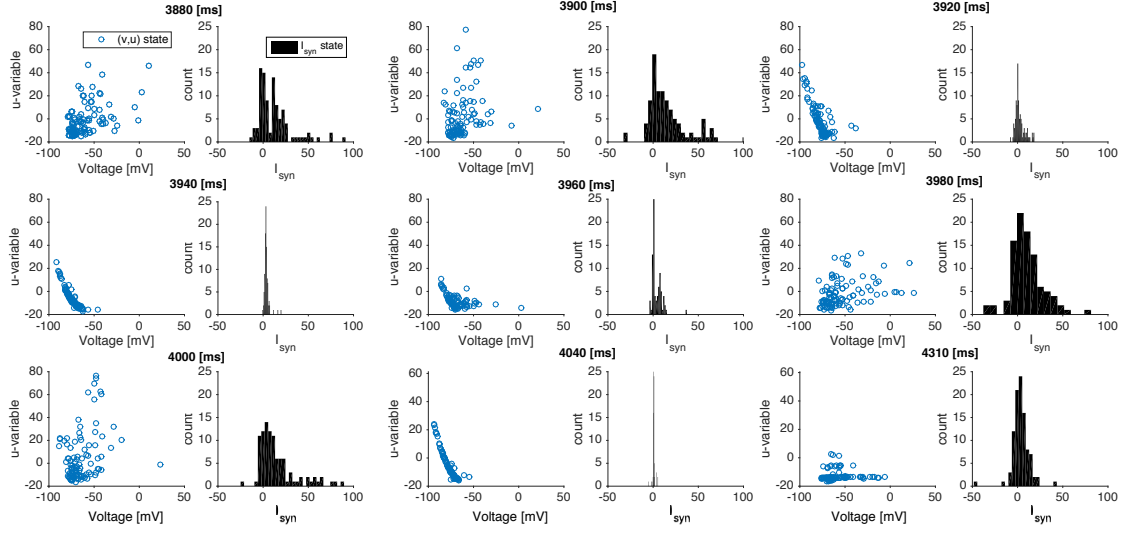
Figure 5.12: *Distribution of the neuron variables and synaptic current at different moments of time. Data in each panel come from 200 neurons pooled together from the same network simulation in Fig 5.7. For different time instants, indicated atop every coupled subpanel, the figure presents scatter plots (left subpanel) of instantaneous (v,u) values, indicated as a blue circles, and histograms (right subpanel) of instantaneous I_{syn} values.*

3920 ms where the voltages progressively move to the left of the graph. As to the I_{syn} histograms, they are mostly dispersed around positive values (with a reduction in the dispersion as T increases) indicating a low inhibitory activity. This confirms an earlier observation that the inhibitory neurons are not the main responsibles for the up-down transition (Tomov et al., 2016). The second row in Fig 5.12 refers to the down-up transition: for $T = 3940$ ms, most neurons are hyperpolarized and the synaptic currents are sharply concentrated around zero, confirming that very few neurons (the quiet ones) are spiking, as shown in Fig 5.7. As time increases, the distribution of neurons in the (v, u) plane becomes more disperse and the voltages v move to depolarized values. This indicates that the neurons are free (without negative feedback) to spike again. Meanwhile, the distribution of synaptic currents widens-up and is dominantly excitatory (although there are some inhibitory currents). The third row in Fig 5.12 refers to the quiescent state: from $T = 4000$ to 4040 ms, the variable u moves down and v moves to hyperpolarized values. As observed in Fig 5.7 for the same condition, there are very few spikes. Only after about 300 ms the voltages start to grow again and firing is re-started in a new active

period.

5.3.5   Influence of synaptic noise upon different states

Having demonstrated in the previous section that synaptic noise affects different phases of activity, we now proceed to a quantitative description. We compute the average duration of active and quiescent periods in sufficiently long (we take the value of 6×10^5 ms) trials. Mean duration is an important measure to characterize and model alternating states, e.g. in the course of transitions between brain rhythms (Lo et al., 2002; Ahn & Rubchinsky, 2013).

Results of simulations confirm that the duration of stay in both active and quiescent periods is affected by the synaptic noise level (Fig 5.13), but in a twofold way: the growth of noise intensity lengthens active periods and shortens the quiescent ones. This implies that synaptic noise influences transitions between the states. Remarkably, the average duration of stay in the quiescent state rapidly falls at the increase of small noise amplitude but seems to reach a certain saturation at moderate noise intensities. Apparently, the minimal time that the neurons need to organize a new collective activity is dynamically constrained by the network topology and deterministic characteristic times in the phase space: in the studied case it cannot be made lower than $\approx$ 80-100 ms.

Depending on the network composition, action of synaptic noise upon the average duration of active and quiescent periods can be weaker or stronger. Although the same common qualitative tendencies persist, quantitative aspects depend on the types of participating neurons as well as on proportions between them. An exemplary comparison is shown in Fig 5.14. Simulations with two types of inhibitory neurons indicate that the LTS neurons, compared to the FS ones, seem to postpone the termination of the active period (top left panel): at low noise the duration of oscillatory activity is higher if LTS neurons are present. This implies that inhibitory neurons influence the transition from active to quiescent period. In contrast, the duration of the quiescent period (bottom right panel) displays no dependence on the type of inhibitory neuron: the corresponding curves in the plot nearly coincide. This indicates that the transition from quiescent to active period is regulated exclusively by excitatory neurons. Indeed, since inhibitory neurons cannot excite a network,
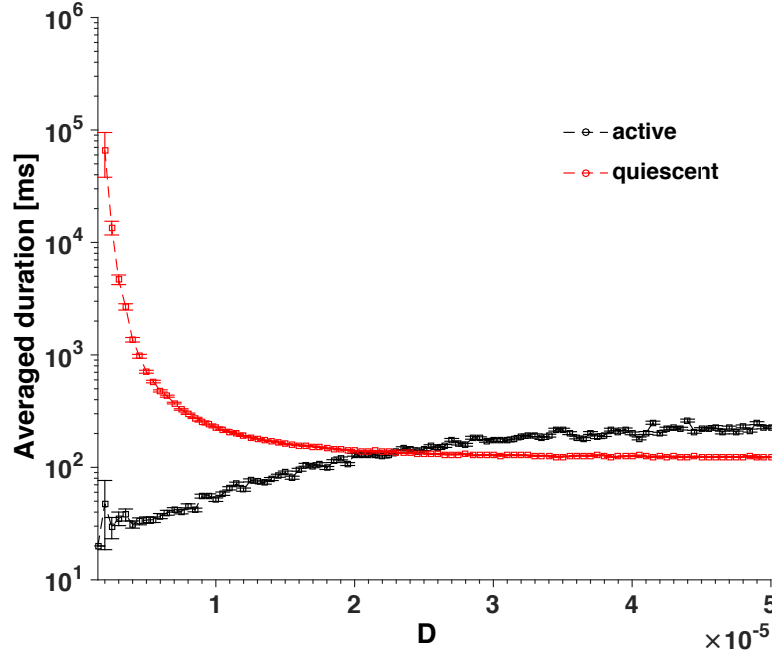
Figure 5.13: *Synaptic noise intensity affects the mean duration of active and quiescent periods. Curves show average durations of active and quiescent periods over the simulation of 10 min as a function of synaptic noise intensity. All inhibitory neurons are of LTS type. Synaptic noise intensity varies in the range $0.05 \times 10^{-5} \leq D \leq 5 \times 10^{-5}$ in discrete steps of size $\Delta D = 0.05 \times 10^{-5}$. Error bars: standard error.*

every period of stay in the quiescent period should be interrupted by an excitatory neuron, or by a group of excitatory neurons.

Introducing diversity among excitatory neurons, we observe certain quantitative changes as well. By replacing 20% of RS neurons by CH neurons, we obtain a network built of 16%CH, 64%RS and 20%LTS. This composition is much less sensitive to the action of synaptic noise. The tendency of growth of active periods under increase of noise is practically absent (see top left panel in Fig 5.14), and at all values of D the average active period is shorter than the corresponding silent one. As for the latter, however, there is a systematic shift. Compared to the case when the whole excitatory population is of the RS type, in the mixture with CH neurons the mean duration of quiescent periods decreases to lower values, below 10^2 ms. This decrease is a combination of synaptic noise- and network-related effects. A quiescent period ends whenever synaptic noise or some of the few quiet excitatory neurons which fire during the quiescent period (or both) drives across the firing threshold one of the majority of typical excitatory neurons which are at rest,
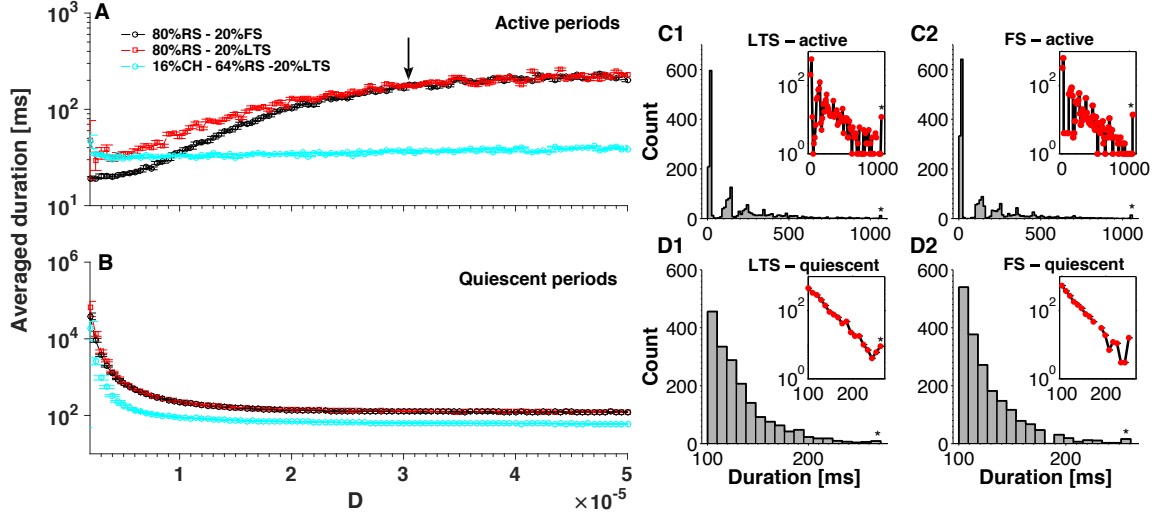
Figure 5.14: *Network composition influences the average duration of stay in active and quiescent periods. **A-B**: Dependence of duration on noise intensity. Legend in the plot indicates the network composition. Curves: average values over the simulation of 10 min. Error bars: standard error. **A**: active periods. **B**: quiescent periods. The value $D = 3 \times 10^{-5}$, denoted by the arrow, is used for calculation of histograms in panels **C1-2** and **D1-2**, characterizing distributions of stay duration in different periods. Stars at the end of the histograms are outliers. Insets show logarithmic representations of the ordinate.*

provided that this neuron is able to activate its postsynaptic neighbors and initiate thereby a wave of activity. If the neighbors fail to fire, the quiescent period continues. The mean time required for the first neuron to fire is the same for the RS and the CH neuron (see Sect.5.3.2.1). However, the RS neuron issues just one isolated action potential, whereas the CH neuron generates a series of spikes, raising with each of them the conductances of its postsynaptic neighbors and creating thereby conditions for their activation and subsequent collective spiking. In this sense, a burst of a CH neuron has higher chances to initiate common activity than a spike of a RS neuron. Therefore, in a network with CH neurons the quiescent periods end earlier. This confirms our conjecture that excitatory neurons influence the length of quiescent periods.

Histograms of duration of stay in the active period in Figs 5.14 **C1-2** show exponential distributions but are somehow fractured (cf. the logarithmic representations in the insets). Distributions of this kind have been reported previously (Duc et al., 2015; Tomov et al., 2016). In the former case the authors related cessation of activity to passages through a specific region in the phase space

of their deterministic network (the "hole" mentioned above), explaining thereby the quantization of cessation times. In our case, the behavior of the system is similar. Assuming the picture of a hole in the network phase space through which the network can escape from active to quiescent state, and a synaptic noise level high enough to allow multiple transitions from quiescent to active state, the quantization of active period durations can be explained keeping in mind that an active period is made of up-down cycles, each one with the same approximate period T. Since the escapes from active to quiescent state always occur at the end of an up-down cycle, the duration of an active state can only increase by integer multiples of T. The distributions of stay duration in the quiescent period, shown in Figs 5.14 **D1-2**, possess exponential character as well, but without a fractured shape. This can be explained by the non-oscillatory nature of the quiescent periods.

Let us have a look at shorter timescales: what happens *inside* the active periods? How does noise influence the collective up and down states? In Fig 5.15 we show dependence of average durations of stay in the up and down states on the noise intensity D, in the same range of D as in Figs 5.13 and 5.14. Whereas the average stay in the down state gets shorter under the growth of noise, lifetime in the up state almost does not change.
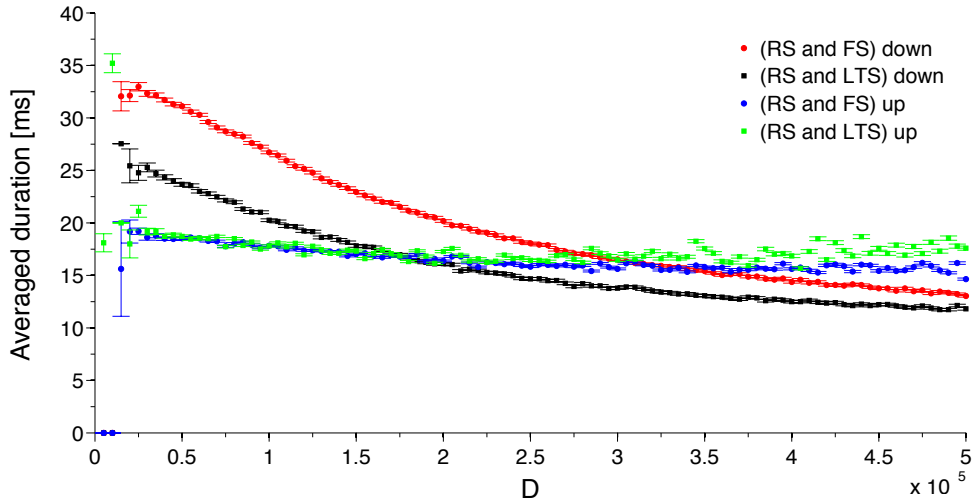

Figure 5.15: *Average duration of stay in the up and down states as a function of noise intensity.* The network contains RS excitatory neurons and either FS or LTS inhibitory neurons. Curves: average values over the simulation of 10 min. Error bars: standard error.

The down state is the only state that is sensitive to the type of inhibitory neuron. There is a clear shift upwards (see red and black curves) if the LTS neurons are replaced with FS ones. This means that transitions from the down state happen faster in the presence of LTS neurons. The sensitivity of the down state can be related to the interpretation in (Tomov et al., 2016) where the cessation of self-sustained oscillatory activity was assigned to passages through a small region of instability (the hole), located in the phase space close to the down state. In our current synaptic noise setup, the more noise, the higher the disturbance in the region of instability at the down state and the shorter its lifetime.

5.3.6 Comparison with other neuron models

We expect the above results on intermittent transitions between states that are active-quiescent and the role of noise upon these transitions to stay qualitatively valid in networks based on other two-variable integrate-and-fire-type neuron models. To support this conjecture, below we apply the same procedure as in Fig 5.7 to the adaptive exponential integrate-and-fire (AdEx) model (Brette & Gerstner, 2005; Gerstner et al., 2014).

The AdEx model is a two-variable neuron that differs from the Izhikevich model by the equation for voltage: instead of a polynomial dependence on v, the AdEx features the exponential one. To run the AdEx network under the same conditions as the Izhikevich one without having to re-scale either the synaptic variables or the noise amplitude, we write the AdEx equations so that the input-frequency relationship and nullclines $\bar{u}$ and u^* are similar to the ones from the Izhikevich model, leading to:

$$
\begin{cases}
\dot{v} &= -g_L(v - E_L) + g_L \Delta_T \exp\left(\dfrac{v - v_T}{\Delta_T}\right) - 46 - u + I(t) \\[2mm]
\dot{u} &= a(b\,v - u),
\end{cases}
\tag{5.6}
$$

where $\Delta_T = 30$, $g_L = 1$, $v_T = -65$, and $E_L = c$. The parameters (a,b,c,d) are the same as in the Izhikevich model. Along with Eq. 5.6, the model includes the fire-and-reset rule given by Eq. 2.4. A comparison of the Izhikevich nullclines to the AdEx nullclines is performed in Figs 5.16 **A** and **B** where one can see that, for

these chosen parameters and at the resting state ($I = 0$), the fixed points for the two models are very close and the shape of the nullcline $\bar{u}$ is similar.
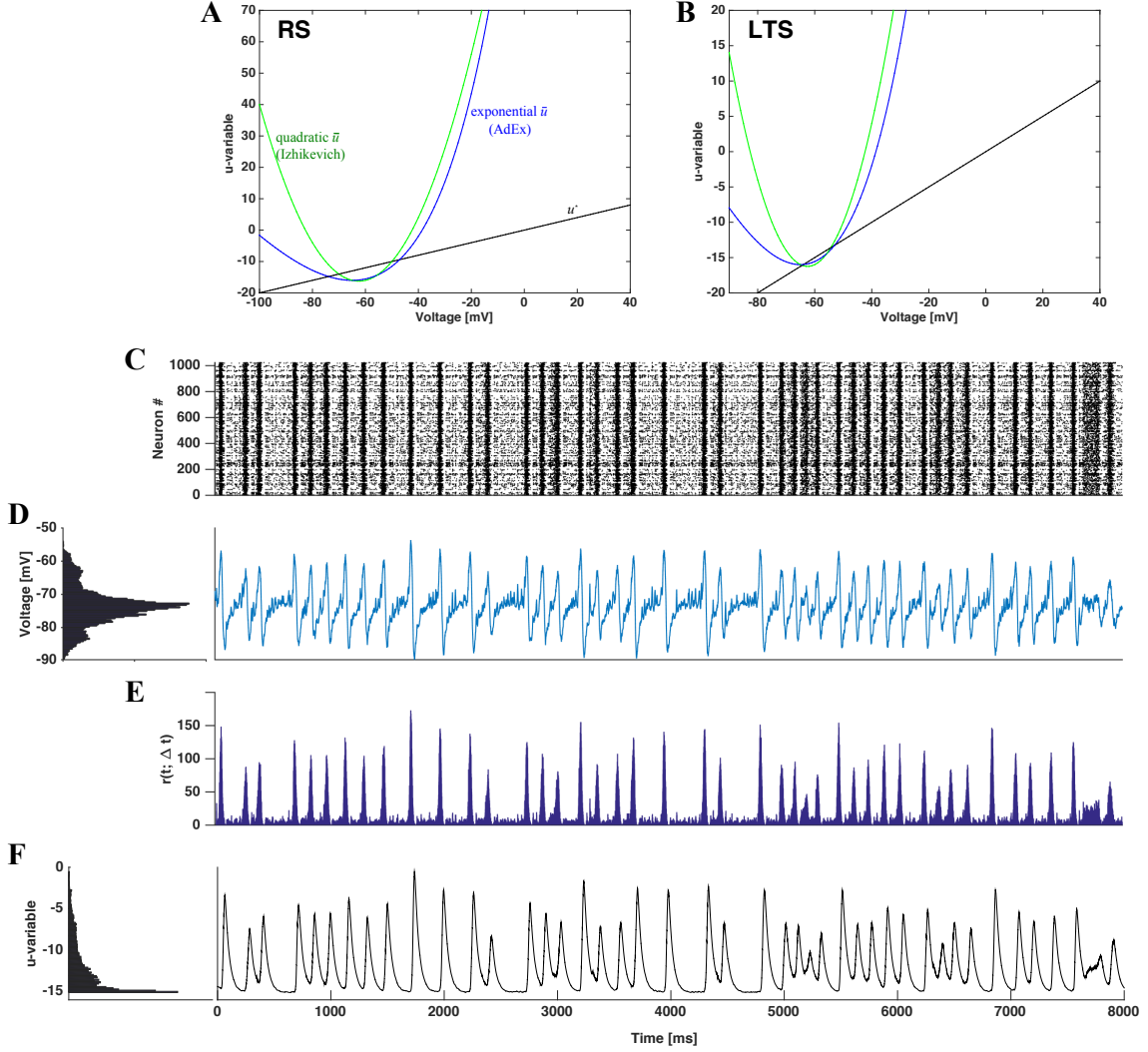
Figure 5.16: Intermittent transitions between active and quiescent regimes in the presence of synaptic noise for network with AdEx neurons. *The network is composed of two AdEx neuron types: the excitatory (RS) and the inhibitory (LTS), in the same proportion 4:1 as in the other networks of this work. Panels **A** and **B**: nullclines on the phase plane, drawn for the Izhikevich and the AdEx models for RS (**A**) and FS (**B**) neurons (see parameters in the text). Panel **C**: raster plot for a network simulation under synaptic noise with $D = 1 \times 10^{-5}$. Panel **D**: averaged voltage histogram (left) and time course of averaged voltage over all network neurons (right). Panel **E**: $r(t; \Delta t)$ extracted from all neurons in the network. Panel **F**: Recovery variable u. Histogram (left) and course of $u(t)$ over all network neurons.*

In Figs 5.16 **C-F** we see a qualitatively close behavior to Figs 5.7 **A-D**: raster plots with $r(t; \Delta t)$ indicating that active (oscillatory) and quiescent (non-oscillatory)

behaviors are switching sporadically, with voltages fluctuating among three different positions (hyperpolarized, resting, and depolarized), and recovery variable u oscillating and featuring accumulation depending on the period. A noticeable difference however occurs when the average voltage in Fig 5.16 **D** for the AdEx model is compared to the one in Fig 5.7 **B** for the Izhikevich model: for the AdEx model the voltage does not stay long enough in the hyperpolarized or depolarized states to create corresponding prominent peaks in the histogram (the peak for resting voltage is much more prominent). This difference is related to the integration of the AdEx neuron model, where the growth of voltage follows an exponential law, which is much faster than the quadratic one. This effect is reflected as well in the average voltage: the peaks and troughs are sharper than those for the Izhikevich neuron model.

5.4 Discussion

Networks of LIF neurons have been extensively scrutinized in the literature to understand their properties under different conditions (Brunel, 2000; Mattia & Del Giudice, 2002; Vogels & Abbott, 2005; Cessac & Viéville, 2008; Wang et al., 2011; Litwin-Kumar & Doiron, 2012; Kriener et al., 2014; Ostojic, 2014; Potjans & Diesmann, 2014; Yim, Kumar, Aertsen, & Rotter, 2014; Landau et al., 2016; Jercog et al., 2017; Tartaglia & Brunel, 2017). Much fewer works have been devoted to systematic investigations of networks of other spiking neuron models. Here we have studied networks of Izhikevich neurons in the presence of synaptic noise. We have found in these networks a rich variety of activity patterns, consisting of synchronous and asynchronous non-oscillatory states and oscillatory states with variable degrees of synchrony. Moreover, these networks exhibit intermittent noise-induced transitions between oscillatory and quiescent states. These transitions are irregular and affected by the synaptic noise level and the network composition.

A systematic analysis of time series, plots of neuron spikes, firing rates, average voltage and membrane recovery variable, and power spectra revealed the characteristics of the oscillatory and quiescent states, similar to observed cortical states (Steriade et al., 2001; El Boustani et al., 2007; Greenberg et al., 2008; Harris &

Thiele, 2011; Sanchez-Vives et al., 2017): during oscillations the membrane voltages of the neurons fluctuate between hyperpolarized (down) and depolarized (up) states like in the so-called "synchronized" states seen in *in vivo* preparations and during slow-wave sleep and anesthesia; in the quiescent state neurons display very low and irregular spiking activity like in the so-called "desynchronized" states seen in quiet rest. As far as we know, phenomena like oscillations between hyperpolarized and depolarized states, and noise-induced intermittent transitions between oscillatory and low activity regimes have not been reported in networks of LIF neurons.

By using the single neuron phase space representation of network dynamics combined with statistical assessments of duration of stay in the oscillatory and quiescent states, we were able to explain the roles played by synaptic noise and network composition in the durations of these states and the transitions between them. Besides, we also were able to explain the origin of the up and down oscillations and the asynchronous non-oscillatory nature of the quiescent states.

Up and down states, in which the average voltage of network neurons is, respectively, depolarized and hyperpolarized, occur during oscillatory (active) periods in the network. They can be understood in terms of the single neuron phase space in the same way as explained in the noiseless case (Tomov et al., 2016). During an up state, when most of the neurons fire tonically, the parabolic-shaped voltage nullcline is kept in the upper part of the phase plane while the recovery variable moves steadily upwards due to neuronal firing. Eventually the neuron finds itself inside the area bounded by the voltage nullcline; it is forced to move to the hyperpolarized region of the phase plane and then downwards, relaxing towards rest. This corresponds to a down state. In the latter, the activity of the network is sustained by quiet neurons, which were inhibited during the up state and became disinhibited during the down state. In the course of time, firing of the quiet neurons is able to excite some of the relaxing post-active neurons; this triggers a new wave of excitation in the network, starting the next up state. This mechanism strongly depends on the recovery variable and its instantaneous increment (cf. Eq.(2.4)), which causes spike-dependent adaptation (Izhikevich, 2007). Together, they constitute a sort of intrinsic negative feedback mechanism which decreases network excitability during the up state, as proposed by other authors in different

contexts (Contreras, Timofeev, & Steriade, 1996; Sanchez-Vives & McCormick, 2000; Bazhenov, Timofeev, Steriade, & Sejnowski, 2002; Compte, Sanchez-Vives, McCormick, & Wang, 2003; Hill & Tononi, 2005; Holcman & Tsodyks, 2006; Parga & Abbott, 2007; Benita, Guillamon, Deco, & Sanchez-Vives, 2012; Chen, Chauvette, Skorheim, Timofeev, & Bazhenov, 2012; Ghorbani, Mehta, Bruinsma, & Levine, 2012; Mattia & Sanchez-Vives, 2012; Jercog et al., 2017; Tartaglia & Brunel, 2017; Levenstein, Buzsaki, & Rinzel, 2018).

The basic mechanism behind up and down oscillations is acting in both the deterministic and the synaptic noise setups. Thus, up-down oscillations are caused not by synaptic noise but by the intrinsic dynamics of the network. Disclosure of the same basic dynamical properties in the network with AdEx neurons (Sect. 5.3.6) allows to expect that this mechanism is common for networks populated by neurons with adaptation variables. In line with what has been pointed out elsewhere (Harris & Thiele, 2011; Mattia & Sanchez-Vives, 2012; Jercog et al., 2017), the up/down oscillations result from an interaction between recurrent synaptic connections and adaptation.

Interestingly, the comparison between networks populated with Izhikevich and AdEx neurons indicates some differences between them: although the global dynamical behavior of the two networks is similar, the local voltage profile of their neurons is different (cf. Fig. 5.7 **B** and Fig. 5.16 **D**). To the best of our knowledge, this is one of the first times in which the Izhikevich and AdEx neuron models are compared through their effects on the network.

The major difference between the deterministic and the synaptic noise setups is that in the deterministic case the oscillations are transient, while in presence of noise they become persistent. But the durations of the up and down phases and an up-down cycle are approximately the same, depending only on the characteristics of network neurons.

The up-down oscillations can be seen as a sort of default activity mode (Sanchez-Vives et al., 2017) of the system (at least in the region of the parameter space considered here). In the deterministic, noiseless, setup this activity eventually dies out, preceded, as we have shown, by the passage of the system through a specific region of its phase space we called a "hole" (Tomov et al., 2016). Through

the hole, located close to the domain traversed by the system during a down phase, the system can escape the up-down oscillations and decay to rest. In the noiseless case the system sooner or later gets into the hole and the network activity dies out. In the synaptic noise setup, this hole-like region in the network's high-dimensional phase space still exists but because of the noise the system does not decay to rest when it passes through it; instead, the system is dragged to the quiescent state.

As in the down state, in the quiescent state the network sustains activity, internally generated by quiet neurons via their recurrent synaptic connections and regulated by the synaptic noise level: it is weak for weak synaptic noise, and strong for strong synaptic noise. Being dictated by noise, activity during a quiescent period is asynchronous and irregular. Because of the passage through the hole the quiescent state has, in general, a longer duration than the down state. Hence, typical neurons which are relaxing in the hyperpolarized region of the single neuron phase space have time to decay to the phase space region around rest. This explains why during quiescent periods the average voltage is close to the resting voltage and is not hyperpolarized as in the down states. For weak synaptic noise, activity generated by the quiet neurons is insufficient to take the network out of the quiescent state: the system remains inactive. For moderate to high synaptic noise intensities, activity of quiet neurons gets stronger and even the neurons that are close to rest can fire, so eventually the global activity is reignited and an up state commences.

The basic effect of the synaptic noise level is to increase/decrease the average duration of the quiescent periods. In other words, synaptic noise can act as a facilitator of transitions between quiescent and active states, and the intermittency between these states results from the stochastic nature of the neuronal firing during quiescent periods as well as from the irregularity of trajectory of the system in its high-dimensional phase space (that determines whether it will hit a hole). Once the system enters the hole, the duration of stay in the quiescent state depends on the noise intensity. For very low noise, the system stays in the quiescent state essentially forever, displaying only residual activity (see Fig 5.4). For moderate to high noise, the system eventually leaves the quiescent state and the up-down oscillations resume. The residence time in the quiescent state gets smaller as the synaptic noise intensity increases. For very strong noise the system may not even enter the hole because,

in such a case, both typical and quiet neurons have high probability of firing at all moments. This explains the disappearance of quiescent periods in the high noise regime. For still higher levels of synaptic noise intensity, even the down periods disappear and the network features constant activity.

Our study also indicates that inhibition affects transitions from active to quiescent periods and the duration of down states. Average stay in the down states is shorter when the inhibitory neurons of the network are of the LTS type than when they are of the FS type (cf. Fig 5.15). This may be related to experimental evidence showing that inhibitory neurons control cortical oscillatory up and down states (Sanchez-Vives et al., 2010). The authors of that study progressively blocked inhibitory cells during a spontaneous up state and showed that this blockage shortened the duration of up states and enlarged the duration of down states. Since the LTS neurons respond to noise faster, a replacement of all LTS neurons in the network by FS neurons can be viewed as a reduction of inhibition; thereby, the corresponding increase of the average duration of down states relates our observations in the model to the experimental evidence. Similar transitions from the up to the down states have been studied before (Holcman & Tsodyks, 2006; Xu, Ni, & Wang, 2016).

One of the objectives of our study was to check whether dynamics in the network of neurons with adaptation is sensitive to the composition of the network and the electrophysiological types of individual neurons. Generic qualitative features of dynamics, like intermittent oscillations between active (up/down) and quiescent states, shape of power spectra, etc, turned out to be persistent for all neuronal subtypes as well as for their mixtures; on the individual level this can be traced back to the common shape of the nullclines. At the same time, we established that certain quantitative measures (like average durations) depend on the proportions of neuron types.

For noise, there are many ways to enter a neural network model (Faisal et al., 2008; Longtin, 2013; Destexhe & Rudolph-Lilith, 2012; Brochini et al., 2016; McDonnell, Goldwyn, & Lindner, 2016). In this work we considered the variant in which it affects the synaptic variables. By doing so, we were able to study the effect of noise at the molecular level on the behavior of the system at the

network level. Since noise at the synaptic level is related to fluctuations in the release of neurotransmitters and the amplitude of miniature postsynaptic currents (Rao et al., 2007; Liu et al., 2010; Tononi & Cirelli, 2014; Kavalali, 2015), which are phenomena at scales of magnitude much smaller than the scale of voltage changes, the weak noise intensities D we considered here capture very small noisy events. Furthermore, because synaptic noise is filtered by the conductance variables, its effect upon neuronal voltages is akin to colored noise input, which is more biologically realistic than if noise were added, via e.g. Poisson processes, to neuron voltages directly.

Our work captures mechanisms at different levels of neural processing with potential contribution to current endeavors to model multiscale brain mechanisms and their role on normal and pathological function (Mejias, Murray, Kennedy, & Wang, 2016; Neymotin et al., 2016; Lytton et al., 2017; Schwalger, Deger, & Gerstner, 2017). As an example, the synaptic noise-induced switches between periods of oscillatory and irregular activity might give support to fast formation and destruction of cell assemblies.

AN ITERATIVE HETEROGENEOUS SELF-CONSISTENT SCHEME THAT EXPLAINS THE EMERGENCE OF SLOW FLUCTUATIONS

6.1 Introduction

The autonomous dynamics of recurrent networks of spiking neurons is an important topic in computational neuroscience. Networks of randomly connected excitatory and inhibitory integrate-and-fire (IF) neurons are often used in the study of this problem, because this model is computationally efficient for numerical simulations and even sometimes permits analytical insights (see e.g. (Abbott & van Vreeswijk, 1993; Brunel, 2000; Lindner, Doiron, & Longtin, 2005; Richardson, 2009; Deger, Schwalger, Naud, & Gerstner, 2014)). Exploring the possible spike statistics in such network models may help us to further our understanding of healthy and pathological neural activity in different brain areas and brain states. Moreover, understanding the autonomous (i.e. spontaneous) activity is also a necessary prerequisite for the comprehension of the network response to external signals and signal transmission and processing capabilities of the network in general.

Recurrent networks of IF neurons can already show a rich repertoire of activity states (Brunel, 2000) shaped by pronounced synchronization and by oscillations on which many computational studies have focused (see e.g. (van Vreeswijk, Abbott, & Ermentrout, 1994; Hopfield & Herz, 1995; Ermentrout, Pascal,

& Gutkin, 2001; Timme, Geisel, & Wolf, 2006; Ladenbauer, Augustin, Shiau, & Obermayer, 2012)). One state that lacks obvious collective effects but still can show a statistically rich behavior is the asynchronous state with low or absent cross-correlations among neurons. This state is found in many network models (van Vreeswijk et al., 1996; Brunel, 2000; Renart et al., 2010; Helias, Tetzlaff, & Diesmann, 2014) and also in experimental recordings in different brain areas in the awake and attentive animal (Poulet & Petersen, 2008; Harris & Thiele, 2011).

Although it is frequently assumed in theoretical studies, approximating the asynchronous activity as Poisson spiking with a total lack of temporal correlations is generally not justified. Despite the characteristic absence or weakness of *spatial* correlations among neurons, neural spike trains in the asynchronous state can still show a pronounced *temporal* correlation: experiments have revealed non-flat (i.e. non-Poissonian) spike-train power spectra exhibiting reduced power at low frequency (Edwards, Wakefield, & Powers, 1993; Bair et al., 1994), peaks attained at frequencies close to the firing rate and multiples (Pesaran, Pezaris, Sahani, Mitra, & Andersen, 2002) or increased power at low frequencies indicating slow fluctuations or bursting (Bair et al., 1994). Some of these features (but also additional ones) have been found for spike-train power spectra from neurons in the sensory periphery (Neiman & Russell, 2011; Grewe, Kruscha, Lindner, & Benda, 2017) that lack synaptic input from other neurons but are subject to channel noise and other signal-unrelated fluctuations. Theoretically, some (but not all) of these spectral shapes can be already understood if we consider simple stochastic models, e.g. a Poisson process with refractory period (Bair et al., 1994; Jarvis & Mitra, 2001) or, more elaborate, integrate-and-fire models driven by white (Lindner, Schimansky-Geier, & Longtin, 2002; Richardson, 2008; Vilela & Lindner, 2009b) or colored noise (Middleton et al., 2003; Bauermeister, Schwalger, Russell, Neiman, & Lindner, 2013; Droste & Lindner, 2017a).

Interestingly, even if completely deterministic neuron models are connected in a random network, corresponding observations of random spiking can be made: the total chaotic input from the network impinging on the single cell acts as an effectively stochastic drive and the resulting spike-train power spectra exhibit in many cases a non-trivial (in particular, non-flat, i.e. non-Poissonian) shape. Depending on cellular

parameters as the reset value after spiking (Dummer, Wieland, & Lindner, 2014) or on the strength of synaptic coupling (Ostojic, 2014; Wieland et al., 2015), the spectrum can change drastically (e.g. from strongly peaked spectra to low-frequency dominated spectra with a $1/f^\alpha$ form). How spike-train power spectra depend on system parameters in a recurrent network is generally poorly understood (for some effects of presynaptic refractoriness, slow presynaptic rate changes and short-term synaptic plasticity, see (Schwalger, Droste, & Lindner, 2015), for effects of the postsynaptic refractory period, see (Bair et al., 1994; Franklin & Bair, 1995)). Some progress has been achieved though for a related but distinct statistics at a higher modeling level, namely, the power spectrum of the population activity, for which different approximations and numerical schemes have been put forward (Knight, 1972; Brunel & Hakim, 1999; Spiridon & Gerstner, 1999; Mattia & Del Giudice, 2002; Lindner et al., 2005; Trousdale, Hu, Shea-Brown, & Josic, 2012; Deger et al., 2014; Schwalger et al., 2017). In this thesis we focus exclusively on single spike-train power spectra.

According to early work by (Mari, 2000) and, particularly, by (Lerchner, Sterner, Hertz, & Ahmadi, 2006), a strong theoretical argument against the white-noise approximation is the self-consistency of the fluctuation statistics. If we think of a homogeneous network of statistically equivalent neurons (identical neural parameters and a fixed number of input connections as in the popular Brunel network (Brunel, 2000)), the output statistics of a cell should be related to the input statistics because in the network every driven cell is also a driving cell. In the simple case of current-pulse-coupled IF neurons without a synaptic filter (homogeneous Brunel network), the power spectrum of the input current should be proportional to the power spectrum of the spike train generated by the neuron. As the output power spectrum of a white-noise driven IF neuron is generally not flat (Poisson-like) (Lindner et al., 2002; Vilela & Lindner, 2009a) and, contrary to some claims in the literature, summing many presynaptic spike trains does not remove the temporal correlations of the single process (Lindner, 2006), the flat white-noise spectrum cannot be a self-consistent solution for the network neuron, unless all neurons are poised deep in the subthreshold fluctuation-driven regime of very rare firing (rates are smaller than 1Hz).

The self-consistency of the temporal correlations of input and output in random networks is not an entirely new idea: in statistical physics it has been used to derive correlation functions of disordered spin systems (Sompolinsky & Zippelius, 1982; Eissfeller & Opper, 1992); in neuroscience, it was applied to random networks of coupled rate units by (Sompolinsky, Crisanti, & Sommers, 1988) (for various recent extensions, see (Aljadeff, Stern, & Sharpee, 2015; Kadmon & Sompolinsky, 2015; Mastrogiuseppe & Ostojic, 2017)). Generally, the self-consistency condition of the asynchronous state can be employed to determine correlation functions or power spectra without actually simulating the network but by simulating a single element iteratively. If we make a Gaussian approximation for the incoming stream of input spikes, we may ask how correlated ('colored') this Gaussian noise has to be to evoke a neural spike train with a temporal correlation proportional to that of the driving noise; equivalently, we can ask about the proportionality of power spectra. This idea can be translated into an iterative scheme that finds this solution numerically (if it exists). Such a scheme has first been developed for a spin system (Eissfeller & Opper, 1992); in the neural context it works essentially as follows (Lerchner, Sterner, et al., 2006; Dummer et al., 2014): A single neuron is driven by a Gaussian noise, the output spike train is recorded, its power spectrum is estimated and serves to generate a new Gaussian noise to again stimulate the neuron in the next generation (step in the iterative scheme). Repeating this procedure over a few generations only, for a network with (nearly) balanced recurrent input and moderate synaptic amplitudes, yields an excellent quantitative agreement with the single-cell statistics of a neuron in a large network (Dummer et al., 2014) [(Lerchner, Sterner, et al., 2006) used the equivalent correlation function]. The simplest version of the procedure fails in the case of strong inhibition and is naturally restricted to homogeneous networks, in which all neurons (excitatory and inhibitory ones) share the same cellular and presynaptic connection parameters. Cortical neural networks are strongly heterogeneous (Meunier et al., 2010; Tomov et al., 2014; Harrison, Badel, Wall, & Richardson, 2015) and, hence, an extension of the method to cases in which neural and connection parameters vary across the network is desirable.

The purpose of the present study is to extend the iterative scheme in several directions. First, we develop a simple method to deal with the instability of the

iterative scheme at strong recurrent inhibition, which makes the scheme applicable to a much broader range of network parameters. Secondly, as sketched in Fig. 6.1, we study a heterogeneous network, in which excitatory and inhibitory neurons have different parameters (either cellular or with respect to their connectivity) or we consider even several (more than two) populations, which differ in their parameters. As indicated in Fig. 6.1, every population is then represented by a single cell in the iterative scheme, and the input statistics to each cell in a certain generation will be determined from all output spectra of the previous generation.
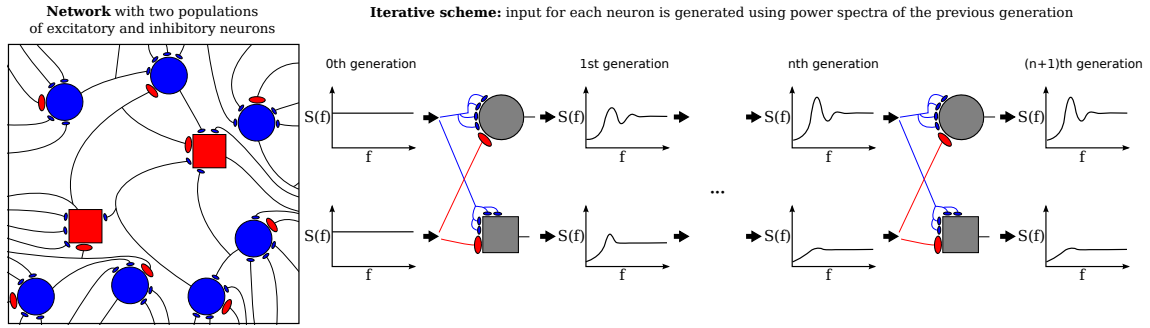
Figure 6.1: *Heterogenous network of excitatory and inhibitory neurons differing in intrinsic parameters. Sketch of the network (left) and the corresponding iterative scheme. where a single neuron is simulated to represent one population (right).The input of a neuron in the next generation is composed of all power spectra from the previous generations. The power spectrum of each population convergences after the nth generation.*

Our motivation for all these extensions of the method is twofold. For once, in cases in which the single-neuron correlation statistics is of interest, e.g. for the emergence of slow fluctuations in (Litwin-Kumar & Doiron, 2012; Ostojic, 2014; Wieland et al., 2015), our extended scheme provides a numerically efficient method that does not require large-network simulations. Hence, if the temporal correlation statistics of the asynchronous state is studied, our results permit to explore the role of network heterogeneity in shaping those correlations. The second purpose of our study is to trigger interest in the self-consistent description of the Gaussian colored noise generated by recurrent spiking networks. Showing that the numerical scheme works in a physiologically relevant parameter regime can also be regarded as a demonstration of the colored-Gaussian-noise approximation's validity and may encourage looking for an analytical description of the network noise via Markovian

embedding (Schwalger et al., 2015).

This chapter is organized as follows. The next section 'Methods' presents the neuron and network models and shows how to stabilize the iterative procedure such that it works also for strong recurrent inhibition and how to incorporate a synaptic filter, and extends the scheme to the different heterogeneous cases. In the following 'Results' section, we consider first the fluctuation statistics of the spike trains in the so-called 'heterogeneous asynchronous state' of a homogeneous network with strong recurrent inhibition (Ostojic, 2014). Here we demonstrate that slow fluctuations emerge due to their preferred amplification by the network. We review briefly the effect of a synaptic filter and then turn to the different heterogeneous cases. All power spectra found with the iterative scheme are compared to numerical simulations of large and sparse networks. We conclude with a brief discussion of our findings.

6.2   Methods

In this section, we introduce the network model with the notation that will be used in the remaining chapter. We also briefly explain the self-consistent iterative scheme as known elsewhere (Dummer et al., 2014; Wieland et al., 2015) and we follow explaining our extensions in the remaining subsections. Results start in the next section.

6.2.1   Network model

Different network compositions are studied, many of which are based on the work of (Brunel, 2000), specifically on his Model B, a heterogeneous random network with fixed in-degree. In contrast to (Brunel, 2000), we use a larger number of neurons, i.e. an excitatory population size $N_E = 10^5$ instead of $N_E = 10^4$. Independently of the number of populations, there is always a mixture of excitatory to inhibitory neurons with a ratio of 4:1, i.e. $N_I = \gamma N_E$ where $\gamma = 0.25$. Therefore, the total network size is $N = N_E + N_I$.

The ℓth neuron from the network has the dynamics

$$\tau_\alpha \dot{v}_\ell \;\; = \;\; -v_\ell + R\left(I_{loc,\ell} + I_{ext,\alpha}\right). \tag{6.1}$$

The external input current to each neuron and its membrane time constant depend on the population it belongs to which is here indicated by index α. The ℓth neuron receives a fixed number of C_ℓ^E (C_ℓ^I) excitatory (inhibitory) randomly selected neurons connections from population $\alpha = \{E, I\}$. The local input is described by:

$$RI_{loc,\ell}(t) = \tau_\alpha \left(\sum_{k=1}^{C_\ell^E} J_{\ell m_{\ell,k}} x_{m_{\ell,k}}(t - \tau_D) - g_\alpha \sum_{i=1}^{C_\ell^I} J_{\ell n_{\ell,i}} x_{n_{\ell,i}}(t - \tau_D) \right) * K(t), \quad (6.2)$$

where g_α is the ratio between average inhibitory and average excitatory synaptic weights, which depends via α on the target neuron ($\alpha \in E, I$) The number of presynaptic neurons $C_\ell^{E,I}$ will be always constant. The excitatory (inhibitory) input neurons are picked randomly from the network and the set of the neuron indexes is denoted by $m_{\ell,k}$ and $n_{\ell,i}$. The synaptic coupling strength (also called synaptic weight or synaptic efficacy) will be constant, $J_{\ell j} = J$. We fix the transmission delay at $\tau_D = 1.5$ ms unless otherwise indicated, and $K(t)$ is a an optional synaptic filter. In most cases, the filter is not used, which means $K(t) = \delta(t)$. Otherwise, it is a simple exponential filter:

$$K(t) = \theta(t) \frac{\exp(-t/\tau_s)}{\tau_s}, \quad (6.3)$$

where $\theta(t)$ is the Heaviside function and τ_s is the synaptic filter time. Note that in the limit $\tau_s \to 0$, the case without synaptic filter is recovered. If not explicitly stated otherwise, parameter values used in our simulations are given in Table 6.1.

6.2.2 The self-consistent scheme

In a large-scale recurrent network with sparse connectivity, we assume that the major source of noise that a single neuron receives comes from the quasi-random input from other cells in the network (see Sect. 2.3 for the different types of noise). In such a scenario, we encounter the following problem of self-consistency: for any arbitrary neuron picked in the network we should observe the same resulting activity, i.e. the statistics extracted from the input spike-trains should be proportional to the statistics (here identified by the second-order statistics given by autocorrelations) of the output spike-trains. The problem is schematically described in Fig. 6.2.

The iterative self-consistent scheme developed by (Lerchner, Sterner, et al., 2006) and (Dummer et al., 2014) is able to reproduce the single neuron spike-train

PARAMETERS

Network connectivity parameters

Name	Value	Description
N_E	10^5	Size of excitatory population
N_I	γN_E	Size of inhibitory population where $\gamma = 0.25$
C^E	1000	Number of excitatory synapses per neuron
C^I	γC^E	Number of inhibitory synapses per neuron

Neuron parameters

Name	Value	Description
v_{th}	20 mV	Firing threshold
v_t	10 mV	Reset potential
τ_R	2 ms	Refractory period
RI_{ext}	30 mV	External input

Table 6.1: *Summary of standard parameters for the iterative scheme with different populations.*

power spectrum for homogeneous populations close to the balanced regime. In this procedure, in one generation a single neuron is stimulated with a colored noise over many trials, the power spectrum of its spike-train is estimated, and using this spectrum and the output firing rate, a new surrogate colored Gaussian noise is generated which is used as the stimulus to the next generation. This procedure is repeated iteratively until the mean value and the spectrum of the driving noise matches in a self-consistent manner approximately to the firing rate and the power spectrum of the resulting spike-train. In Fig. 6.3 we summarize the procedure.

6.2.3 Self-consistent scheme for a homogeneous population – stabilization of the scheme for strong recurrent inhibition

In the previous section, we presented a summary of the self-consistent scheme, here we introduce our version of a heterogeneous self-consistent scheme. For further
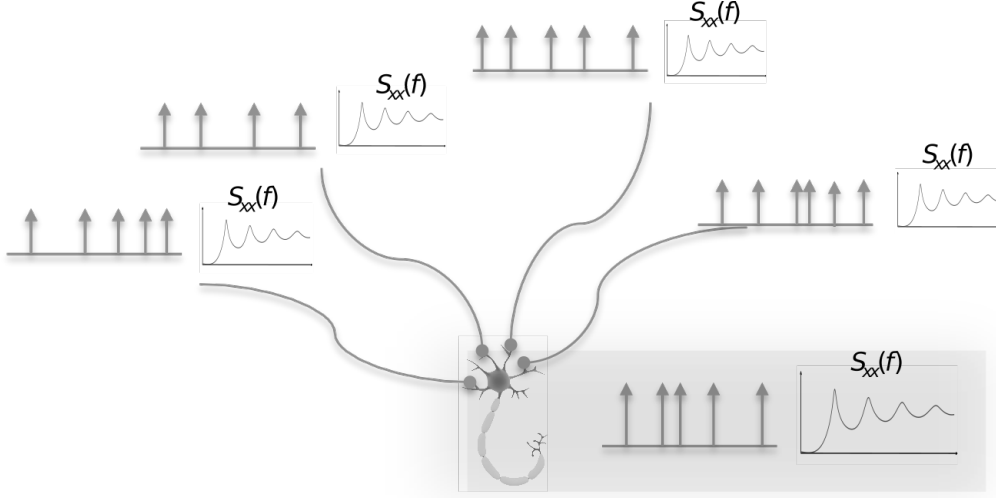
Figure 6.2: ***The problem of self consistency.*** *In a homogeneous sparse recurrent network, we expect that any neuron in the network should have the same second-order statistics. This generates a problem of self-consistency: the input should correspond to the output.*

details of the homogeneous scheme we refer to (Dummer et al., 2014).

As previously stated, the version of the scheme by (Lerchner, Sterner, et al., 2006) and (Dummer et al., 2014) is unable to reproduce self-consistently the statistics of single neurons in a recurrent network with strong relative inhibition g. More specifically, in cases where the inhibition is high, the scheme loses stability and the measured firing rate ν oscillates as a function of the generations (Dummer et al., 2014) [a numerical instability in the balanced case is reported in (Lerchner, Sterner, et al., 2006), which is unrelated to the instability at strong recurrent inhibition]. As a result, network regimes of low firing rate (such as those seen in cortex) cannot be captured.

Here, we propose a method to ensure convergence even with strong recurrent inhibition. We observed that the firing rate oscillations are around the target firing rate, therefore we can use the average firing rate over all past n generations as input
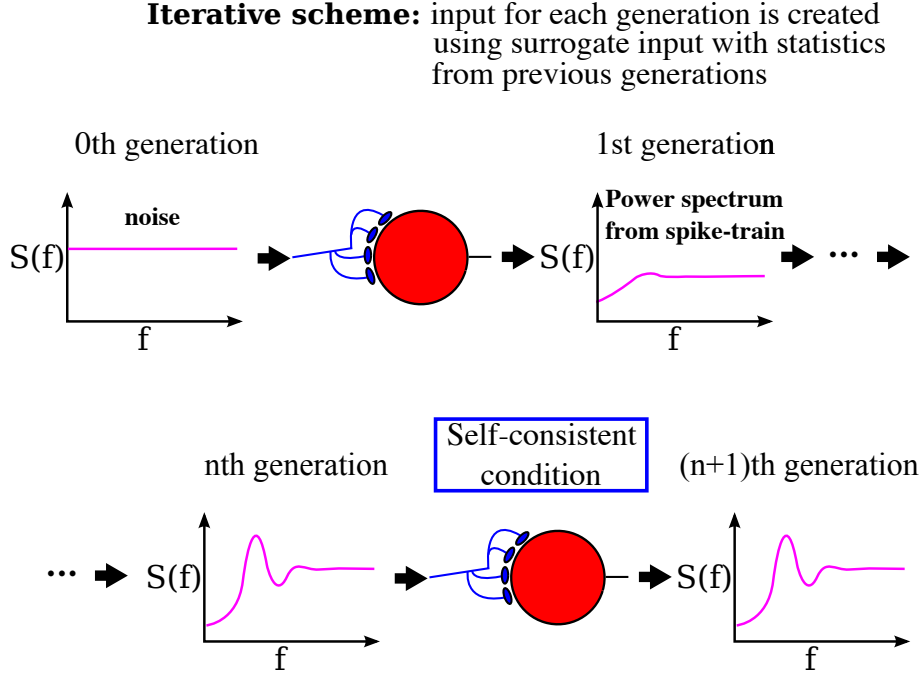
Figure 6.3: *Iterative self-consistent scheme. A neuron is introduced to a noise input in the 0th generation. Then, statistics from its output are extracted and used to produce input to the next generation of neurons. This procedure is iteratively repeated until a self-consistent condition is achieved.*

to the next generation.

$$\hat{\nu}_n = \frac{1}{n} \sum_{q=1}^{n} \nu_q. \tag{6.4}$$

This procedure stabilizes the scheme, see Fig. 6.4 for a numerical example. Note that averaging over a higher number of past generations can yield a faster convergence (cf. Fig. 6.4 **(b)** and **(c)**). The effect can be visualized using a similar approach as in (Dummer et al., 2014): a map from the input rate to the output rate. We calculate the output rate from the input rate with the approximation for synaptically filtered white noise (Brunel & Sergi, 1998). The effect of the averaging over resulting output rate and input can be captured by the functions $\nu_{out,0} = \nu_{out}(\nu_{in})$, $\nu_{out,1} = \nu_{out}\left(\frac{\nu_{in} + \nu_{out}(\nu_{in})}{2}\right)$,..., which are shown in Fig. 6.4 **(d)**. These functions display an increasingly flatter shape in the dependence on the initial firing rate illustrating the stabilizing effect of the averaging.
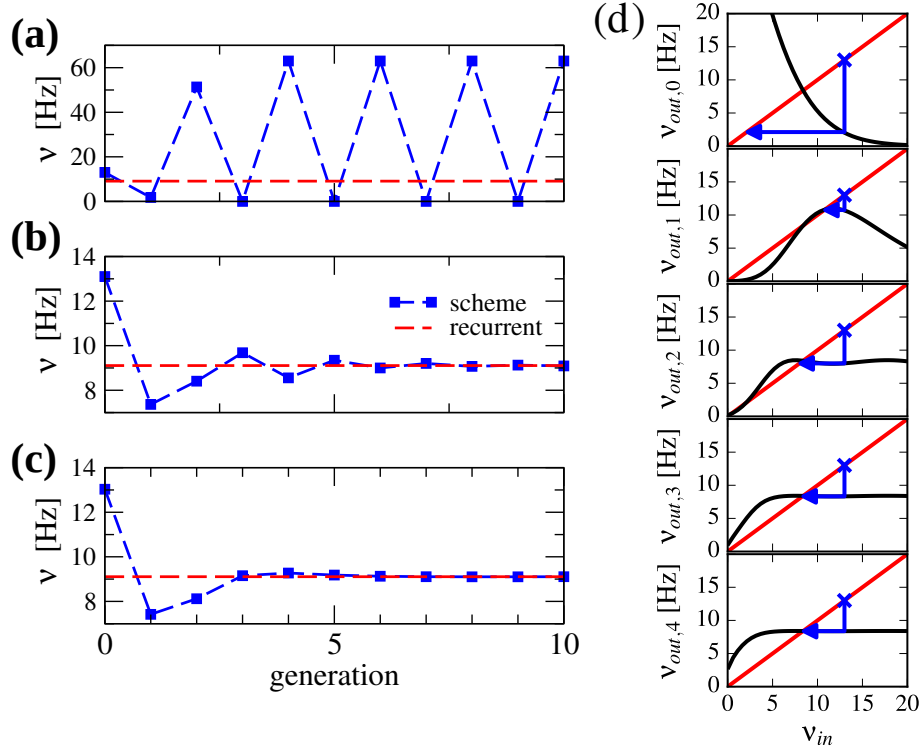
Figure 6.4: *Stabilization of the iterative scheme by averaging over previous generations. (inhibition-dominated regime) Convergence of the firing rate in the iterative scheme (blue line) using different procedures. Parameters are g=5.5, J=0.2 mV, τ_s = 10 ms, γ = 0.25, and RI_{ext} = 30 mV. Recurrent network (red line) is firing at ν = 9.1 Hz. (a) no average is considered, only the previous generation. (b) firing rate is averaged over the past two generations. (c) firing rate is averaged over all past generations. (d) visualization of the averaging procedure: firing rate resulting from i iterations of the averaging procedure $\nu_{out,i}$ of a neuron driven by the firing rate ν_{in} (see text). The function $\nu_{out}(\nu_{in})$ is approximated using the expression for a LIF neuron driven by synaptically filtered white noise (Brunel & Sergi, 1998). The fixed point $\nu_{in} = \nu_{out,1}$ is unstable because $|d\nu_{out}/d\nu_{in}| > 1$ (see (Dummer et al., 2014)). Few iterations suffice to yield a flat curve indicating a stable fixed point.*

The procedure of averaging the rate over the past generations will be used only in cases of unstable convergence. Typically, if excitation and inhibition are (nearly) balanced, the scheme is stable and we do not need to apply the averaging procedure.

6.2.4   The self-consistent scheme for several populations

The self-consistent scheme for a homogeneous population can be generalized in different ways. First of all, real networks consist of several types of neurons, that

all differ with respect to their physiological parameters. A first important step is to distinguish between excitatory and inhibitory neurons not solely with respect to their postsynaptic effect but to endow inhibitory neurons also with different cellular parameters (membrane time constant, leak potential, mean input current) than excitatory cells. Generally, we distinguish between P^E excitatory and P^I inhibitory populations. In the self-consistent scheme each population is represented by one neuron.

6.2.4.1 Determination of the second-order statistics

In the situation considered here, every neuron in the network receives a fixed number of inputs. First of all, the mean recurrent input to a given population α is determined by the firing rates of the presynaptic neurons and by the connection parameters in the network:

$$\mu_\alpha = \tau_\alpha J \left(\sum_k^{P^E} C_k^E \nu_{E,k} - \sum_k^{P^I} g_k C_k^I \nu_{I,k} \right), \tag{6.5}$$

where $\nu_{E,k}$ and $\nu_{I,k}$ are the excitatory and inhibitory firing rates determined by the kth presynaptic neuron. Furthermore, by writing the effective input in the Fourier domain, we can obtain the power spectrum of the effective input $\bar{S}_\alpha(f)$ to a neuron in the α population given by:

$$\bar{S}_\alpha(f) = \frac{\left\langle R\tilde{I}(f)_\alpha R\tilde{I}^*(f)_\alpha \right\rangle}{T}$$
$$= \tau_\alpha^2 J^2 \left(\sum_k^{P^E} |\tilde{K}(f)|^2 C_k^E S_k^E(f) + \sum_l^{P^I} g_l^2 |\tilde{K}(f)|^2 C_l^I S_l^I(f) \right), \tag{6.6}$$

where $S_k^E(f)$ and $S_l^I(f)$ are the spike-train power spectra from the kth E and lth I-cells that provide synaptic input to the population α, respectively, and $\tilde{K}(f)$ is the Fourier transformed synaptic filter in Eq. (6.3). Note that in order to distinguish it from the output spectra, the input spectra to the population α is identified by a bar, i.e. $\bar{S}_\alpha$. If more than two populations are present, in Eq. (6.5) and Eq. (6.6) their contributions are taken into account by the number P^E and P^I of populations.

6.2.4.2 Gaussian approximation of the input

We want to use Eq. (6.5) and Eq. (6.6) to create an input with the same first- and second-order statistics. For a large number of presynaptic neurons that are only weakly correlated, this statistics will be approximately Gaussian by virtue of the central limit theorem[1]. To generate an input to a neuron embedded in the αth population with a prescribed power spectrum, we generate the Fourier transform

$$R\tilde{I}_{G,\alpha}(f) = \sqrt{\frac{\bar{S}_\alpha(f)}{2\Delta f}}\left(\tilde{\eta}_r + i\tilde{\eta}_i\right) \tag{6.7}$$

of a time-dependent function $RI_{G,\alpha}(t)$ by drawing two independent Gaussian numbers $\tilde{\eta}_r$, $\tilde{\eta}_i$ with unit variance and zero mean in each frequency bin. The frequency resolution is set by the length of the time window, $\Delta f = T^{-1}$. Finally, we generate the time-dependent current $RI_{G,\alpha}(t)$ by inverse Fourier transformation of $R\tilde{I}_{G,\alpha}(f)$.

We start with Gaussian white noise as input as the 0-*th* generation in the scheme and drive P neurons, where $P = P^E + P^I$ is the number of populations. The neurons are simulated over a number of trials, the output spike-trains are measured and their power spectra, $S_k^{E,I}(f)$, are estimated (1st generation). For the next generation, an input is created using the spike-train power spectra of the first generation in the Gaussian approximation described above. The procedure is repeated until the output power spectra matches the input power spectra, i.e. self-consistency is achieved. In all simulations of the scheme we observed that iterating up to the 30th generation and using 10,000 trials for each generation was enough to reach a self-consistent solution, provided that the scheme converged for the given parameters.

In summary, we simulate the single LIF neuron representing the population

---

[1] This is evident for a finite synaptic filter, that leads to a summation of many independent continuous functions. For delta synapses, we add up spike trains and so it becomes questionable, how they can approach a Gaussian statistics. In this latter case we should consider the effect of the summed shot noise on a dynamical system such as the integrate-and-fire neuron: the sum over a small time interval (smaller than the membrane time constant but large enough to collect many independent spikes from the presynaptic neurons) yields a spike count which can be well approximated by a Gaussian variable; this is similar to the common diffusion approximation (Tuckwell, 1988), which, however, additionally involves the assumption of a Poissonian input spike train. In this sense, the Gaussian approximation can be applied to sums of spike trains.

α with

$$\tau_\alpha \dot{v}_\alpha = -v_\alpha + \mu_\alpha + R[I_{ext,\alpha} + I_{G,\alpha}(t)]. \tag{6.8}$$

6.3 Results

6.3.1 Homogeneous network with strong recurrent inhibition and additional synaptic filtering

We would like to start with results for the inhibition-dominated network ($g > 4$), in which firing rates are low. In this regime, the iterative scheme as proposed by (Dummer et al., 2014) is highly unstable and we only obtain convergence with the averaging procedure described in section 6.2.3. To demonstrate that the averaging procedure works in such a situation, we consider in Fig. 6.5 the network studied by (Ostojic, 2014) who found two contrasting asynchronous states when varying the synaptic strength J.

In Fig. 6.5 **(a)** spike-train spectra for strong recurrent inhibition ($g = 5$) for different values of J and different network sizes are shown. The power spectra of these network simulations are close to those of the iterative scheme in most cases. For weak coupling, the agreement between spectra is always good; discrepancies for large J become smaller with increasing network size because cross-correlations become less important in this limit. An additional reason for discrepancy is that the Gaussian approximation becomes less accurate for strong synaptic strength. The change in spike-train power spectra upon increase of the synaptic coupling does not hinge on the specific nature of the subthreshold function in the IF model. If we replace the leaky IF model by an exponential IF model (Fourcaud-Trocmé, Hansel, van Vreeswijk, & Brunel, 2003) in the network and in the recurrent scheme, we observe a similarly drastic change in low-frequency power if the synaptic strength is doubled (inset of Fig. 6.5 **(a)**). Also for this single-neuron model the agreement between spectra from the network and from the self-consistent scheme is fairly good.

When the coupling strength J increases, the firing rate first decreases and then increases (Fig. 6.5 **(d)**). More interestingly, with increasing coupling we see a transition from Poisson-like irregular firing (Fig. 6.5 **(b)**) to bursty firing of single neurons (Fig. 6.5 **(c)**), i.e. periods of strong firing are separated by pauses. In the
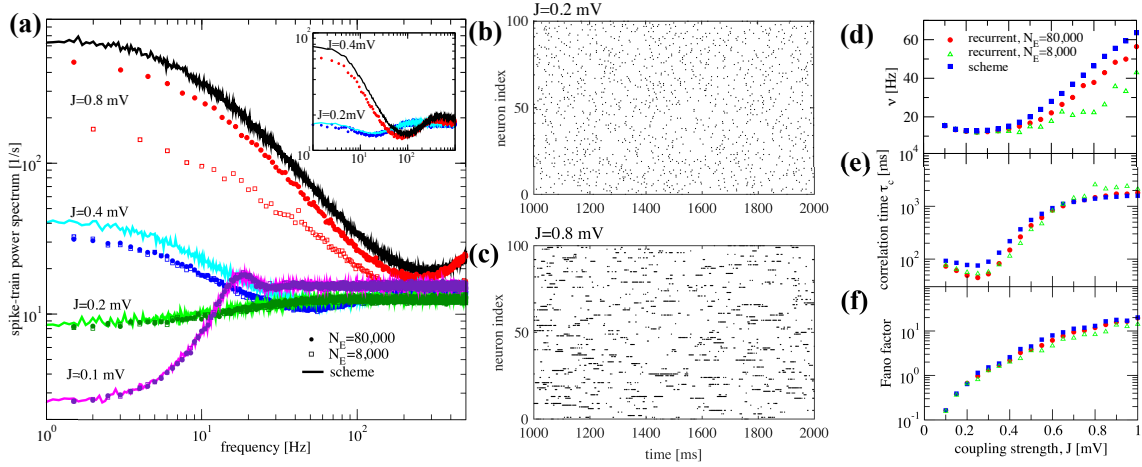
Figure 6.5: *Large amplification of slow fluctuations explain heterogeneous asynchronous state in a homogeneous network. Same set-up as in (Ostojic, 2014), $\tau_E = \tau_I = 20$ ms, $RI_{ext} = 24$ mV, $\gamma = 0.25$, $\tau_D = 0.55$ ms, $g = 5$, and $\tau_R = 0.5$ ms. This is an unstable parameter region where the network fires at low-frequency regime and high inhibition $g = 5$ is set. (a): single-neuron spike-train power spectra from recurrent network (circles for $N_E =80,000$ and squares for $N_E =8,000$) and self-consistent scheme (solid lines) for different values of J. Inset: power spectra for a large network ($N_E = 100,000$) of exponential IF neurons (single-neuron dynamics is $\tau_m \dot{v} = -v + \Delta_T \exp(\frac{v - v_{th}}{\Delta_T}) + RI(t)$ where $\tau_E = \tau_I = 20$ ms, $RI_{ext} = 30$ mV, $\gamma = 0.25$, $\tau_D = 0.55$ ms, $g = 5$, $\tau_R = 0.5$ ms, and $\Delta_T = 0.2$) for two different values of the synaptic coupling, showing the same qualitative difference in low-frequency power as the LIF networks. (b) and (c): raster plots containing 100 neurons from the LIF network with $N_E =80,000$ for $J = 0.2$ mV and $J = 0.8$ mV, respectively. (d), (e), and (f): firing rate ν, correlation time τ_c, and Fano factor for different values of J for both recurrent and self-consistent scheme evaluated in a simulation of $T = 100$ s.*

latter state one can observe a broad distribution of spike counts, and that is why this state has been referred to as heterogeneous asynchronous state (Ostojic, 2014). In terms of the power spectrum this transition becomes manifest as an amplification at low frequencies (Wieland et al., 2015); correspondingly the Fano factor increases (Fig. 6.5 **(f)**). Together with the minimum in the correlation time (Fig. 6.5 **(e)**) (attained at a coupling where the Fano factor is about unity), our results confirm that the transition described by (Ostojic, 2014) in the inhibition-dominated regime is essentially the same as the one observed and explained by (Wieland et al., 2015) for the balanced case $g = 4$.

In summary, the results in Fig. 6.5 indicate that the emergence of a new heterogeneous asynchronous state for strong synaptic coupling can be explained

only using the properties of a single neuron and the self-consistency condition, here demonstrated by our iterative single-neuron scheme.

We now investigate the effect of a finite synaptic filter, Eq. (6.3). Not surprisingly, a pronounced synaptic filter (large τ_s) leads to a long time scale in the network dynamics, as revealed by the increased power at low frequencies (Fig. 6.6). The synaptic filter, Eq. (6.3) is scaled such that the total charge per input spike remains constant. Therefore, an increased time constant for the exponential decay renders the postsynaptic response smaller in amplitude and longer in duration. This longer duration of postsynaptic responses extends the range of temporal correlations in the input to the neuron, which in turn causes the slow fluctuations in the neuron's activity. The resulting power spectrum (Fig. 6.6 **(a)**), especially for long synaptic time constant, looks similar to that of a colored-noise driven perfect IF model (see Fig.9 in (Middleton et al., 2003)). We emphasize that the emergence of the slow time scale is here imposed by the long-lasting synaptic filter which is in marked contrast to the network amplification of slow fluctuations for strong synaptic coupling discussed before in Fig. 6.5.
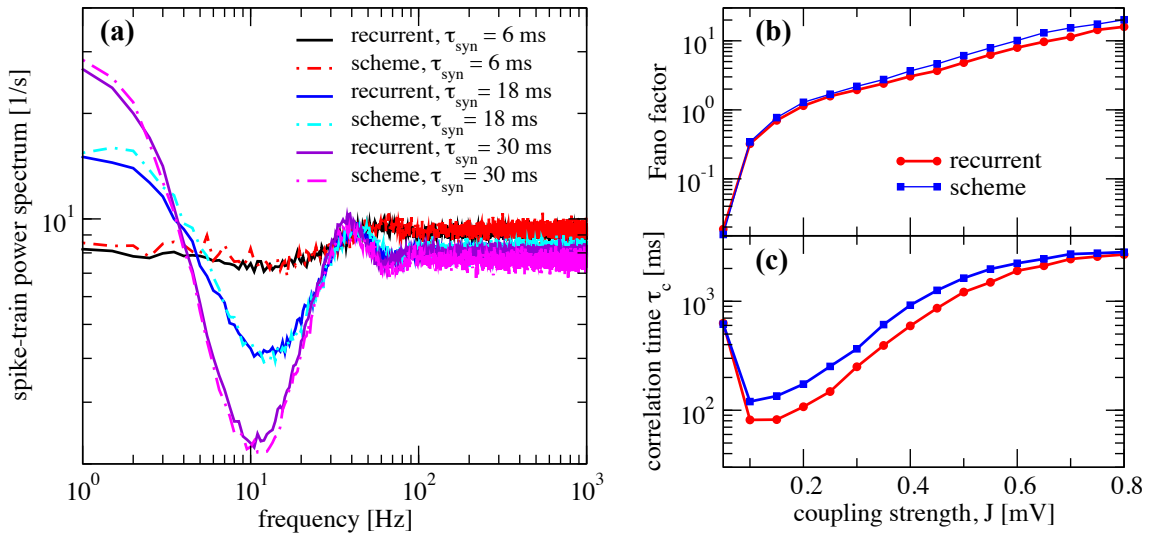
Figure 6.6: *Self-consistent scheme also works for a network with synaptic filtering.* **(a)** *Effect of τ_s on the recurrent network and iterative scheme, the plot displays power spectra for different values of τ_s. This is an inhibition-dominated regime with exponential synapses and $J = 0.2$ mV. In this region, the network fires at low firing rates. In **(b-c)** we fix τ_s at 10 ms and show Fano factor and correlation time τ_c for different values of J for both recurrent and self-consistent scheme. Other parameters as in Fig. 6.5.*

We also verified that the synaptic filter does not change qualitatively the emergence of slow fluctuations for strong coupling (i.e. the heterogeneous asynchronous state discussed above). Using $\tau_s = 10$ ms we still see the characteristic strong increase in Fano factor (Fig. 6.6 **(b)**) and a minimum in the correlation time (Fig. 6.6 **(c)**).

6.3.2 Networks with different parameters for excitatory and inhibitory neurons

In the following, we return to the limit of instantaneous synapses $\tau_s \to 0$, i. e. $K(t) = \delta(t)$, and introduce different parameter values for excitatory neurons (E-cells) and inhibitory neurons (I-cells). First of all, in order to test whether the applicability of the scheme hinges on the exact value of crucial parameters, we choose a small change of the membrane time constant between E and I-cells: $\tau_I = 19$ ms and $\tau_E = 20$ ms. Secondly, we make the relative strength of recurrent inhibition, g_E and g_I, different for the two populations in order to see whether the generalized iterative scheme with two neurons can cope with this heterogeneous situation.

In Fig. 6.7 we show power spectra obtained from simulations of the recurrent network and of the iterative scheme for different combinations (g_E, g_I). In Fig. 6.7 **(a)** the two populations are statistically rather different with an E-cell firing rate of $\nu_E = 3.2$ Hz whereas I-cells fire at $\nu_I = 9.7$ Hz. Both spectra are well reproduced by the iterative scheme and show a "green" shape (in the colored noise lingo, this is white minus red noise). That means, the spectra exhibit a dip at low frequencies, but this is much more pronounced for the I-cells. Even when we increase the difference in recurrent inhibition and the two types of neurons fire at lower frequencies of $\nu_E = 0.1$ Hz and $\nu_I = 7.4$ Hz, the agreement of the spectra from the iterative scheme and from the network simulations is excellent (Fig. 6.7 **(c)**). If we choose the relative recurrent inhibition to be the same, the neural dynamics differ only by the small difference of the membrane time constants, which does neither cause significant differences in the firing rates ($\nu_E = 128.9$ Hz and $\nu_I = 129.9$ Hz) nor in the shape of the power spectra (cf. Fig. 6.7 **(b)**).

In order to explore the quality of the approximation systematically, we
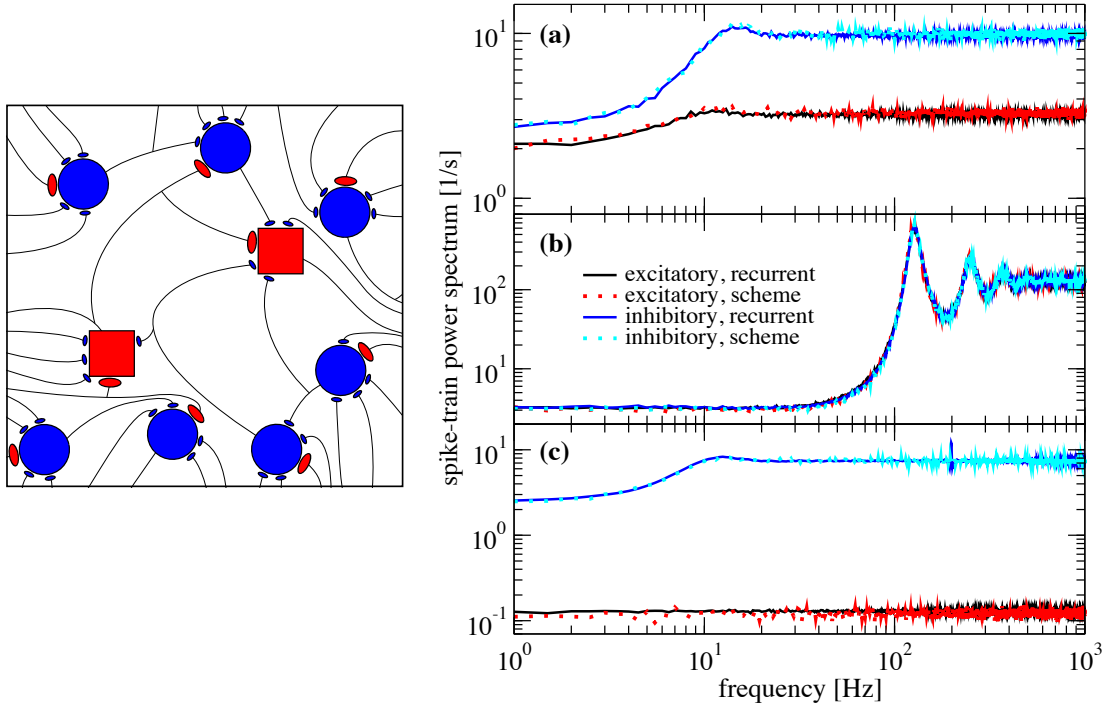
Figure 6.7: *Example spectra for heterogeneous network of excitatory and inhibitory neurons differing in their parameters.* Comparison of power spectra of the recurrent network with two different populations and the self-consistent iterative scheme with two neurons. Parameters are in *(a)* $(g_E, g_I) = (4.2, 4.0)$, in *(b)* $(g_E, g_I) = (3.7, 3.7)$, and in *(c)* $(g_E, g_I) = (4.25, 3.6)$.

evaluated the discrepancy using the relative integrated error

$$\Delta = \frac{\int_0^{f_{cut}} df \, (S_{xx,net}(f) - S_{xx,scheme}(f))^2}{\int_0^{f_{cut}} df \, S_{xx,net}^2(f)}, \tag{6.9}$$

where $f_{cut} = 2\nu_I$ (we use the inhibitory firing rate because it is usually higher).

In our scheme the assumption of weak cross-correlations among neurons in the network is crucial - indeed we assume an infinitely sparse system that is in a perfectly asynchronous state. This is, of course, a somewhat artificial limit and thus it is interesting how, for a fixed number of connections (about 10^3), the squared deviation as well as important statistics such as the Fano factor depend on the system size. In Fig. 6.8 this dependence is illustrated for the case where $g_E = 4.2$ and $g_I = 4.0$, the same parameters as in Fig. 6.7 **(a)**. For the chosen connectivity, a minimal number of $N_E = 20,000$ E-cells seems to be required to reach a good approximation (relative error below 1% for both E and I cells) with the self-consistent scheme. This plot

illustrates that although sparsity is an important assumption for the self-consistent determination of spike-train power spectra, it does not lead to the necessity to consider exorbitantly large networks.
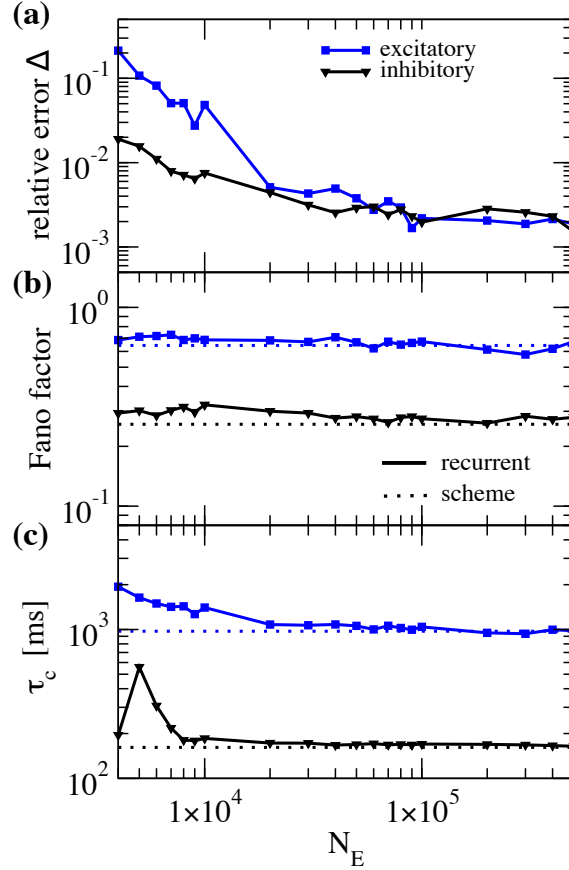
Figure 6.8: *Performance of iterative scheme improves with network size. The performance of the iterative scheme depends on the network size. Curves were produced for the case $g_E = 4.2$ and $g_I = 4.0$, same parameters as in Fig. 6.7 (a). (a) Relative error dependence of the scheme for a network size N_E evaluated with the integrated relative error defined in Eq. (6.9). (b) Fano factor dependence where dotted line represents the iterative scheme prediction and solid lines the recurrent network. (c) correlation time τ_c dependence.*

6.3.3 Networks with three distinct populations and distinct modules

In principle, the proposed iterative scheme is applicable to any number of populations. As long as the resulting activity is sufficiently asynchronous (implying weak cross-correlations) and the synaptic strength is not excessively large

(needed for the Gaussian approximation), the iterative scheme should converge to a self-consistent result. Here we demonstrate that the extended scheme also works for networks with more than two populations and study two cases: a network with three distinct populations and a modular network.

An example of three populations is given by a combination of one excitatory and two inhibitory populations (Fig. 6.9 **(a)**), biologically inspired by a cortical network with excitatory regular spiking neurons (RS), inhibitory fast-spiking (FS) and low-threshold spiking (LTS) neurons (see (Izhikevich, 2003) and (Tomov et al., 2014) and references therein). Their firing rates are ordered such that $\nu_{FS} > \nu_{LTS} > \nu_{RS}$. This heterogeneous situation is achieved by changing both membrane time constants, which are chosen to be $\tau_{FS} = 21$ ms, $\tau_{LTS} = 20$ ms, and $\tau_{RS} = 19$ ms, and making one of the synaptic weights in the network (connecting RS neurons to FS neurons) 1.4 times stronger (indicated by the thick arrow in Fig. 6.9**(a)**, left). This setting illustrates how heterogeneity of connectivity and membrane time constants shape the power spectra statistics.

The resulting spectra are well captured by the iterative scheme; they all display the effect of neural refractoriness by the dip at low frequencies (Bair et al., 1994; Franklin & Bair, 1995) but to a different degree. The dip is most pronounced for the fast spiking neurons; the regular spiking neurons fire with a statistics that is closest to a Poisson process with a flat power spectrum.

According to a common view, the cortex possesses a modular structure (Boucsein et al., 2011; Tomov et al., 2014, 2016), a feature that we take into account in the next setup. We consider two different modules as shown in Fig. 6.9 **(b)**. The two modules are equal to each other with respect to the population size and each consists of an E-I network with $N_E = 100,000$ and membrane time constants $\tau = 20$ ms, requiring the simulation of two neurons in total in the self-consistent scheme. For module 1 and 2 we choose $J = 0.1$ mV and $J = 0.27$ mV, respectively. With this choice, the two modules operate in different regimes: module 1 in a fast-fluctuation mode with low Fano factor and peaked power spectrum, module 2 in a regime of dominating slow fluctuations (cf. section 6.3.1). In module 2, we rewired 50% of the connections so that they come from module 1, i.e. it receives $0.5C_E$ excitatory inputs and $0.5C_I$ inhibitory inputs from module 1. This results in a highly heterogeneous
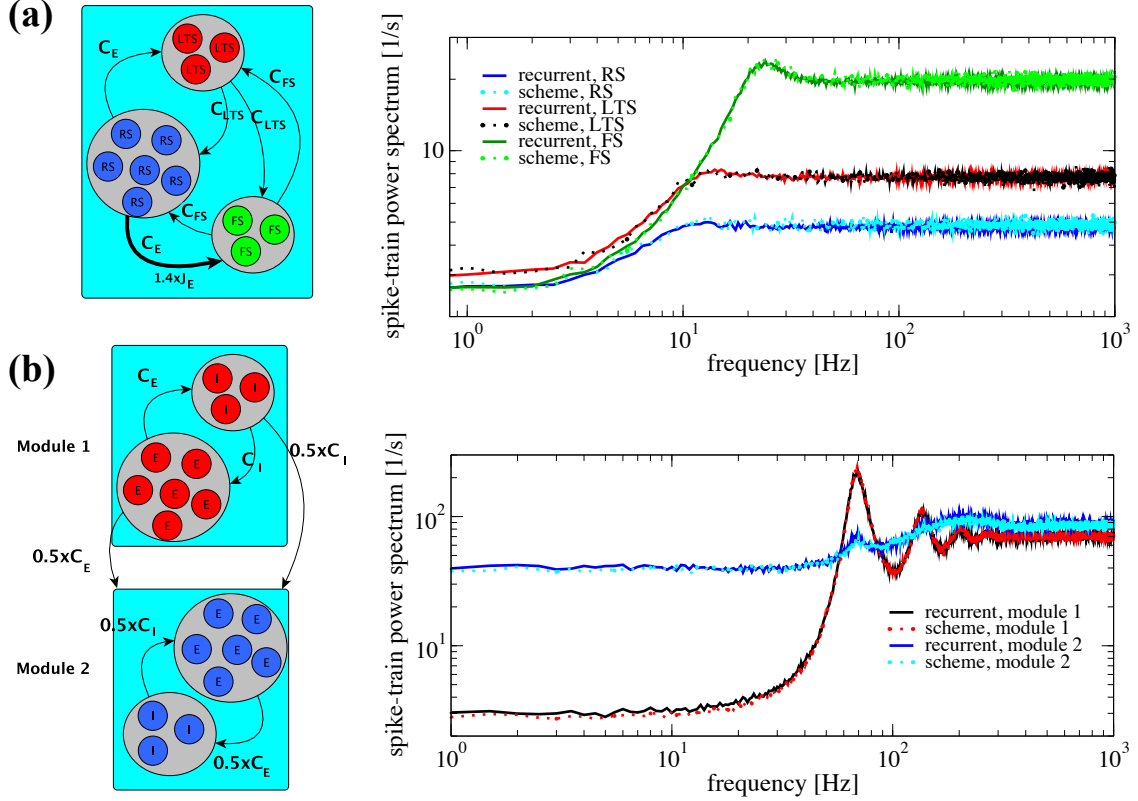
Figure 6.9: *Heterogeneous networks with more than two populations.*
Comparison between power spectra of the recurrent network (solid lines) with the iterative
scheme (dashed lines). **(a)** *Three different populations (RS, LTS, and FS) whereby the*
inhibitory population is composed of LTS ($N_{LTS} = 0.25 \times N_E$, $C_{LTS} = 0.25 \times C_E$) and
of FS ($N_{FS} = 0.05 \times N_E$, $C_{FS} = 0.05 \times C_E$). Parameters are $g = 4.0$, $\tau_{RS} = 20$ ms,
$\tau_{LTS} = 19$ ms, $\tau_{FS} = 21$ ms. We multiply the synaptic strength by 1.4 for the excitatory
weight to inhibitory neuron from population 2. **(b)** *Modular network, modules 1 and*
2 communicate through connections represented at the sketch in the left. Each module
contains 1.25×10^5 cells with E:I ratio 4:1. In both modules $\tau = 20$ ms. At module 1
$J = 0.1$ mV and at module 2 $J = 0.27$ mV, for all modules $g = 4.0$. Module 2 exhibits a
spectral hump around 80 Hz which comes from the interaction with module 1.

situation which is reflected in the power spectrum of module 2: in contrast to the
behavior observed in Fig. 6.5, the power spectrum of module 2 contains an additional
hump around 80 Hz. The power spectra of all different neurons in this setup are
well represented by the iterative scheme, cf. Fig. 6.9 **(b)**.

The result in Fig. 6.9 **(b)** demonstrates that the iterative scheme can capture
complex situations involving the interaction among different modules. The simulated
network contained in total 250,000 neurons and the iterative scheme reproduced the
single neuron correlation statistics with high accuracy using only two neurons.

6.4   Discussion

In this chapter we extended the self-consistent scheme described by (Dummer et al., 2014) to situations with strong inhibition, synaptic filtering, and networks with subpopulations of distinct neuron types. In all cases we employed the Gaussian approximation. Despite these approximations, our comparison of the determined spike-train power spectra with those found by numerical simulations of large and sparse recurrent networks revealed a good quantitative agreement.

Admittedly, with an increasing number of subtypes of neurons, we loose some of the numerical advantages of the scheme compared to a network simulation because in order to get reliable estimates of the power spectrum, we have to simulate the few neurons in each generation many times. If the convergence of the scheme is slow then, adding up all neurons in all generations and all trials, we may have to simulate in the end as many neurons as in the network (however, the typical bottleneck of many simulations, to keep track of all synaptic connections, is still absent in the scheme). It is thus questionable, whether much more complicated situations than discussed here can be studied in depth by our scheme.

Another short-coming of the approach concerns cases in which neural cross-correlations (a very vivid topic of current research, see (Doiron, Litwin-Kumar, Rosenbaum, Ocker, & Josić, 2016)) cannot be neglected anymore or in which weak cross-correlations still have a significant impact on the population activity (Schneidman, Berry, Segev, & Bialek, 2006). There are different causes for cross-correlations including common (shared) input, spatially homogeneous external stimuli, and a slight overall synchronization in the network (some of which are reviewed by (Helias et al., 2014; Doiron et al., 2016)). Not all of these factors can be taken into account by extending the scheme to pairs of neurons that are stimulated by correlated Gaussian noise processes[2]. We may still learn something from finding situations in which neural cross-correlations can quantitatively be described by extensions of the scheme to pairs of neurons in each generation.

---

[2] For the simpler but still formidable problem of how neuron pairs respond to cross-correlated Gaussian white noise sources, see, for instance, (Doiron, Lindner, Longtin, Maler, & Bastian, 2004; de la Rocha, Doiron, Shea-Brown, Josic, & Reyes, 2007; Shea-Brown, Josić, de la Rocha, & Doiron, 2008; Ostojic, Brunel, & Hakim, 2009; Vilela & Lindner, 2009b; Deniz & Rotter, 2017).

Nevertheless, the results and the approach put forward in this thesis are useful in several respects. If the single-neuron statistics is of interest (because this is what is recorded or this is what shows particularly interesting features), our method provides a computationally cheap solution to calculate the spike-train power spectrum and to study its dependence on cellular and network parameters without the need to simulate a network. The scheme is particularly suited for the idealized case of a perfectly asynchronous network that is difficult to study numerically because an almost completely asynchronous state can be reached only in a very sparse, hence, very large network. This case is interesting because it often permits analytical calculations via a density equation for the membrane voltage (Knight, 1972; Abbott & van Vreeswijk, 1993; Amit & Brunel, 1997a; Brunel, 2000; Mattia & Del Giudice, 2002) and thus our scheme might be useful for comparison to simpler theories.

As already mentioned in the introduction, we can regard our results as a confirmation that the approximation of the synaptic input by a correlated Gaussian noise is a reasonable one over a physiological range of parameters for a sparse recurrent network in the asynchronous state. Using Markovian embedding, an arbitrary colored Gaussian noise can be described by a (possibly very high-dimensional) Ornstein-Uhlenbeck process, an idea that has been worked out in the neural context by (Schwalger et al., 2015); for examples from the physics literature, see, for instance, (Schimansky-Geier & Zülicke, 1990; Hänggi & Jung, 1995; Siegle, Goychuk, Talkner, & Hänggi, 2010). Hence, a stochastic mean-field theory in terms of the corresponding multidimensional Fokker-Planck equation seems to be in reach, generalizing the successful framework of the diffusion approximation, which was based on the Poissonian (white-noise) approximation and thus led to a one-dimensional Fokker-Planck equation. A theory using the colored-noise Fokker-Planck equation would faithfully reproduce the second-order temporal correlations of the spiking neurons and, possibly, provide novel insights into the bifurcation between asynchronous and synchronous states. This may be particularly relevant for larger synaptic amplitudes (Ostojic, 2014; Wieland et al., 2015), for which the color of the noise becomes more and more important.

CHAPTER 7

ENHANCEMENT OF ACTIVITY PROPAGATION IN HIERARCHICAL AND MODULAR NETWORKS WITH SLOW FLUCTUATIONS

7.1 Introduction

Neural fluctuations are ubiquitous phenomena in the brain. There is ample evidence that cortical neurons generate and receive temporally fluctuating rhythmic and non-rhythmic signals that relate to behavior (Britten, Shadlen, Newsome, & Movshon, 1993; Buzsáki & Draguhn, 2004; Buzsáki, 2006; Bonifazi et al., 2009; Colgin, 2011). In particular, slow voltage fluctuations that emerge in single neurons can upscale to influence network behavior with possible consequences to learning processes like working memory (Brunel & Wang, 2001; Kane & Engle, 2002; Curtis & D'Esposito, 2003; Mongillo, Barak, & Tsodyks, 2008; Leszczyński, Fell, & Axmacher, 2015). This problem is attractive from a theoretical standpoint, and has received attention from the computational neuroscience community (Durstewitz & Deco, 2008; Ostojic, 2014).

The question of how fluctuations are generated in single neuron and network models has been studied with different approaches. In a classic study of a random network model composed of leaky integrate-and-fire (LIF) neurons (Brunel, 2000), the interplay between relative inhibitory synaptic strength and external input can lead to different dynamic activity regimes ranging from the asynchronous irregular

(AI) state, with uniform population firing rate and irregular single neuron spikes, to the synchronous regular (SR) state, where both the population and the single neuron rate oscillate. The same network can display the so-called heterogeneous AI state where individual neurons fire irregularly with intermittent bursts (Ostojic, 2014). Using a self-consistent scheme that captures the spectral properties of network firing in terms of a single neuron, it has been shown that heterogeneous AI bursts emerge from slow fluctuations in single neuron firing (Wieland et al., 2015; R. F. Pena et al., 2018). Nevertheless, few works have tackled the problems of how slow fluctuations can emerge in a network composed of fast elements like neurons (Wieland et al., 2015) and how these fluctuations influence information processing in the network (Salinas & Sejnowski, 2001; Droste & Lindner, 2017b).

The cerebral cortex has a non-random anatomical structure (Mountcastle, 1997; Bullmore & Sporns, 2009; Kaiser & Hilgetag, 2010; Meunier et al., 2010) and displays activity fluctuations at the level of both individual neurons and neural populations. Many computational models have studied activity patterns that emerge from networks with non-random topologies inspired on cortical anatomy (Izhikevich & Edelman, 2008; Wang et al., 2011; Litwin-Kumar & Doiron, 2012; Potjans & Diesmann, 2014; Tomov et al., 2014, 2016). Spontaneous neural firing that appear in simulations of these models can display slow fluctuations. However, a mechanistic explanation of the coupling between network topology and activity fluctuations is still missing.

In this chapter we explore how topology and synaptic strength can work together to generate and enhance slow activity fluctuations in a spiking network model. We study networks with hierarchical modular topologies and find parameter ranges for which slow fluctuations emerge. These fluctuations can appear and be enhanced in two different ways: (i) by increasing the synaptic efficacy; and (ii) by increasing the number of modules via the increase of the hierarchical level. Interestingly, while mechanism (i) causes the build up of slow fluctuations in individual neurons, mechanism (ii) causes slow fluctuations by increasing single-neuron spike-train cross-correlations. Thus, although similar effects can appear through increases in both synaptic strength and network hierarchical level, the underlying mechanisms are different.

Moreover, using information-theoretical measures we show that the slow fluctuations enhance activity propagation in hierarchical modular networks. In particular, we analyze information transmission between single neurons and between modules, and show that the latter is not straightforwardly predictable from the former, disclosing the complexity behind communication dynamics in such networks.

The remainder of this chapter is structured as follows. In the next section we introduce the neuron and network models used in our simulations, and the spike-train correlation and information-theoretical methods used to characterize results. Next, we present the results section for networks with varying synaptic strengths and hierarchical levels analyzed via the methods described. Finally, in the last section we discuss our results and possible implications of them.

7.2   Methods

7.2.1   Neuron Model

In this Chapter we choose the leaky integrate-and-fire (LIF) neuron model (Gerstner et al., 2014) (see Sect. 2). All parameters from the single-neurons and network are displayed in Table 7.1.

7.2.2   Network

The hierarchical and modular network (HMN) is the subject of study here. The construction of a HMN follows an algorithmic that creates different levels of hierarchy (cf. (Tomov et al., 2014, 2016) and Sect. 2.2.3.2). In that sense, all networks built in this work are classified in different hierarchical and modular levels (H). The zeroth level is a standard Erdős-Rényi topology with $N = 2^{17} = 131,072$ neurons connected with a given connectivity $\epsilon = 0.01$. The term ϵ is the ratio between the expected number of connection by the number of neurons.

The following $H \geq 1$ levels are build following the same algorithm: (i) the network is divided in equal portions which will be different modules; (ii) connections *between* the modules are rewired with probability $R_{\text{ex/in}}$ to excitatory/inhibitory connections, respectively; (iii) connections *within* the modules are kept. This procedure is iteratively repeated until the Hth hierarchical and modular level is

PARAMETERS

Neuron parameters		
Name	**Value**	**Description**
v_{th}	20 mV	Firing threshold
v_{r}	10 mV	Reset potential
τ_{R}	0.5 ms	Refractory period
RI_{ext}	30 mV	External input

Network connectivity parameters		
Name	**Value**	**Description**
N	2^{17}	Size of excitatory population
ϵ	0.01	Connectivity
R_{ex}	0.9	Excitatory rewiring probability
R_{in}	1	Inhibitory rewiring probability

Synaptic parameters		
Name	**Value**	**Description**
J	$\in [0; 1]$ mV	Excitatory efficacy
g	5	Relative inhibition
τ_{D}	0.55 ms	Synaptic delay

Table 7.1: *Summary of standard parameters in this chapter.*

obtained.

7.2.3 Statistics

Here we define the specific measures used in this chapter. To evaluate the spike train's long-term variability we will use the Fano factor (FF) as in Eq. (3.7). Note that a large value of FF indicates an enhancement of slow fluctuations. In our simulations, we extract FF from $\bar{S}_{xx}(f)$ (the averaged spike-train power spectrum over K neurons) since both are relate by $\lim_{f \to 0} \bar{S}_{xx}(f) = \nu \times FF$. From $\bar{S}_{xx}(f)$ we also extract the firing-rate by the relationship $\lim_{f \to \infty} \bar{S}_{xx}(f) = \nu$ (cf. (Grün & Rotter, 2010)).

For spike-trains we compute the autocorrelation function

$$c_{xx}(\tau) = \frac{1}{K} \sum_{j \in K} \left(\langle x_j(t) x_j(t+\tau) \rangle - \langle x_j(t) \rangle \langle x_j(t+\tau) \rangle \right), \qquad (7.1)$$

which in our work is always an average over $K = 10,000$ randomly chosen neurons and normalized by $c_{xx}(0)$. Similarly, the cross-correlation function $c_{xy}(\tau)$ is computed by taking $K = 10,000$ randomly chosen pairs of spike-train $x(t)$ and $y(t)$.

Following (Neiman et al., 2007; Wieland et al., 2015), we also extract the correlation time τ_c from $\bar{S}_{xx}(f)$ by means of the Parseval theorem as we defined in Eq. (3.8).

To measure information flow in the network we make use of the well known Transfer Entropy (TE)(Schreiber, 2000). This quantity measures how predictable is the future of the spike train $x(t)$ if we have knowledge about the spike train $y(t)$ in the present time (for simplicity we will denote the spike-trains at a given time t by x_t and y_t). In other words, TE tells how much information of y is present in the future of x, that is why it is commonly related to information flow, given that the measure is asymmetric it also give a directional sense, i.e. whether information is flowing from x to y or vice-versa.

Here we use a version of TE called delayed transfer entropy as described in Ito et al. (2011) (Ito et al., 2011), and it is given by Eq. (7.2). The procedure to evaluate it is done by taking four spike-trains y_t, x_t, and the spike train of the receiving neuron shifted by a delay d (x_{t+d}) and by the delay $d+1$ (x_{t+d+1}). In the following, we simply have to determinate the probability $p(y_t)$, and the joint probabilities $p(y_{t+1}, y_t)$, $p(x_t, y_t)$, and $p(x_{t+1+d}, x_{t+d}, y_t)$ to finally "plug" them into Eq. (7.2)

$$TE_{y \to x}(d) = \sum p(x_{t+1+d}, x_{t+d}, y_t) \log_2 \left(\frac{p(x_{t+1+d}, x_{t+d}, y_t) p(y_t)}{p(y_{t+1}, y_t) p(x_t, y_t)} \right), \qquad (7.2)$$

where the summation is taken over the set of all possible combinations of symbols for the spike-trains. Since the value of the spike-train in each time step is either 0 (for silence) and 1 (for a spike), for the joint probabilities $p(x_t, y_t)$ we have $2^2 = 4$ combinations, and for $p(x_{t+1+d}, x_{t+d}, y_t)$ we have $2^3 = 8$ combinations. In Fig. 7.1 we summarize the procedure to measure the delayed transfer entropy explained above to measure the $TE_{y \to x}$. In Fig. 7.1(a) the spike-trains were made in such a way that

whereas $TE_{y \to x}$ is maximum for $d = 2$, $TE_{x \to y}$ is maximum for $d = 3$ (cf. Fig. 7.1(c); this was artificially generated by making x to fire two steps after y whereas y fires three steps after x). The delay for which TE is maximum can be interpreted not only as the time that information takes to go from y to x but also as the time delay of a functional connection of this pair. In fact, many studies use this approach to determine and retrieve the connectivity map of a network (de Abril, Yoshimoto, & Doya, 2018).
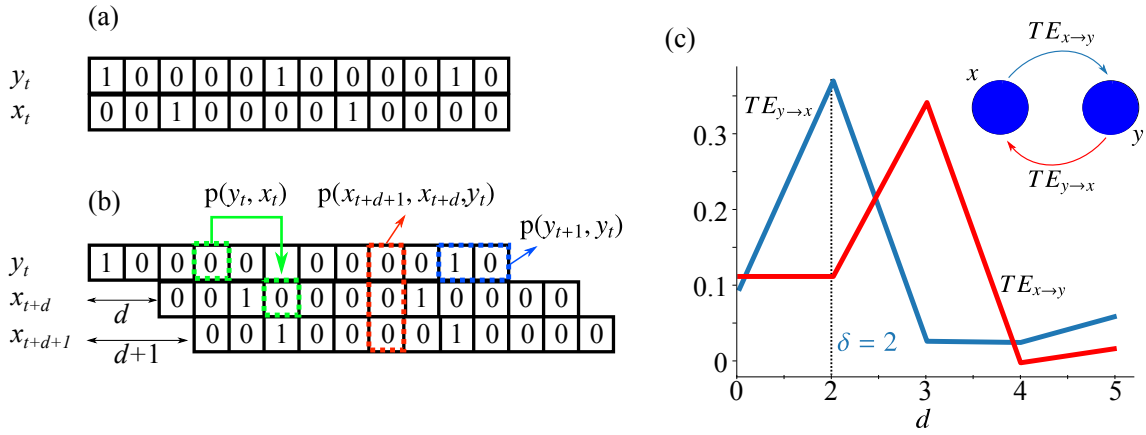

Figure 7.1: *Method to measure the delayed transfer entropy using the joint probability distributions.* (a) First we take two spike trains of a pair of neurons embedded in the network. (b) Then we apply a delay d in one of them to determine the joint probabilities distributions $p(x_t, y_t)$ (indicated by the green arrow), $p(x_{t+1+d}, x_{t+d}, y_t)$ (indicated by the red arrow), and $p(y_{t+1}, y_t)$ (indicated by the blue arrow) then we estimate the transfer entropy by "plugging" this distributions into Eq. (7.2), in (c) we show that TE is maximized by the delay close to the time delay of the connection and the asymmetry of the measure ($TE_{y \to x} \neq TE_{x \to y}$).

In the network, TE is taken by selecting $K = 10,000$ randomly chosen pairs of neurons. For each pair, TE was measured within the range $d \in [200; 300]$ bins which is a reasonable considering the spiking delay communication τ_D and the time expected to observe an action potential rise. In the end, we extracted the averaged TE over

$$\langle TE(J) \rangle = \frac{1}{K} \sum_{j \in K} \max\{TE_j(d)\}, \tag{7.3}$$

where TE_j is the Transfer Entropy for the jth pair.

To estimate information flow in the macroscopic level, we also use the transfer entropy but taken from the activity $r(t; \Delta t)$ of the different modules. Here we

take adjacent modules and compute the TE between them in such a way that for each hierarchical level the mean information flow will be given by $\langle TE^{(H)} \rangle = 1/(2^H - 1) \sum_{i=1}^{2^H - 1} TE_{i \to i+1}$, where $TE_{i \to i+1}$ is given by Eq. (7.2) with $d = 0$. The main reason for a delay zero is that here we are taking adjacent modules and that their activity is sampled with $\Delta t = 1$ ms (see Eq. (3.3)). Observe that to distinguish from the spike-train transfer entropy we identify this one with a superscript (H), i.e. $\langle TE^{(H)} \rangle$. Since the activity of a module is continuous we used a kernel estimator to estimate the joint probabilities (Schreiber, 2000).

To evaluate statistical dependency among modules, we extracted the mutual information (de Abril et al., 2018) among adjacent modules as aforesaid for $\langle TE^{(H)} \rangle$, the mutual information reads

$$MI(x; y) = \sum_{\substack{x \in x_t \\ y \in y_t}} p(x, y) \log_2 \frac{p(x, y)}{p(x)p(y)}. \tag{7.4}$$

We will also measure multivariate mutual information using three module activities, which can be written as

$$MI(x; y; z) = \sum_{\substack{x \in x_t \\ y \in y_t \\ z \in z_t}} p(x, y, z) \log_2 \frac{p(x, y)p(x, z)p(y, z)}{p(x, y, z)p(x)p(y)p(z)}, \tag{7.5}$$

we average these quantities over a certain number of modules and identify them by $\langle MI^{(H)} \rangle$.

7.3 Results

7.3.1 Slow fluctuations emerge in both Erdős-Rényi topology and HMNs

We start our results section with a comparison of general characteristics observed in the Erdős-Rényi topology and HMNs with varying synaptic strength. According to observations elsewhere (Ostojic, 2014; Wieland et al., 2015; R. F. Pena et al., 2018), in an AI state where neurons are firing without apparent correlation, an increase of J creates a second type of AI activity which is characterized by a build up of slow fluctuations (Wieland et al., 2015; R. F. Pena et al., 2018). At the

level of the single neurons, cells in this latter regime have a rather heterogeneous firing pattern with bursts of spikes intercalated with periods of silence.

In (Ostojic, 2014), aspects related with a better information processing in the second type of AI pattern have been discussed. Here, by simulating several configurations where combinations of J with H were our parameters, we obtained different patterns as displayed in Fig. 7.2.
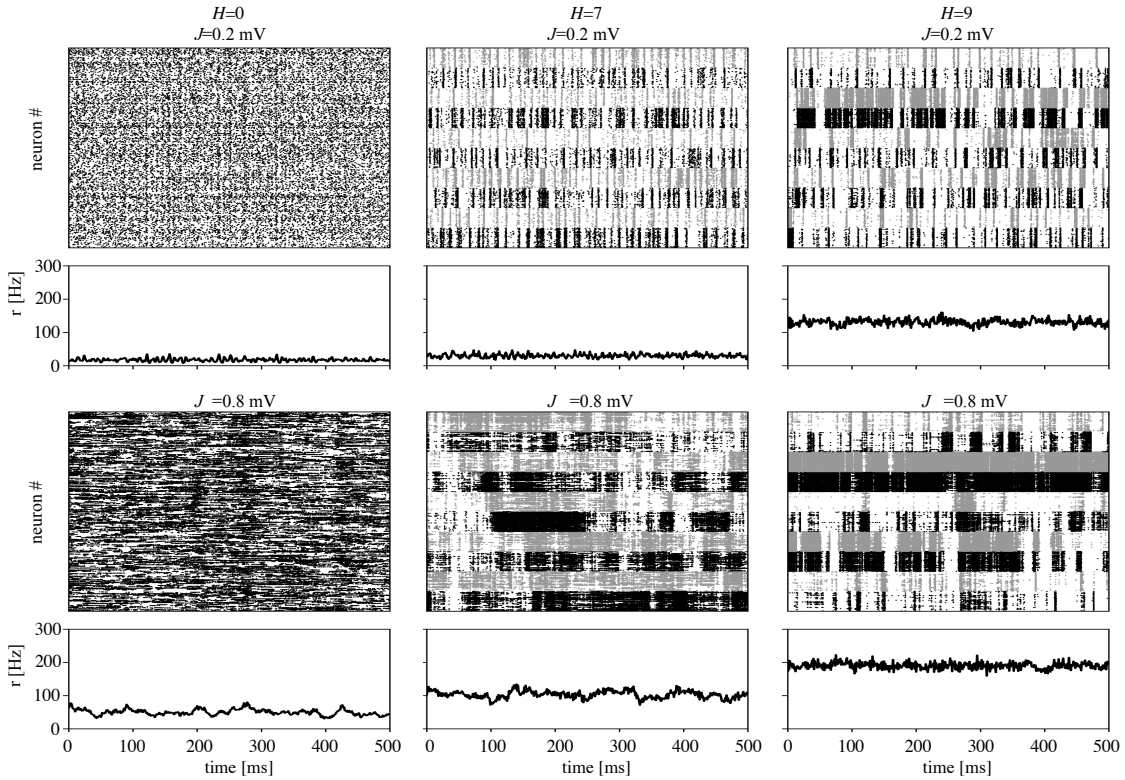
Figure 7.2: *Raster plots and activity representing different network behaviors with varying J and H. Each pair of subpanel shows a raster plot with 2560 neurons and activity $r(t)$ taken over all neurons in the network. In the columns we present $H = 0, 7,$ and 9, respectively. Upper row: $J = 0.2$ mV. Bottom row: $J = 0.8$ mV. Specifically for $H = 7$ and 9, the selected neurons to be presented in the raster plots follow the same number of neurons per module to allow comparison, moreover the different modules have their spike times presented with dots intercalated by black and gray to allow module distinction.*

In the first column of Fig. 7.2 we see the two types of asynchronous activity as reported elsewhere (Ostojic, 2014). For $J = 0.2$ mV, neurons fire rather irregular and no synchronous behavior is observed. As the synaptic strength increases to $J = 0.8$ mV, the activity changes drastically to a more heterogeneous behavior where

single-neurons tend to fire with intercalated bursts separated by short time windows and the network time-dependent firing rate has a less homogeneous dynamics.

In the second and third column of Fig. 7.2 we compare activity dynamics in hierarchical levels $H = 7$ and $H = 9$ as well as different values of J (from top to bottom $J = 0.2$ mV and $J = 0.8$ mV). In both levels of hierarchy, a marked neuronal and network dynamics appears as J increases following the same transition observed in the Erdős-Rényi topology ($H = 0$). Interestingly, as H increases modules begin to act more individually as can be noted by different spike patterns observed in each module. In the following, we will argue that both HMN and high synaptic efficacy J have advantages on information transmission due to the build up of slow fluctuations that emerge in these setups.

In Fig. 7.3 we present extended statistics to show that there are similarities in increasing either J or H. Comparisons of the spike-train power spectra in Figs. 7.3(a,b) with varying J and H show that a similar effect of build up of slow fluctuations emerge upon increasing of these parameters. However, the effect is more pronounced for J than H, e.g. for fixed $H = 0$ note that changing $J = 0.2$ mV to $J = 0.8$ mV the slow fluctuations (identified by initial values of the spectrum) increase by 2 orders of magnitude, whereas for fixed $J = 0.2$ mV changing H from 0 to 9 slow fluctuations increase these values by 1 order of magnitude. The spectral characteristics are similar to cortical neurons (Bair et al., 1994).

In Figs. 7.3(c–e) we present the dependency of the firing rate ν, Fano factor FF and correlation time τ_c with J where the different curves correspond to different H (colors correspond to the same values of H as in Figs. 7.3(a)). Similar results for J and $H = 0$ were presented in (R. F. Pena et al., 2018) where a similar network to ours was discussed. Here we see that while J increases (in Figs. 7.3(c–e)), FF (indicative of long-term variability) also increases pointing to the build-up of slow fluctuations. The ν and τ_c are non-monotonic for low H typically $H < 7$ where they present a minimum value marking a transition from the two asynchronous behaviors (compare raster plots in Fig. 7.2). For $H > 7$ the ν and τ_c have a marked change, both curves become monotonic and the transition point disappears: only an increase of ν and τ_c is observed as J increases.

The sets of Figs. 7.3(c–e) depict different characteristics. Increase of H
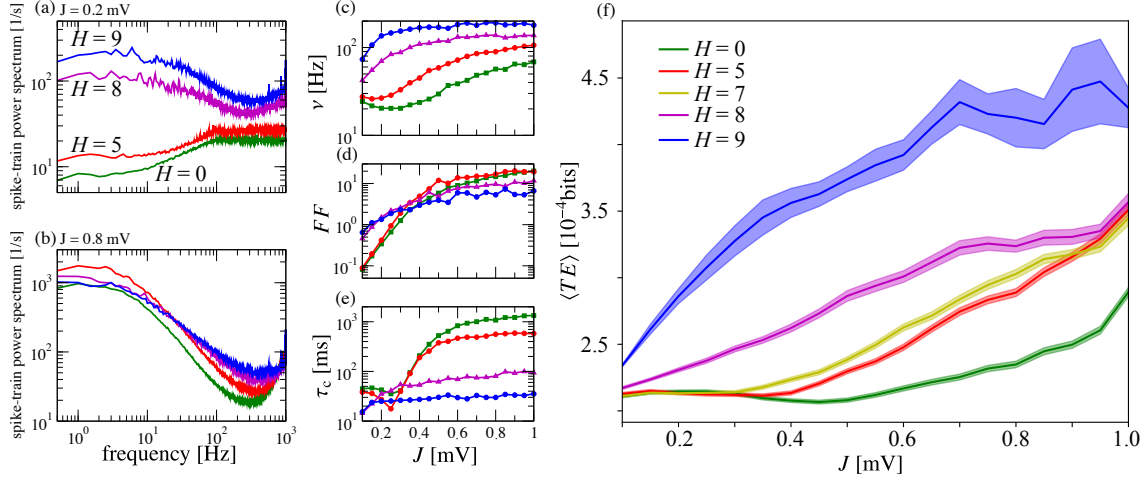
Figure 7.3: *Large amplification of slow fluctuations caused by both increase of J and of H. (a) Spike-train power spectra computed for different values of H as indicated in the plot for J = 0.2 mV and (b) J = 0.8 mV. (c–e) Firing rate ν, Fano factor FF, and correlation time τ_c for different values of J and whereby H follows the same colors as in (a,b). (f) Transfer entropy computed as in Eq. (7.3), shaded curves are standard errors.*

produces undoubtedly slow fluctuations. However, different from J which enhance slow fluctuations until some saturation value, the increase of hierarchy does enhance slow fluctuations but the saturation value gets lower if hierarchy is increased at high hierarchical level, i.e. too much hierarchy hinders slow fluctuations: observe that for high J and high H, the higher the H the lower the FF.

So far, we have shown that it is possible to achieve slow fluctuations both by increasing J or by increasing the hierarchical level. To characterize information flow in the network, in Fig. 7.3, we show that for networks with low hierarchical level ($H \leq 7$), $\langle TE \rangle$ increases for $J \gtrapprox 0.4$ mV, i.e., the regime where the network starts to exhibit slow fluctuations. Furthermore, as H increases, values of $\langle TE \rangle$ increase until we reach $H = 8$ which seems to behave as a transition point. In this exact point, the shape of the $\langle TE \rangle$ curve becomes more linear and all values in the curve are bigger than the ones observed for $H < 8$. For $H = 9$, $\langle TE \rangle$ exhibits even higher values independently of J. These results are in accordance with what has been reported elsewhere (Ostojic, 2014; Droste & Lindner, 2017b) on the enhancement of information propagation in networks embedded in slow fluctuations regime.

We propose that, as H increases the modules start to act as a functional unit. This effect is largely enhanced when high J and H are combined. By acting as a

modular functional unit, it is easier for information to be transmitted throughout the network. Note for example in Fig. 7.2 that networks with high J and H have modules acting very differently from each other.

7.3.2 Effects of J and H on single neurons spike-train's autocorrelation and cross-correlation

We decided to investigate the spike-trains autocorrelation and the cross-correlation in order to clarify the individual properties of neurons upon build up of slow fluctuations as reported above. In Fig. 7.4 we present the obtained $c_{xx}(\tau)$ and $c_{xy}(\tau)$ for different values of H and J (see caption in the figure). Note that discussing the properties of the autocorrelation function reflects directly on observations of the power spectrum, this happens because the power spectrum and autocorrelation function are connected by the Wiener-Khinchin theorem $\bar{S}_{xx}(f) = \int_{-\infty}^{\infty} c_{xx}(\tau)e^{-2\pi i f \tau} d\tau$.

Figure 7.4 demonstrates that although the increase of J increases spike-train autocorrelation, its effect on the cross-correlation is not straightforward. For low values of H, J has apparent very little effect on the cross-correlation function. This indicates that at these parameters, an increasing on the synaptic efficacy J affects mainly the single-neuron behavior which is in line with the idea that the network activity is still asynchronous.

Next, at values of high H, J can affect cross-correlations. Observe that in the $c_{xy}(\tau)$ plot for high H an exponential decay starting at $c_{xy}(0)$ takes place indicating that a more complex pattern emerges at population level which was not present at $H = 0$. In addition, at high H the effect of J is slightly less pronounced at $c_{xx}(\tau)$ than it is in $c_{xy}(\tau)$.

These results indicate that without a hierarchical and modular topology, the build up of slow fluctuations affects mainly the single-neuron behavior but there is nearly no population communication present. However, when the hierarchical and modular topology is introduced, the build up of slow fluctuations also emerge but different from $H = 0$, a population communication takes place. The latter is indeed more advantageous for information propagation as indicated in our last section.

But why does spike-train's cross-correlation increases with the hierarchical
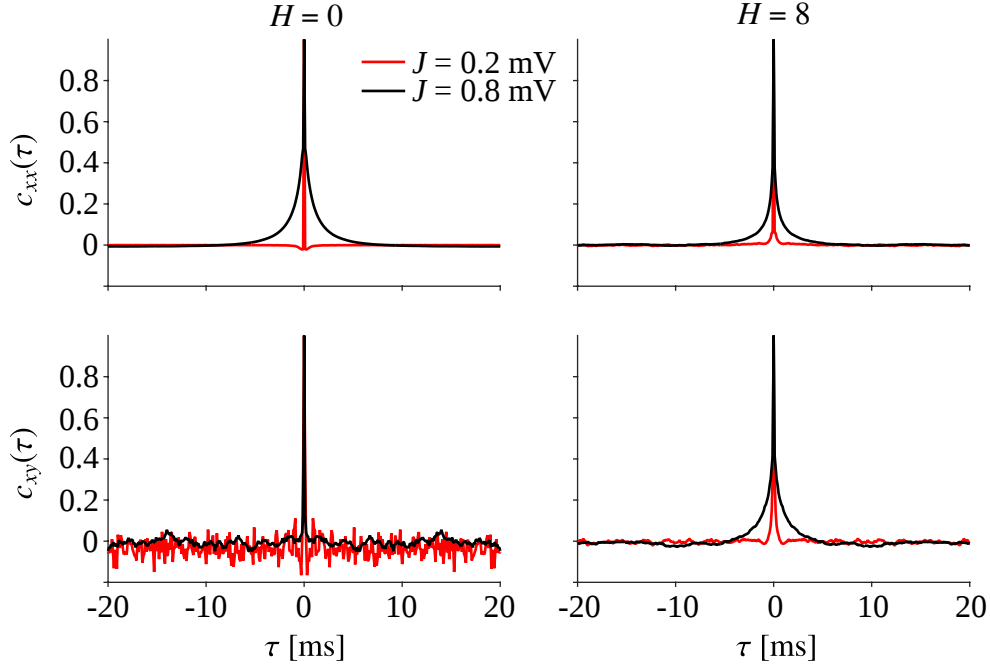
Figure 7.4: *Spike-train autocorrelations $c_{xx}(\tau)$ and cross-correlations $c_{xy}(\tau)$ for varying J and H. The c_{xx} is extracted from $K = 10,000$ randomly chosen neurons and the c_{xy} from $K = 10,000$ randomly chosen pairs of neurons. First column: $H = 0$. Second column: $H = 8$. First row: $c_{xx}(\tau)$. Second row: $c_{xy}(\tau)$. Red lines: $J = 0.2$ mV. Black lines: $J = 0.8$ mV.*

level? To understand that we have derived equations to investigate how the number of connections is rewired. In our derivation we will not make any distinction among excitatory/inhibitory connections keeping everything in general terms.

Let's start with the network where $H = 0$, we note that the expected number of connections in a neuron that comes from inside the module $n_{in}^{(H=0)} = N\epsilon$, where the superscript indicates the hierarchical level $H = 0$.

In the next step, when $H = 1$, the algorithm tells that one should divide the network and rewire its connections, this means that the expected number of connections in the divided module will be half of the previous plus half of what the probabilistic rewiring (which, by simplicity, will be denoted by R) of connections provided, i.e.

$$n_{in}^{(H=1)} = \frac{n_{in}^{(H=0)}}{2} + \frac{n_{in}^{(H=0)}}{2} \times R. \tag{7.6}$$

In Eq. (7.6) we only show the average number of connections to a neuron that comes from inside the same module, but we can also calculate the remaining

connections that come from outside the module which is

$$n_{\text{out}}^{(H=1)} = n_{\text{in}}^{(H=0)} - n_{\text{in}}^{(H=1)} = N\epsilon - n_{\text{in}}^{(H=1)}. \tag{7.7}$$

Note that we can re-write Eq. (7.7) for any hierarchical level $H > 0$ because the remaining outside connections will always the expected number of connections inside minus what was rewired:

$$n_{\text{out}}^{(H)} = N\epsilon - n_{\text{in}}^{(H)}. \tag{7.8}$$

For the 2nd hierarchical level, we follow the same procedure and obtain the expression for $n_{\text{in}}^{(H=2)}$, but now outside connections are also rewired:

$$\begin{aligned} n_{\text{in}}^{(H=2)} &= \frac{n_{\text{in}}^{(H=1)}}{2} + \frac{n_{\text{in}}^{(H=1)}}{2} \times R + n_{\text{out}}^{(H=1)} \times R \\ &= \frac{n_{\text{in}}^{(H=1)}}{2}(1 - R) + N\epsilon \times R. \end{aligned} \tag{7.9}$$

For hierarchical levels $H + 1 > 2$, we recursively apply the above equations and obtained the expression

$$n_{\text{in}}^{(H+1)} = \frac{N\epsilon}{2}\left[\left(\frac{1-R}{2}\right)^H + 2R\sum_{k=0}^{H}\left(\frac{1-R}{2}\right)^k\right]. \tag{7.10}$$

In summary, Eq. 7.10 gives the expected number of connections to a neuron that come from its own module at the hierarchical level $H + 1 > 2$, and Eq. (7.8) gives the respective connections that come from outside the module at any $H > 0$.

The set of Eqs. (7.6) – (7.10) can elucidate why cross-correlations increase with in a module as H increases. By dividing the expected number of connections inside a module by the number of neurons in the module we can obtain a rough approximation of the connectivity inside the module (ϵ_{in}).

In Fig. 7.5(a) we show how the value of ϵ_{in} changes according to the hierarchical level H, observe the clear exponential growth. More surprisingly, this plot also gives us a hint that indeed cross-correlations play a major role in shaping slow fluctuations in the hierarchical and modular network: as ϵ_{in} exponentially increases so does the cross-correlations. In fact, it is expected that a random rewiring of connections would lead to their exponential growth.
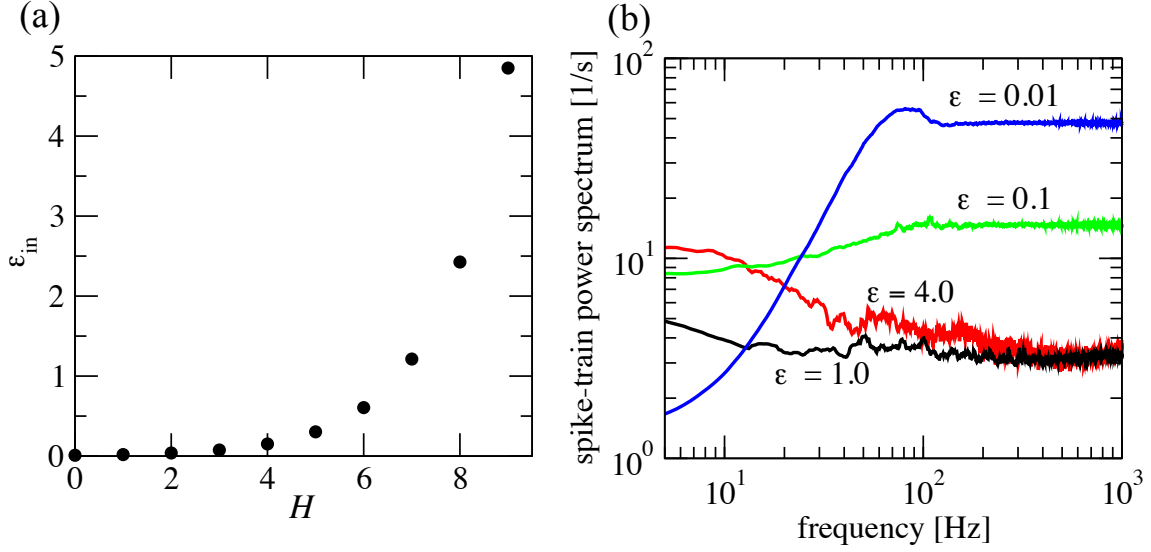
Figure 7.5: *Relation of connectivity and slow fluctuations.* *(a) Values of connectivity inside a module (ϵ_{in}) as H increases (cf. Eqs. 7.6 – 7.10). (b) Spike-train power spectra extracted for a small network of with $N = 2^{14}$ and $H = 0$ for different values of ϵ.*

In spite of that, to make really sure that cross-correlations are responsible for increasing slow-fluctuations, we simulated small networks with $N = 2^{14}$ and $H = 0$ while varying the value of ϵ. This latter experiment has the purpose of checking how slow fluctuations build up upon increasing connectivity as it happens along with the increasing of H. In Fig. 7.5(b) we present the spike-train power spectra of such experiment where one can see that in fact slow fluctuations start to build up as ϵ increases (note the initial values on the left side of the power spectra).

7.3.3 Propagation and processing and information flow in HMNs

Given the fact that a hierarchical and modular topology has an increased graph complexity, and observing that slow fluctuations can be achieved as well by the increase of J and ϵ, what could be the differences in communication and processing related with the use of such an intricate topology? This section focus on addressing this question and compares the single-neuron with the hierarchical and modular structure.

First, we recall Fig. 7.3(f), where we have observed that increasing H causes a significant enhancement in information flow calculated by selecting a randomly

chosen number of neuron pairs, which can be interpreted as an increase in the "usefulness" of a given spike train in predicting the future behavior of a second one. Here, to contrast communication in micro- (single neurons) and macroscopic (modules activity) levels, we evaluated information flow among modules activity $\langle TE^{(H)} \rangle$ as explained in the Methods section.

In Fig. 7.6(a) we can observe that the communication between modules is indeed very different from the one observed in Fig. 7.3(f). A most compelling difference is the change in behavior for low H where a non-monotonic curve is observed with a maximum close to $J = 0.2$ mV which decays for higher values of J. For high H this behavior is somewhat mirrored, see for instance that for $H = 7$ the maximum in $H = 5$ became a minimum and that the curve starts to grow after $J \gtrsim 0.2$ mV. As H increases even further, the through (peak for low H) vanishes and only a monotonic behavior remains.

Despite these differences, similarities are still found. Clearly there is a transition which changes the behavior of the $\langle TE^{(H)} \rangle$ curves with both H and J dependencies. In the case of H, one can observe that above and below $H = 7$ there are two contrasting behaviors similar to Fig. 7.3(f). In addition, the build up of slow fluctuations created by an increase of J also has an evident role in shaping the curves which may differ if the network is constructed with low or high H. Overall, the results in Fig. 7.6(a) express that a modular communication clearly takes place in the HMNs and that this communication is influenced by a microscopic parameter such as the synaptic strength J, although the single-neuron communication does not necessarily reflect what takes place in the modular communication as is depicted by Fig. 7.6(a).

The inset in Fig. 7.6(a) where we show the same data for each H in a boxplot presents an interesting information. We see that at $H = 6$ the $\langle TE^{(H)} \rangle$ is maximum and little distributed. This indicates that at $H = 6$ the communication is robust independently of J.

In the following, we remind the reader our discussion above where we argued that the higher the H the more individually modules become in the network, i.e. they start to work as functional units. To test this idea we computed the mutual information among modules which can be interpreted as a measure of statistical
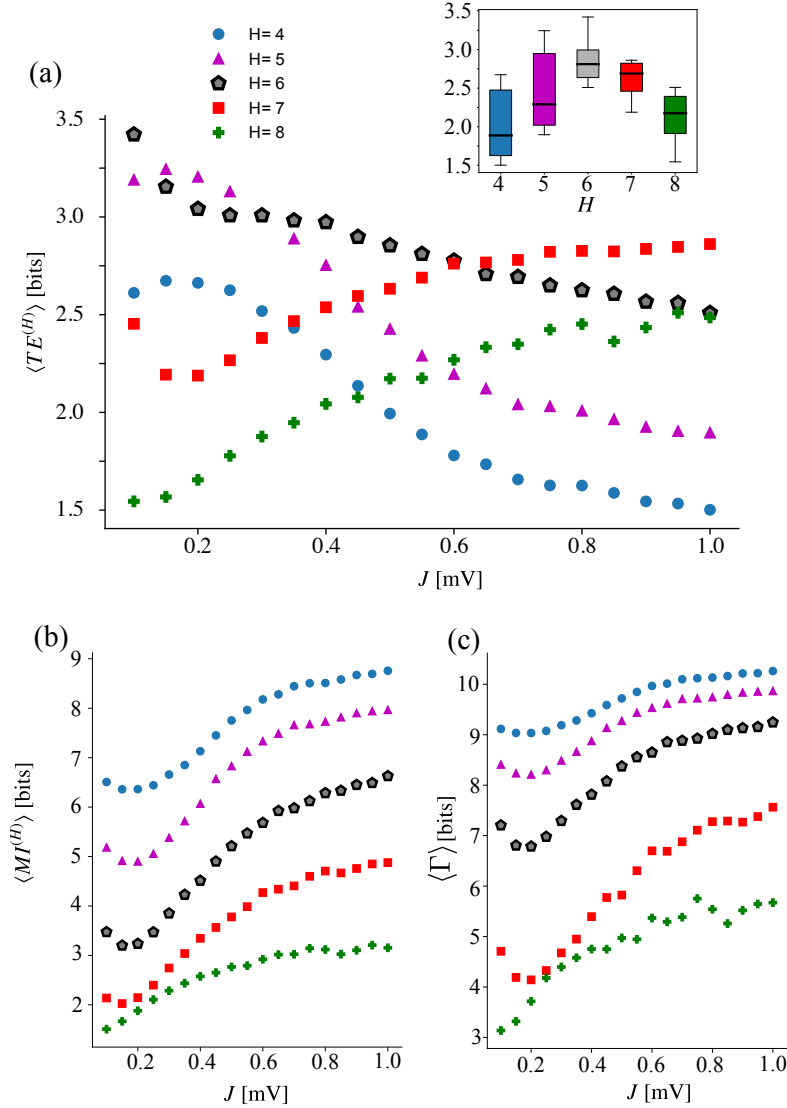
Figure 7.6: *Transfer entropy and mutual information among modules. The measures are extracted among modules evaluated for different values of J, see legend for H values in each curve. (a) $\langle TE^{(H)} \rangle$. (b) $\langle MI^{(H)} \rangle$. (c) $\langle \Gamma \rangle$.*

dependency (de Abril et al., 2018). We present these results in Fig. 7.6(b) where one can see that as H increases $\langle MI^{(H)} \rangle$ decreases indicating that the modules are acting more independently. Coupled with that, we see here how the synaptic efficacy J also plays a role in raising statistical dependency among modules, in cases of high hierarchy we see that for every configuration the higher the J the more dependent the modules become. The latter is similar to low H but a transition point takes place. These observations again suggest that the microscopic parameter J associated

with the slow fluctuations make the modules more dependent. Thus, we suggest that in our model slow fluctuations may endow modular statistical dependency.

We further analyzed how information is segregated in the network by extracting a multivariate mutual information among three modules activity and comparing it with the mutual information among pairs of the same modules (Williams & Beer, 2010; Wibral, Lizier, & Priesemann, 2015; Chicharro & Panzeri, 2017), we call this measure Γ which reads

$$\Gamma = MI^{(H)}(x; z) + MI^{(H)}(y; z) - MI^{(H)}(x; y; z), \tag{7.11}$$

where for Γ it is possible to assume every real value. If $\Gamma > 0$ we have redundant information, i.e. some information is repeated in different modules. Otherwise we have synergy. This analysis is displayed in Fig. 7.6(c) where we show the averaged Γ over the groups of every three adjacent modules. This measure shows that our HMN has redundant information. We see that increasing J facilitates the emergence of redundant information, nevertheless we see that increasing H removes redundancy.

7.4   Discussion

An interesting question in computational neuroscience has been the investigation of different dynamics achieved by networks composed of spiking neurons (Brunel, 2000; Renart et al., 2010; Wang et al., 2011; R. F. O. Pena et al., 2018) and in particular the ones that enhance information processing such as networks embedded in slow fluctuations (Litwin-Kumar & Doiron, 2012; Ostojic, 2014; Wieland et al., 2015). Structural characteristics and how they interact with the dynamics are also of great interest (Sporns, Chialvo, Kaiser, & Hilgetag, 2004; Reijneveld, Ponten, Berendse, & Stam, 2007) and, in this regard, a hierarchical and modular topology faithfully represents generic characteristics of a cortical network (Mountcastle, 1997; Kaiser & Hilgetag, 2010; Tomov et al., 2014). In this work, we have constructed large-scale networks populated by spiking neurons with increasing levels of hierarchy which we extracted information theory grounded measures. In addition, we investigated how the synaptic efficacy affects the slow fluctuations build up in these networks. Our goal was to analyze how the interplay of intrinsic neuronal

parameters and topological features influences activity propagation.

Our main finding is that the hierarchical and modular topology creates an effect of slow fluctuations, similar to the one created by an increase of synaptic efficacy, which in turn shapes information propagation and processing through those modules. Previous studies have shown that hierarchical and modular networks are advantageous in the sense of activity sustainment (Tomov et al., 2014) and can present critical behaviors (Wang et al., 2011) that are connected to optimal transmissions (Kinouchi & Copelli, 2006), here we see that modularity may also create optimal transmission. In particular, this does not necessarily happens due to high magnitude of information transfer, but may happen at a transition point in the level of hierarchical organization which endows a robust communication independently of synaptic strength.

In the work of Ostojic (Ostojic, 2014), augmentation of the synaptic strength creates a new type of asynchronous irregular activity which was argued by the author as a regime that favors information processing capability. Notwithstanding, in another work it was built an iterative scheme (Dummer et al., 2014) where only a single neuron is simulated over several generations whereby its input is statistically computed from the previous generation and this work was able to capture the very same statistics as in the network of (Ostojic, 2014; R. F. Pena et al., 2018). Our analysis of spike-trains' autocorrelation and cross-correlation functions are in accordance with the latter because they indicate no cross-correlation (population behavior) build up as the synaptic efficacy grows, i.e. the regime of Ostojic (Ostojic, 2014) seems to be rich in the neuronal level but not in the network level. In this way, our results show that an information propagation is unfavored in such a network where neurons are statistically equal.

On the contrary, in our simulations when hierarchical and modular architecture was increased, despite the similarities on build up of slow fluctuations that were found to an increase of the synaptic coupling, the spike-trains' cross-correlation function also increased. Recent studies have been putting forward the influence of correlations in neurons (Galán, Fourcaud-Trocme, Ermentrout, & Urban, 2006; Moreno-Bote, Renart, & Parga, 2008; Barreiro & Ly, 2018). Here, our transfer entropy measure shows an undoubtedly increase in the information

propagation of single-neurons at high hierarchical levels which we showed to be related to the raise of cross-correlations through their rewiring process.

As one of the objectives of our work was to understand the topological benefits for a hierarchical and modular structure, we compared the transfer entropy taken from pairs of single-neurons' spike-train and among modules. At high hierarchical levels, we observed a marked difference in orders of magnitude indicating that a communication over modules is preferred than through single-neurons. In like manner, networks with higher hierarchical and modular structure seem to optimized the communication through the population mechanisms. Surely, a signal sent from a population will be noted whereas a signal sent from a single neuron may be subjected to noise and other disturbances on its way.

In addition to that, we also saw that as hierarchy is increased modules start to act more individually, as demonstrated by the mutual information extracted among modules. In fact, it has been suggested elsewhere that activity in modular networks provides functional segregation and integration (Sporns, Tononi, & Edelman, 2000; Wang et al., 2011) which is certainly an advantage. To test this idea we evaluated the multivariate mutual information which demonstrated that information is redundant in the hierarchical and modular networks. Our analysis showed that the higher the number of modules the less redundancy is found. Notably, redundancy can be either seen as an advantage, so that information is robustly maintained, or as a disadvantage in the sense that modules do not possess unique information.

Overall, we believe that our work captures with simple network modeling, computational, and theoretical analyzes important properties for its communication and processing. We put forward a crucial understanding of how slow fluctuations build up in networks through individual and population mechanisms. Our study can be well applied to future research focusing on the discernment of how cortical networks optimize information processing and propagation.

<div align="right">

CHAPTER **8**

</div>

CONCLUSIONS

The work developed in this thesis had as objective the investigation of the emergence of fluctuations in cortical network models with heterogeneous populations. Heterogeneity was approached by either increasing topological complexity or by adding different neuronal classes to the problem. In Sect. 2.3 we defined differences among (i) rhythmic fluctuations, (ii) non-rhythmic fluctuations, and (iii) noise. Having these differences stated, in each chapter we investigated (i–iii) with the help of neuronal modeling.

- In Chapter 4 we started our work by investigating the global characteristics of a network composed of different electrophysiological classes and varying its hierarchical and modular level. We aimed parameter regions where rhythmic (oscillatory) self-sustained activity appears. Our investigations showed the role of both classes and topology in sustaining activity. In addition, we have identified that the network displays transient chaos through statistical analysis of its escape rate over a large ensemble of initial conditions. We observed that trajectories leave the chaotic set in a very narrow unstable region which we called "hole" in a phenomenological description. The concept of hole was used to explain why higher levels of hierarchy sustain activity longer.

- In Chapter 5 we studied random networks with mixtures of different neurons and showed how synaptic noise influences these networks. Our results show that both rhythmic and non-rhythmic fluctuations emerge upon synaptic noise inclusion. Markedly, the two types of fluctuations develop intermittent transitions between each other which are regulated by the level of noise: if

<div align="center">

133

</div>

the noise amplitude is higher, rhythmic fluctuations are more apparent. The development of such activity was carefully studied by means of dynamical systems analysis. Results were compared with different neuronal models.

- In Chapter 6 we developed a reduced iterative self-consistent scheme to describe second-order statistics without the use of costly simulations. This consisted in an extension of the iterative scheme proposed by Lerchner, Ursta, et al. (2006) and extended by Dummer et al. (2014). In this scheme, instead of simulating a network, two single neurons were simulated for several generations: in each generation, surrogate noise with statistics based on the output of the previous generation was injected as input in the neurons. It was shown that the the power spectra of the neurons converge to self-consistent results in several situations. By using the iterative scheme we managed to explain various scenarios where build up of slow fluctuations is found in neurons, with special emphasis on scenarios where heterogeneities are in the cells or inbuilt in modules.

- In Chapter 7 we investigated more specifically the emergence of slow fluctuations. We observed that not only the synaptic strength but also the hierarchical and modular levels are responsible for the build up of slow fluctuations. We attributed the latter to an increase in cross-correlations which was not observed in the former. We tried to link these observations with advantages by means of information processing and measures of propagation where we managed to find optimal hierarchical and modular levels and synaptic strength amplitudes. These results bring new ideas on how the interplay of topology and synaptic efficacy acts upon information processing and information flow.

As future expectations, we believe that results from this thesis bring new conceptual advances that could be potentially used and extended in several directions that were not approached here:

- The results in Chapter 4 could be tested in experiments involving *in vitro* or *in vivo* self-sustained activity where a phenomenological understanding of

the existence of a "hole" could be advantageous. For instance, a sustained pathological focus could be terminated with an application of a well oriented input that would lead the system to its "hole". Moreover, the results reported in that chapter are restricted to very periodic behavior, further development has to be made in the direction of aperiodic oscillations such as the ones that are usually reported in several experiments (Wilson, 2008).

- Results from Chapter 5 could be extended to different types of noise, for instance, additive noise in the voltage variables. Moreover, the analysis using dynamical systems that was developed in that chapter could be used as a tool to investigate network behavior generated by networks that differ only by their neuronal composition. This is a study that deserves some attention, to the best of our knowledge there is no such comparison in the literature.

- Further extensions of the iterative scheme developed in Chapter 6 can be done as well. For example, they could include cross-correlations. This would allow a wider range of situations which cannot be reproduced by the present development.

- Results in Chapter 7 could be used to predict the propagation of inputs in a network. The opposite has also some importance: breaking the propagation of some pathological input indirectly by removing slow-fluctuations from the network could be tested. This could be done by selecting inputs with second-order statistics prescribed in a way that low frequencies would be affected.

These are only examples of possible extensions, other ideas are reported in the respective chapters.

Most of the results shown here were published in prestigious journals as described in Chapter 1. In this regard, we believe that the results reported in this thesis helped to move forward the knowledge on how fluctuations emerge in and affect cortical network models.

In summary, we believe that the initial proposal was achieved justifying this Ph.D. Thesis.

CHAPTER 9

REFERENCES

Abbott, L., & van Vreeswijk, C. (1993). Asynchronous states in networks of pulse-coupled oscillators. *Phys. Rev. E*, *48*, 1483–1490.

Ahn, S., & Rubchinsky, L. L. (2013). Short desynchronization episodes prevail in synchronous dynamics of human brain rhythms. *Chaos*, *23*, 013138.

Ahn, S., & Rubchinsky, L. L. (2017). Potential mechanisms and functions of intermittent neural synchronization. *Front. Comput. Neurosci.*, *11*, 44.

Aljadeff, J., Stern, M., & Sharpee, T. (2015). Transition to Chaos in Random Networks with Cell-Type-Specific Connectivity. *Phys. Rev. Lett.*, *114*, 088101.

Amit, D. J., & Brunel, N. (1997a). Dynamics of a recurrent network of spiking neurons before and following learning. *Networ. Comput. Neural Syst.*, *8*, 373–404.

Amit, D. J., & Brunel, N. (1997b). Model of global spontaneous activity and local structured activity during delay periods in the cerebral cortex. *Cereb. Cortex*, *7*, 237–252.

Aydore, S., Pantazis, D., & Leahy, R. M. (2013). A note on the phase locking value and its properties. *NeuroImage*, *74*, 231–244.

Bair, W., Koch, C., Newsome, W., & Britten, K. (1994). Power spectrum analysis of bursting cells in area mt in the behaving monkey. *J. Neurosci.*, *14*, 2870–2892.

Baranauskas, G., Maggiolini, E., Vato, A., Angotzi, G., Bonfanti, A., Zambra, G., ... Fadiga, L. (2011). Origins of $1/f^2$ scaling in the power spectrum of intracortical local field potential. *J. Neurophysiol.*, *107*, 984–994.

Barreiro, A. K., & Ly, C. (2018). Investigating the correlation–firing rate relationship in heterogeneous recurrent networks. *J. Math. Neurosci.*, *8*, 8.

Bassett, D. S., Greenfield, D. L., Meyer-Lindenberg, A., Weinberger, D. R., Moore, S. W., & Bullmore, E. T. (2010). Efficient physical embedding of topologically complex information processing networks in brains and computer circuits. *PLoS Comput. Biol.*, *6*, e1000748.

Battaglia, D., Brunel, N., & Hansel, D. (2007). Temporal decorrelation of collective oscillations in neural networks with local inhibition and long-range excitation. *Phys. Rev. Lett.*, *99*, 238106.

Bauermeister, C., Schwalger, T., Russell, D., Neiman, A. B., & Lindner, B.

(2013). Characteristic effects of stochastic oscillatory forcing on neural firing: Analytical theory and comparison to paddlefish electroreceptor data. *PLoS Comput. Biol.*, *9*, e1003170.

Bazhenov, M., Timofeev, I., Steriade, M., & Sejnowski, T. J. (2002). Model of thalamocortical slow-wave sleep oscillations and transitions to activated states. *J. Neurosci.*, *22*, 8691–8704.

Bear, M. F., Connors, B. W., & Paradiso, M. A. (2007). *Neuroscience* (Vol. 2). Lippincott Williams & Wilkins.

Bédard, C., & Destexhe, A. (2009). Macroscopic models of local field potentials and the apparent $1/f$ noise in brain activity. *Biophys. J.*, *96*, 2589–2603.

Beggs, J. M., & Plenz, D. (2003). Neuronal avalanches in neocortical circuits. *J. Neurosci.*, *23*, 11167–11177.

Benita, J. M., Guillamon, A., Deco, G., & Sanchez-Vives, M. V. (2012). Synaptic depression and slow oscillatory activity in a biophysical network model of the cerebral cortex. *Front. Comput. Neurosci.*, *6*, 64.

Benzi, R., Sutera, A., & Vulpiani, A. (1981). The mechanism of stochastic resonance. *J. Phys. A-Math Gen.*, *14*, L453.

Binzegger, T., Douglas, R. J., & Martin, K. A. (2004). A quantitative map of the circuit of cat primary visual cortex. *J. Neurosci.*, *24*, 8441–8453.

Blanco, S., Garay, A., & Coulombie, D. (2013). Comparison of frequency bands using spectral entropy for epileptic seizure prediction. *ISRN Neurol.*, *2013*, 287327.

Bonifazi, P., Goldin, M., Picardo, M. A., Jorquera, I., Cattani, A., Bianconi, G., . . . Cossart, R. (2009). Gabaergic hub neurons orchestrate synchrony in developing hippocampal networks. *Science*, *326*, 1419–1424.

Bosking, W. H., Zhang, Y., Schofield, B., & Fitzpatrick, D. (1997). Orientation selectivity and the arrangement of horizontal connections in tree shrew striate cortex. *J. Neurosci.*, *17*, 2112–2127.

Boucsein, C., Nawrot, M. P., Schnepel, P., & Aertsen, A. (2011). Beyond the cortical column: abundance and physiology of horizontal connections imply a strong role for inputs from the surround. *Front. Neurosci.*, *5*, 32.

Brette, R., & Gerstner, W. (2005). Adaptive exponential integrate-and-fire model as an effective description of neuronal activity. *J. Neurophysiol.*, *94*, 3637–3642.

Britten, K. H., Shadlen, M. N., Newsome, W. T., & Movshon, J. A. (1993). Responses of neurons in macaque mt to stochastic motion signals. *Visual Neurosci.*, *10*, 1157–1169.

Brochini, L., de Andrade Costa, A., Abadi, M., Roque, A. C., Stolfi, J., & Kinouchi, O. (2016). Phase transitions and self-organized criticality in networks of stochastic spiking neurons. *Sci. Rep.*, *6*, 35831.

Brunel, N. (2000). Dynamics of sparsely connected networks of excitatory and inhibitory spiking neurons. *J. Comput. Neurosci.*, *8*, 183–208.

Brunel, N., & Hakim, V. (1999). Fast global oscillations in networks of integrate-and-fire neurons with low firing rates. *Neural Comput.*, *11*, 1621–1671.

Brunel, N., & Sergi, S. (1998). Firing frequency of leaky intergrate-and-fire neurons with synaptic current dynamics. *J. Theor. Biol.*, *195*, 87–95.

Brunel, N., & Wang, X. J. (2001). Effects of neuromodulation in a cortical network model of object working memory dominated by recurrent inhibition. *J. Comput. Neurosci.*, *11*, 63–85.

Bullmore, E., & Sporns, O. (2009). Complex brain networks: graph theoretical analysis of structural and functional systems. *Nat. Rev. Neurosci.*, *10*, 186–198.

Buzsáki, G. (2006). *Rhythms of the brain*. New York, Oxford: Oxford University Press.

Buzsáki, G., & Draguhn, A. (2004). Neuronal oscillations in cortical networks. *Science*, *304*, 1926–1929.

Celka, P. (2007). Statistical analysis of the phase-locking value. *IEEE Signal Proc. Let.*, *14*, 577–580.

Cessac, B., & Viéville, T. (2008). On dynamics of integrate-and-fire neural networks with conductance based synapses. *Front. Comput. Neurosci.*, *2*, 2.

Chen, J.-Y., Chauvette, S., Skorheim, S., Timofeev, I., & Bazhenov, M. (2012). Interneuron-mediated inhibition synchronizes neuronal activity during slow oscillation. *J. Physiol.-London*, *590*, 3987–4010.

Chicharro, D., & Panzeri, S. (2017). Synergy and redundancy in dual decompositions of mutual information gain and information loss. *Entropy*, *19*, 71.

Colgin, L. L. (2011). Oscillations and hippocampal–prefrontal synchrony. *Curr. Opin. Neurobiol.*, *21*, 467–474.

Compte, A., Brunel, N., Goldman-Rakic, P. S., & Wang, X.-J. (2000). Synaptic mechanisms and network dynamics underlying spatial working memory in a cortical network model. *Cereb. Cortex*, *10*, 910–923.

Compte, A., Sanchez-Vives, M. V., McCormick, D. A., & Wang, X.-J. (2003). Cellular and network mechanisms of slow oscillatory activity ($<$ 1 Hz) and wave propagations in a cortical network model. *J. Neurophysiol.*, *89*, 2707–2725.

Connors, B., Gutnick, M., & Prince, D. (1982). Electrophysiological properties of neocortical neurons in vitro. *J. Neurophysiol.*, *48*, 1302–1320.

Contreras, D. (2004). Electrophysiological classes of neocortical neurons. *Neural Networks*, *17*, 633–646.

Contreras, D., & Steriade, M. (1995). Cellular basis of eeg slow rhythms: a study of dynamic corticothalamic relationships. *J. Neurosci.*, *15*, 604–622.

Contreras, D., Timofeev, I., & Steriade, M. (1996). Mechanisms of long-lasting hyperpolarizations underlying slow sleep oscillations in cat corticothalamic networks. *J. Physiol.-London*, *494*, 251–264.

Curtis, C. E., & D'Esposito, M. (2003). Persistent activity in the prefrontal cortex during working memory. *Trends Cogn. Sci.*, *7*, 415–423.

Dayan, P., & Abbott, L. F. (2001). *Theoretical neuroscience*. Cambridge, MA: MIT Press.

de Abril, I. M., Yoshimoto, J., & Doya, K. (2018). Connectivity inference from

neural recording data: Challenges, mathematical bases and research directions. *Neural Networks*, *102*, 120–137.

Deger, M., Schwalger, T., Naud, R., & Gerstner, W. (2014). Fluctuations and information filtering in coupled populations of spiking neurons with adaptation. *Phys. Rev. E*, *90*, 062704.

de la Rocha, J., Doiron, B., Shea-Brown, E., Josic, K., & Reyes, A. (2007). Correlation between neural spike trains increases with firing rate. *Nature*, *448*, 802–6.

Deniz, T., & Rotter, S. (2017). Solving the two-dimensional Fokker-Planck equation for strongly correlated neurons. *Phys. Rev. E*, *95*, 012412.

Destexhe, A. (2009). Self-sustained asynchronous irregular states and up–down states in thalamic, cortical and thalamocortical networks of nonlinear integrate-and-fire neurons. *J. Comput. Neurosci.*, *27*, 493–506.

Destexhe, A., Rudolph, M., Fellous, J.-M., & Sejnowski, T. J. (2001). Fluctuating synaptic conductances recreate in vivo-like activity in neocortical neurons. *Neuroscience*, *107*, 13–24.

Destexhe, A., & Rudolph-Lilith, M. (2012). *Neuronal noise*. New York: Springer.

Doiron, B., Lindner, B., Longtin, A., Maler, L., & Bastian, J. (2004). Oscillatory activity in electrosensory neurons increases with the spatial correlation of the stochastic input stimulus. *Phys. Rev. Lett.*, *93*, 048101.

Doiron, B., Litwin-Kumar, A., Rosenbaum, R., Ocker, G. K., & Josić, K. (2016). The mechanics of state-dependent neural correlations. *Nat. Neurosci.*, *19*, 383–393.

Droste, F., & Lindner, B. (2017a). Exact analytical results for integrate-and-fire neurons driven by excitatory shot noise. *J. Comp. Neurosci.*, *43*, 81–91.

Droste, F., & Lindner, B. (2017b). Up-down-like background spiking can enhance neural information transmission. *eNeuro*, ENEURO–0282-17.

Duc, K. D., Parutto, P., Chen, X., Epsztein, J., Konnerth, A., & Holcman, D. (2015). Synaptic dynamics and neuronal network connectivity are reflected in the distribution of times in up states. *Front. Comput. Neurosci.*, *9*, 96.

Dummer, B., Wieland, S., & Lindner, B. (2014). Self-consistent determination of the spike-train power spectrum in a neural network with sparse connectivity. *Front. Comput. Neurosci.*, *8*, 104.

Durstewitz, D., & Deco, G. (2008). Computational significance of transient dynamics in cortical networks. *Eur. J. Neurosci.*, *27*, 217–227.

Edwards, B. W., Wakefield, G. H., & Powers, N. L. (1993). The spectral shaping of neural discharges by refractory effects. *J. Acoust. Soc. Am.*, *93*, 3353.

Eissfeller, H., & Opper, M. (1992). New Method for Studying the Dynamics of Disordered Spin Systems Without Finite-Size Effects. *Phys. Rev. Lett.*, *68*, 2094.

El Boustani, S., Pospischil, M., Rudolph-Lilith, M., & Destexhe, A. (2007). Activated cortical states: experiments, analyses and models. *J. Physiol.-Paris*, *101*, 99–109.

Erdős, P., & Rényi, A. (1959). On random graphs, i. *Publ. Math.-Debrecen*, *6*, 290–297.

Ermentrout, B., Pascal, M., & Gutkin, B. (2001). The effects of spike frequency adaptation and negative feedback on the synchronization of neural oscillators. *Neural Comput.*, *13*, 1285–1310.

Faisal, A. A., Selen, L. P., & Wolpert, D. M. (2008). Noise in the nervous system. *Nat. Rev. Neurosci.*, *9*, 292–303.

Fourcaud-Trocmé, N., Hansel, D., van Vreeswijk, C., & Brunel, N. (2003). How spike generation mechanisms determine the neuronal response to fluctuating inputs. *J. Neurosci.*, *23*, 11628–40.

Franklin, J., & Bair, W. (1995). The effect of a refractory period on the power spectrum of neuronal discharge. *SIAM J. Appl. Math.*, *55*, 1074–1093.

Galán, R. F., Fourcaud-Trocme, N., Ermentrout, G. B., & Urban, N. N. (2006). Correlation-induced synchronization of oscillations in olfactory bulb neurons. *J. Neurosci.*, *26*, 3646–3655.

Gerstner, W., Kistler, W. M., Naud, R., & Paninski, L. (2014). *Neuronal dynamics: From single neurons to networks and models of cognition*. Cambridge: Cambridge University Press.

Ghorbani, M., Mehta, M., Bruinsma, R., & Levine, A. J. (2012). Nonlinear-dynamics theory of up-down transitions in neocortical neural networks. *Phys. Rev. E*, *85*, 021908.

Gillespie, D. T. (1996). The mathematics of brownian motion and johnson noise. *Am. J. Phys.*, *64*, 225–240.

Girones, Z., & Destexhe, A. (2016). Enhanced responsiveness in asynchronous irregular neuronal networks. *arXiv preprint arXiv:1611.09089*.

Gray, C. M., & McCormick, D. A. (1996). Chattering cells: superficial pyramidal neurons contributing to the generation of synchronous oscillations in the visual cortex. *Science*, *274*, 109–13.

Greenberg, D. S., Houweling, A. R., & Kerr, J. N. (2008). Population imaging of ongoing neuronal activity in the visual cortex of awake rats. *Nat. Neurosci.*, *11*, 749–751.

Grewe, J., Kruscha, A., Lindner, B., & Benda, J. (2017). Synchronous Spikes are Necessary but not Sufficient for a Synchrony Code. *P. Natl. Acad. Sci. USA*, *114*, E1977—E1985.

Grün, S., & Rotter, S. (2010). *Analysis of parallel spike trains* (Vol. 7). Springer.

Guillery, R. W. (2005). Observations of synaptic structures: origins of the neuron doctrine and its current status. *Philos. T. Roy. Soc. B*, *360*, 1281–1307.

Hahn, G., Ponce-Alvarez, A., Monier, C., Benvenuti, G., Kumar, A., Chavane, F., . . . Frégnac, Y. (2017). Spontaneous cortical activity is transiently poised close to criticality. *PLoS Comput. Biol.*, *13*, e1005543.

Haider, B., Häusser, M., & Carandini, M. (2013). Inhibition dominates sensory responses in the awake cortex. *Nature*, *493*, 97–100.

Hänggi, P., & Jung, P. (1995). Colored noise in dynamical-systems. *Adv. Chem. Phys.*, *89*, 239–326.

Harris, K. D., & Thiele, A. (2011). Cortical state and attention. *Nat. Rev. Neurosci.*, *12*, 509–523.

Harrison, P. M., Badel, L., Wall, M. J., & Richardson, M. J. E. (2015). Experimentally Verified Parameter Sets for Modelling Heterogeneous Neocortical Pyramidal-Cell Populations. *PLoS Comput. Biol.*, *11*, 8.

Helias, M., Tetzlaff, T., & Diesmann, M. (2014). The Correlation Structure of Local Neuronal Networks Intrinsically Results from Recurrent Dynamics. *PLoS Comput. Biol.*, *10*, e1003428.

Hill, S., & Tononi, G. (2005). Modeling sleep and wakefulness in the thalamocortical system. *J. Neurophysiol.*, *93*, 1671–1698.

Hodgkin, A. L., & Huxley, A. F. (1952). A quantitative description of membrane current and its application to conduction and excitation in nerve. *J. Physiol.*, *117*, 500–544.

Holcman, D., & Tsodyks, M. (2006). The emergence of up and down states in cortical networks. *PLoS Comput. Biol.*, *2*, e23.

Hopfield, J. J., & Herz, A. V. M. (1995). Rapid local synchronization of action potentials: Towards computation with coupled integrate-and-fire neurons. *Proc. Natl. Acad. USA*, *92*, 6655–6662.

Ito, S., Hansen, M. E., Heiland, R., Lumsdaine, A., Litke, A. M., & Beggs, J. M. (2011). Extending transfer entropy improves identification of effective connectivity in a spiking cortical network model. *PloS One*, *6*, e27431.

Izhikevich, E. M. (2000). Neural excitability, spiking and bursting. *Int. J. Bifurcat. Chaos*, *10*, 1171–1266.

Izhikevich, E. M. (2003). Simple model of spiking neurons. *IEEE T. Neural Networ.*, *14*, 1569–1572.

Izhikevich, E. M. (2007). *Dynamical systems in neuroscience*. Cambridge, MA: MIT Press.

Izhikevich, E. M., & Edelman, G. M. (2008). Large-scale model of mammalian thalamocortical systems. *Proc. Natl. Acad. Sci. USA*, *105*, 3593–3598.

Jarvis, M., & Mitra, P. (2001). Sampling properties of the spectrum and coherency of sequences of action potentials. *Neural Comput.*, *13*, 717–49.

Jercog, D., Roxin, A., Barthó, P., Luczak, A., Compte, A., & de la Rocha, J. (2017). Up-down cortical dynamics reflect state transitions in a bistable network. *eLife*, *6*, e22425.

Kadmon, J., & Sompolinsky, H. (2015). Transition to Chaos in Random Neuronal Networks. *Phys. Rev. X 5*, *5*, 041030.

Kaiser, M., & Hilgetag, C. C. (2010). Optimal hierarchical modular topologies for producing limited sustained activation of neural networks. *Front. Neuroinform.*, *4*, 8.

Kandel, E. R., Schwartz, J. H., Jessell, T. M., et al. (2000). *Principles of neural science* (Vol. 4). McGraw-Hill New York.

Kane, M. J., & Engle, R. W. (2002). The role of prefrontal cortex in working-memory capacity, executive attention, and general fluid intelligence: An individual-differences perspective. *Psychon. B Rev.*, *9*, 637–671.

Kang, Y., & Kayano, F. (1994). Electrophysiological and morphological characteristics of layer vi pyramidal cells in the cat motor cortex. *J. Neurophysiol.*, *72*, 578–591.

Kavalali, E. T. (2015). The mechanisms and functions of spontaneous neurotransmitter release. *Nat. Rev. Neurosci.*, *16*, 5–16.

Kinouchi, O., & Copelli, M. (2006). Optimal dynamical range of excitable networks at criticality. *Nat. Phys.*, *2*, 348–351.

Knight, B. W. (1972). Relationship Between Firing Rate of a Single Neuron and Level of Activity in a Population of Neurons - Experimental Evidence for Resonant Enhancement in Population Response. *J. Gen. Physiol.*, *59*, 767–78.

Kriener, B., Enger, H., Tetzlaff, T., Plesser, H. E., Gewaltig, M.-O., & Einevoll, G. T. (2014). Dynamics of self-sustained asynchronous-irregular activity in random networks of spiking neurons with strong synapses. *Front. Comput. Neurosci.*, *8*, 136.

Kumar, A., Schrader, S., Aertsen, A., & Rotter, S. (2008). The high-conductance state of cortical networks. *Neural Comput.*, *20*, 1–43.

Lachaux, J.-P., Rodriguez, E., Martinerie, J., & Varela, F. J. (1999). Measuring phase synchrony in brain signals. *Hum. Brain Mapp.*, *8*, 194–208.

Ladenbauer, J., Augustin, M., Shiau, L., & Obermayer, K. (2012). Impact of adaptation currents on synchronization of coupled exponential integrate-and-fire neurons. *PLoS Comput. Biol.*, *8*, e1002478.

Lai, Y.-C., & Tél, T. (2011). *Transient chaos: complex dynamics on finite time scales* (Vol. 173). Springer Science & Business Media.

Landau, I. D., Egger, R., Dercksen, V. J., Oberlaender, M., & Sompolinsky, H. (2016). The impact of structural heterogeneity on excitation-inhibition balance in cortical networks. *Neuron*, *92*, 1106–1121.

Lapicque, L. (1907). Recherches quantitatives sur l'excitation électrique des nerfs traitéecomme une polarization. *J. Physiol. Pathol. Gen.*, *9*, 620—635.

Lerchner, A., Sterner, G., Hertz, J., & Ahmadi, M. (2006). Mean field theory for a balanced hypercolumn model of orientation selectivity in primary visual cortex. *Networ. Comput. Neural Syst.*, *17*, 131–50.

Lerchner, A., Ursta, C., Hertz, J., Ahmadi, M., Ruffiot, P., & Enemark, S. (2006). Response variability in balanced cortical networks. *Neural Comput.*, *18*, 634–659.

Leszczyński, M., Fell, J., & Axmacher, N. (2015). Rhythmic working memory activation in the human hippocampus. *Cell Rep.*, *13*, 1272–1282.

Levenstein, D., Buzsaki, G., & Rinzel, J. (2018). Excitable dynamics of nrem sleep: a unifying model for neocortex and hippocampus. *bioRxiv*, 312587.

Lindner, B. (2006). Superposition of many independent spike trains is generally not a poisson process. *Phys. Rev. E*, *73*, 022901.

Lindner, B. (2009). A brief introduction to some simple stochastic processes. *Stochastic Methods in Neuroscience*, 1.

Lindner, B., Doiron, B., & Longtin, A. (2005). Theory of oscillatory firing induced by spatially correlated noise and delayed inhibitory feedback. *Phys. Rev. E.*,

72, 061919.

Lindner, B., Schimansky-Geier, L., & Longtin, A. (2002). Maximizing spike train coherence or incoherence in the leaky integrate-and-fire model. *Phys. Rev. E.*, *66*, 031916.

Litwin-Kumar, A., & Doiron, B. (2012). Slow dynamics and high variability in balanced cortical networks with clustered connections. *Nat. Neurosci.*, *15*, 1498–1505.

Liu, Z.-W., Faraguna, U., Cirelli, C., Tononi, G., & Gao, X.-B. (2010). Direct evidence for wake-related increases and sleep-related decreases in synaptic strength in rodent cortex. *J. Neurosci.*, *30*, 8671–8675.

Lo, C.-C., Amaral, L. N., Havlin, S., Ivanov, P. C., Penzel, T., Peter, J.-H., & Stanley, H. E. (2002). Dynamics of sleep-wake transitions during sleep. *Europhys. Lett.*, *57*, 625–631.

Longtin, A. (2013). Neuronal noise. *Scholarpedia*, *8*, 1618.

Lowet, E., Roberts, M. J., Bonizzi, P., Karel, J., & De Weerd, P. (2016). Quantifying neural oscillatory synchronization: a comparison between spectral coherence and phase-locking value approaches. *PloS One*, *11*, e0146443.

Lytton, W. W., Arle, J., Bobashev, G., Ji, S., Klassen, T. L., Marmarelis, V. Z., . . . Sanger, T. D. (2017). Multiscale modeling in the clinic: diseases of the brain and nervous system. *Brain Inform.*, *4*, 219–230.

Maimon, G., & Assad, J. A. (2009). Beyond poisson: increased spike-time regularity across primate parietal cortex. *Neuron*, *62*, 426–440.

Mannella, R. (2002). Integration of stochastic differential equations on a computer. *Int. J. Mod. Phys. C*, *13*, 1177–1194.

Mari, C. F. (2000). Random networks of spiking neurons: instability in the xenopus tadpole moto-neural pattern. *Phys. Rev. Lett.*, *85*, 210.

Mastrogiuseppe, F., & Ostojic, S. (2017). Intrinsically-generated fluctuating activity in excitatory-inhibitory networks. *PLoS Comput. Biol.*, *13*, e1005498.

Mattia, M., & Del Giudice, P. (2002). Population dynamics of interacting spiking neurons. *Phys. Rev. E*, *66*, 051917.

Mattia, M., & Sanchez-Vives, M. V. (2012). Exploring the spectrum of dynamical regimes and timescales in spontaneous cortical activity. *Cogni. Neurodynamics*, *6*, 239–250.

McCormick, D. A., Connors, B. W., Lighthall, J. W., & Prince, D. A. (1985). Comparative electrophysiology of pyramidal and sparsely spiny stellate neurons of the neocortex. *J. Neurophysiol.*, *54*, 782–806.

McDonnell, M. D., Goldwyn, J. H., & Lindner, B. (2016). Neuronal stochastic variability: influences on spiking dynamics and network activity. *Front. Comput. Neurosci.*, *10*, 38.

Mejias, J. F., Murray, J. D., Kennedy, H., & Wang, X.-J. (2016). Feedforward and feedback frequency-dependent interactions in a large-scale laminar network of the primate cortex. *Sci. Adv.*, *2*, e1601335.

Meunier, D., Lambiotte, R., & Bullmore, E. T. (2010). Modular and hierarchically modular organization of brain networks. *Front. Neurosci.*, *4*, 200.

Middleton, J., Chacron, M., Lindner, B., & Longtin, A. (2003). Firing statistics of a neuron model driven by long-range correlated noise. *Phys. Rev. E*, *68*, 021920.

Miller, J. K., Ayzenshtat, I., Carrillo-Reid, L., & Yuste, R. (2014). Visual stimuli recruit intrinsically generated cortical ensembles. *Proc. Natl. Acad. Sci. USA*, *111*, E4053–E4061.

Millman, D., Mihalas, S., Kirkwood, A., & Niebur, E. (2010). Self-organized criticality occurs in non-conservative neuronal networks during 'up' states. *Nat. Phys.*, *6*, 801–805.

Mongillo, G., Barak, O., & Tsodyks, M. (2008). Synaptic theory of working memory. *Science*, *319*, 1543–6.

Moreno-Bote, R., Renart, A., & Parga, N. (2008). Theory of input spike auto- and cross-correlations and their effect on the response of spiking neurons. *Neural Comput.*, *20*, 1651—705.

Moreno-Bote, R., Rinzel, J., & Rubin, N. (2007). Noise-induced alternations in an attractor network model of perceptual bistability. *J. Neurophysiol.*, *98*, 1125–1139.

Mountcastle, V. B. (1997). The columnar organization of the neocortex. *Brain*, *120*, 701–722.

Neiman, A. B., & Russell, D. F. (2011). Sensory coding in oscillatory electroreceptors of paddlefish. *Chaos*, *21*, 047505.

Neiman, A. B., Yakusheva, T. A., & Russell, D. F. (2007). Noise-induced transition to bursting in responses of paddlefish electroreceptor afferents. *J. Neurophysiol.*, *98*, 2795–2806.

Neymotin, S. A., McDougal, R. A., Bulanova, A. S., Zeki, M., Lakatos, P., Terman, D., ... Lytton, W. W. (2016). Calcium regulation of hcn channels supports persistent activity in a multiscale model of neocortex. *Neuroscience*, *316*, 344–366.

Nowak, L. G., Azouz, R., Sanchez-Vives, M. V., Gray, C. M., & McCormick, D. A. (2003). Electrophysiological classes of cat primary visual cortical neurons in vivo as revealed by quantitative analyses. *J. Neurophysiol.*, *89*, 1541–1566.

Okun, M., Steinmetz, N. A., Cossell, L., Iacaruso, M. F., Ko, H., Barthó, P., ... others (2015). Diverse coupling of neurons to populations in sensory cortex. *Nature*, *521*, 511–515.

Ostojic, S. (2014). Two types of asynchronous activity in networks of excitatory and inhibitory spiking neurons. *Nat. Neurosci.*, *17*, 594–600.

Ostojic, S., Brunel, N., & Hakim, V. (2009). How connectivity, background activity, and synaptic properties shape the cross-correlation between spike trains. *J. Neurosci.*, *29*, 10234–10253.

Paltridge, B. (2002). Thesis and dissertation writing: an examination of published advice and actual practice. *Engl. Specif. Purp.*, *21*, 125–143.

Parga, N., & Abbott, L. F. (2007). Network model of spontaneous activity exhibiting synchronous transitions between up and down states. *Front. Neurosci.*, *1*, 57–66.

Pena, R. F., Vellmer, S., Bernardi, D., Roque, A., & Lindner, B. (2018). Self-consistent scheme for spike-train power spectra in heterogeneous sparse networks. *Front. Comput. Neurosci.*, *12*, 9.

Pena, R. F. O., Zaks, M. A., & Roque, A. C. (2018). Dynamics of spontaneous activity in random networks with multiple neuron subtypes and synaptic noise. *J. Comput. Neurosci.*, *45*, 1–28.

Pesaran, B., Pezaris, J., Sahani, M., Mitra, P., & Andersen, R. (2002). Temporal structure in neuronal activity during working memory in macaque parietal cortex. *Nat. Neurosci.*, *5*, 805–811.

Plenz, D., & Aertsen, A. (1996). Neural dynamics in cortex-striatum co cultures ii. spatiotemporal characteristics of neuronal activity. *Neuroscience*, *70*, 893–924.

Potjans, T. C., & Diesmann, M. (2014). The cell-type specific cortical microcircuit: relating structure and activity in a full-scale spiking network model. *Cereb. Cortex*, *24*, 785–806.

Poulet, J. F. A., & Petersen, C. C. H. (2008). Internal brain state regulates membrane potential synchrony in barrel cortex of behaving mice. *Nature*, *454*, 881–5.

Pulido, C., & Marty, A. (2017). Quantal fluctuations in central mammalian synapses: Functional role of vesicular docking sites. *Physiol. Rev.*, *97*, 1403–1430.

Rao, Y., Liu, Z.-W., Borok, E., Rabenstein, R. L., Shanabrough, M., Lu, M., . . . Gao, X.-B. (2007). Prolonged wakefulness induces experience-dependent synaptic plasticity in mouse hypocretin/orexin neurons. *J. Clin. Invest.*, *117*, 4022–4033.

Reijneveld, J. C., Ponten, S. C., Berendse, H. W., & Stam, C. J. (2007). The application of graph theoretical analysis to complex networks in the brain. *Clin. Neurophysiol.*, *118*, 2317–2331.

Renart, A., Brunel, N., & Wang, X.-J. (2003). Mean-field theory of recurrent cortical networks: Working memory circuits with irregularly spiking neurons. In J. Feng (Ed.), *Computational neuroscience* (pp. 432–490). Boca Raton, FL: CRC Press.

Renart, A., De La Rocha, J., Bartho, P., Hollender, L., Parga, N., Reyes, A., & Harris, K. D. (2010). The asynchronous state in cortical circuits. *Science*, *327*, 587–590.

Richardson, M. J. E. (2008). Spike-train spectra and network response functions for non-linear integrate-and-fire neurons. *Biol. Cybern.*, *99*, 381–392.

Richardson, M. J. E. (2009). Dynamics of populations and networks of neurons with voltage-activated and calcium-activated currents. *Phys. Rev. E.*, *80*, 021928.

Rosenblum, M., Pikovsky, A., Kurths, J., Schäfer, C., & Tass, P. A. (2001). Phase synchronization: from theory to data analysis. In *Handbook of biological physics* (Vol. 4, pp. 279–321). North-Holland: Elsevier.

Rössler, O. E. (1976). An equation for continuous chaos. *Phys. Lett. A*, *57*, 397–398.

Sachidhanandam, S., Sreenivasan, V., Kyriakatos, A., Kremer, Y., & Petersen, C. C. (2013). Membrane potential correlates of sensory perception in mouse barrel

cortex. *Nat. Neurosci.*, *16*, 1671–1677.

Sahasranamam, A., Vlachos, I., Aertsen, A., & Kumar, A. (2016). Dynamical state of the network determines the efficacy of single neuron properties in shaping the network activity. *Sci. Rep.*, *6*, 26029.

Salinas, E., & Sejnowski, T. J. (2001). Correlated neuronal activity and the flow of neural information. *Nat. Rev. Neurosci.*, *2*, 539–550.

Sanchez-Vives, M. V., Massimini, M., & Mattia, M. (2017). Shaping the default activity pattern of the cortical network. *Neuron*, *94*, 993–1001.

Sanchez-Vives, M. V., Mattia, M., Compte, A., Perez-Zabalza, M., Winograd, M., Descalzo, V. F., & Reig, R. (2010). Inhibitory modulation of cortical up states. *J. Neurophysiol.*, *104*, 1314–1324.

Sanchez-Vives, M. V., & McCormick, D. A. (2000). Cellular and network mechanisms of rhythmic recurrent activity in neocortex. *Nat. Neurosci.*, *3*, 1027–1034.

Schimansky-Geier, L., & Zülicke, C. (1990). Harmonic noise: Effect on bistable systems. *Z. Phys. B*, *79*, 451–460.

Schneidman, E., Berry, M. J., Segev, R., & Bialek, W. (2006). Weak pairwise correlations imply strongly correlated network states in a neural population. *Nature*, *440*, 1007–1012.

Schreiber, T. (2000). Measuring information transfer. *Phys. Rev. Lett.*, *85*, 461.

Schwalger, T., Deger, M., & Gerstner, W. (2017). Towards a theory of cortical columns: From spiking neurons to interacting neural populations of finite size. *PLoS Comput. Biol.*, *13*, e1005507.

Schwalger, T., Droste, F., & Lindner, B. (2015). Statistical structure of neural spiking under non-poissonian or other non-white stimulation. *J. Comput. Neurosci.*, *39*, 29–51.

Sejnowski, T. J., Churchland, P. S., & Movshon, J. A. (2014). Putting big data to good use in neuroscience. *Nat. Neurosci.*, *17*, 1440–1441.

Shea-Brown, E., Josić, K., de la Rocha, J., & Doiron, B. (2008). Correlation and synchrony transfer in integrate-and-fire neurons: basic properties and consequences for coding. *Phys. Rev. Lett.*, *100*, 108102.

Shepherd, G. M. (2003). *The synaptic organization of the brain*. Oxford University Press.

Shu, Y., Hasenstaub, A., Badoual, M., Bal, T., & McCormick, D. A. (2003). Barrages of synaptic activity control the gain and sensitivity of cortical neurons. *J. Neurosci.*, *23*, 10388–10401.

Shu, Y., Hasenstaub, A., & McCormick, D. A. (2003). Turning on and off recurrent balanced cortical activity. *Nature*, *423*, 288–293.

Siegert, A. J. (1951). On the first passage time probability problem. *Phys. Rev.*, *81*, 617–623.

Siegle, P., Goychuk, I., Talkner, P., & Hänggi, P. (2010). Markovian embedding of non-markovian superdiffusion. *Phys. Rev. E*, *81*, 011136.

Softky, W. R., & Koch, C. (1993). The highly irregular firing of cortical cells is inconsistent with temporal integration of random epsps. *J. Neurosci.*, *13*,

334–350.

Sompolinsky, H., Crisanti, A., & Sommers, H. J. (1988). Chaos in Random Neural Networks. *Phys. Rev. Lett.*, *61*, 259.

Sompolinsky, H., & Zippelius, A. (1982). Relaxational dynamics of the edwards-anderson model and the mean-field theory of spin-glasses. *Phys. Rev. B*, *25*, 6860.

Spiridon, M., & Gerstner, W. (1999). Noise spectrum and signal transmission through a population of spiking neurons. *Networ. Comput. Neural Syst.*, *10*, 257.

Sporns, O., Chialvo, D. R., Kaiser, M., & Hilgetag, C. C. (2004). Organization, development and function of complex brain networks. *Trends Cogn. Sci.*, *8*, 418–25.

Sporns, O., Tononi, G., & Edelman, G. M. (2000). Theoretical neuroanatomy: relating anatomical and functional connectivity in graphs and cortical connection matrices. *Cereb. Cortex*, *10*, 127–141.

Steriade, M. (2001). Impact of network activities on neuronal properties in corticothalamic systems. *J. Neurophysiol.*, *86*, 1–39.

Steriade, M. (2004). Neocortical cell classes are flexible entities. *Nat. Rev. Neurosci.*, *5*, 121–134.

Steriade, M., Nunez, A., & Amzica, F. (1993). A novel slow (< 1hz) oscillation of neocortical neurons in vivo: depolarizing and hyperpolarizing components. *J. Neurosci.*, *13*, 3252–3265.

Steriade, M., Timofeev, I., Dürmüller, N., & Grenier, F. (1998). Dynamic properties of corticothalamic neurons and local cortical interneurons generating fast rhythmic (30–40 hz) spike bursts. *J. Neurophysiol.*, *79*, 483–490.

Steriade, M., Timofeev, I., & Grenier, F. (2001). Natural waking and sleep states: a view from inside neocortical neurons. *J. Neurophysiol.*, *85*, 1969–1985.

Tartaglia, E. M., & Brunel, N. (2017). Bistability and up/down state alternations in inhibition-dominated randomly connected networks of lif neurons. *Sci. Rep.*, *7*, 11916.

Thomson, A. M., West, D. C., Wang, Y., & Bannister, A. P. (2002). Synaptic connections and small circuits involving excitatory and inhibitory neurons in layers 2–5 of adult rat and cat neocortex: triple intracellular recordings and biocytin labelling in vitro. *Cereb. Cortex*, *12*, 936–953.

Timme, M., Geisel, T., & Wolf, F. (2006). Speed of synchronization in complex networks of neural oscillators: Analytic results based on random matrix theory. *Chaos*, *16*, 015108.

Timofeev, I., Grenier, F., Bazhenov, M., Sejnowski, T., & Steriade, M. (2000). Origin of slow cortical oscillations in deafferented cortical slabs. *Cereb. Cortex*, *10*, 1185–1199.

Tomov, P., Pena, R. F., Roque, A. C., & Zaks, M. A. (2016). Mechanisms of self-sustained oscillatory states in hierarchical modular networks with mixtures of electrophysiological cell types. *Front. Comput. Neurosci.*, *10*, 23.

Tomov, P., Pena, R. F., Zaks, M. A., & Roque, A. C. (2014). Sustained oscillations,

irregular firing, and chaotic dynamics in hierarchical modular networks with mixtures of electrophysiological cell types. *Front. Comput. Neurosci.*, *8*, 103.

Tononi, G., & Cirelli, C. (2014). Sleep and the price of plasticity: from synaptic and cellular homeostasis to memory consolidation and integration. *Neuron*, *81*, 12–34.

Tranel, D., Cooper, G., & Rodnitzky, R. L. (2003). Higher brain functions. In *Neuroscience in medicine* (pp. 621–639). Springer.

Trousdale, J., Hu, Y., Shea-Brown, E., & Josic, K. (2012). Impact of network structure and cellular response on spike time correlations. *PLoS Comput. Biol.*, *8*, e1002408.

Tuckwell, H. C. (1988). *Introduction to theoretical neurobiology*. Cambridge: Cambridge University Press.

Uhlenbeck, G. E., & Ornstein, L. S. (1930). On the theory of the brownian motion. *Phys. Rev.*, *36*, 823–841.

Uhlhaas, P. J., Pipa, G., Lima, B., Melloni, L., Neuenschwander, S., Nikolić, D., & Singer, W. (2009). Neural synchrony in cortical networks: history, concept and current status. *Front. Integr. Neurosci.*, *3*, 17.

van Vreeswijk, C., Abbott, L., & Ermentrout, G. (1994). When inhibition not excitation synchronizes neural firing. *J. Comput. Neurosci.*, *1*, 313–21.

van Vreeswijk, C., Sompolinsky, H., et al. (1996). Chaos in neuronal networks with balanced excitatory and inhibitory activity. *Science*, *274*, 1724–1726.

Vilela, R. D., & Lindner, B. (2009a). Are the input parameters of white-noise-driven integrate & fire neurons uniquely determined by rate and CV? *J. Theor. Biol.*, *257*, 90–9.

Vilela, R. D., & Lindner, B. (2009b). A comparative study of three different integrate-and-fire neurons: spontaneous activity, dynamical response, and stimulus-induced correlation. *Phys. Rev. E.*, *80*, 031909.

Vogels, T. P., & Abbott, L. F. (2005). Signal propagation and logic gating in networks of integrate-and-fire neurons. *J. Neurosci.*, *25*, 10786–10795.

Vogels, T. P., Rajan, K., & Abbott, L. F. (2005). Neural network dynamics. *Annu. Rev. Neurosci.*, *28*, 357–376.

Voges, N., Schüz, A., Aertsen, A., & Rotter, S. (2010). A modeler's view on the spatial structure of intrinsic horizontal connectivity in the neocortex. *Prog. Neurobiol.*, *92*, 277–292.

Vyazovskiy, V. V., Olcese, U., Hanlon, E. C., Nir, Y., Cirelli, C., & Tononi, G. (2011). Local sleep in awake rats. *Nature*, *472*, 443–447.

Wang, S.-J., Hilgetag, C. C., & Zhou, C. (2011). Sustained activity in hierarchical modular neural networks: self-organized criticality and oscillations. *Front. Comput. Neurosci.*, *5*, 30.

Wibral, M., Lizier, J. T., & Priesemann, V. (2015). Bits from brains for biologically inspired computing. *Front. Robot. AI*, *2*, 5.

Wieland, S., Bernardi, D., Schwalger, T., & Lindner, B. (2015). Slow fluctuations in recurrent networks of spiking neurons. *Phys. Rev. E*, *92*, 040901.

Williams, P. L., & Beer, R. D. (2010). Nonnegative decomposition of multivariate information. *arXiv preprint arXiv:1004.2515*.

Wilson, C. (2008). Up and down states. *Scholarpedia*, *3*, 1410.

Xu, X., Ni, L., & Wang, R. (2016). A neural network model of spontaneous up and down transitions. *Nonlinear Dynam.*, *84*, 1541–1551.

Yim, M. Y., Kumar, A., Aertsen, A., & Rotter, S. (2014). Impact of correlated inputs to neurons: modeling observations from *in vivo* intracellular recordings. *J. Comput. Neurosci.*, *37*, 293–304.